Unterschrift des Betreuers

TECHNISCHE UNIVERSITÄT WIEN
Vienna University of Technology

D I P L O M A R B E I T

CHARACTERIZATION OF DOPED CaF$_2$ CRYSTALS
towards a solid-state optical clock
Thema

Ausgeführt am

Atominstitut
der Technischen Universität Wien

unter der Anleitung von Univ.Prof. Dipl.-Phys. Dr.rer.nat. Thorsten Schumm

durch

Bianka Ullmann
Name

Dieselgasse 5B/2/41
A-1100 Wien
Anschrift

13.09.2012
Datum

_____
Unterschrift (Studentin)

CHARACTERIZATION OF DOPED CaF$_2$ CRYSTALS
towards a solid-state optical clock

Diploma Thesis

Technical Physics

written by

Bianka Ullmann
Matriculation number 0425601

Institute:

Institute of Atomic and Subatomic Physics

Thesis advisior:

Univ.Prof. Dipl.-Phys. Dr.rer.nat. Thorsten Schumm

Vienna, 13/09/2012   _____   _____

(Signature Author)   (Signature Thesis Advisor)

Abstract

It is generally agreed, that the next generation frequency standards will be based on optical transitions in atoms. An interesting candidate for realizing such a novel frequency standard could be the low-energy isomer transition in the nucleus of ^{229}Thorium. This unique long-lived (order seconds to minutes) isomer state is expected at an energy of $7.6\,\text{eV} \pm 0.5\,\text{eV}$. It has not yet been directly observed experimentally.

One approach to determine the exact energy of the isomer state is to implant ^{229}Th into crystals, transparent for vacuum ultraviolet (VUV) light, and then perform spectroscopy. In this diploma thesis, initial steps in the characterization of VUV transparent crystals, especially CaF_2 were made. In particular, properties of ^{232}Th-doped CaF_2 single crystals were characterized for the first time and compared to un-doped CaF_2 and various other possible host crystals.

For the characterization of the crystals we used radiological (neutron activation analysis and gamma spectroscopy), optical (transmittance and luminescence), and surface characterization methods (atomic force microscopy). We demonstrate that uniform doping with ^{232}Thorium can be successfully performed with a significant doping concentration ($10^{18}\,\text{cm}^{-3}$) while maintaining VUV transparency of the crystal. The study reveals several material property correlations, like the dependence of the transmittance and the spectrally resolved luminescence performance on the crystal surface preparation or on impurities and crystal defects. We conclude how the transmittance and luminescence performance is affected by defects, crystal doping, and crystal surface preparation. In addition some sample preparation methods like cutting, polishing, and cleaving of crystals were tested.

Further characterization steps should focus on the characteristic parameters of luminescence, like the decay time for different wavelength to unambiguously identify the microscopic processes. At this stage, ^{232}Th-doped CaF_2 seems to be a promising candidate for precision spectroscopy of the ^{229}Th isomer state.

Contents

1. Introduction

Time is one of the most fundamental parameter of human life and its measuring instrument, the clock, one of the oldest human inventions. The development of the clock took millennia, from the sundial to the atomic clock. Nowadays the base unit of time in the International System of Units is defined as the duration of 9,192,631,770 periods of the radiation corresponding to the transition between the two hyperfine levels of the ground state of the ^{133}Cs atom. With this transition frequency the accuracy of the atomic clock has reached a level of 10^{-16} [20].

For a better accuracy a next generation frequency standard based on optical transitions in atoms is needed. An interesting candidate for realizing such a novel frequency standard could be the low-energy isomer transition in the nucleus of ^{229}Th. This unique long-lived (order seconds to minutes) isomer state is expected at an energy of $7.6\,\mathrm{eV} \pm 0.5\,\mathrm{eV}$ [4]. This energy corresponds to a wavelength about $160\,\mathrm{nm}$. It has not yet been directly observed experimentally. Initial steps to determine the exact energy and lifetime of the isomer state are aim of this diploma thesis.

To determine the nature of the long-lived isomer state of ^{229}Th, the nucleus must be excited so that optical spectroscopy can be performed. However, an excitation with vacuum ultraviolet (VUV) light could induce unwanted transitions in the electron shell. During relaxation to the ground state, the electron shell would emit photons with an energy in the spectral range of the searched nuclear transition. This could mean, that the nucleus transition remains immeasurable because of the strong emission of the electron shell.

There are two main approaches how to counteract the excitation of the electron shell. One approach is ion trapping and cooling of ^{229}Th^{3+} ions. The second approach to determine the exact energy of the isomer state is to implant ^{229}Th into

1

crystals, transparent for VUV light. Advantages of the second approach over the ion trapping method are simple fabrication, no complex experimental techniques and simultaneously excitation of up to 10^{18} ^{229}Th nuclei. In this diploma thesis the approach of implanting ^{229}Th into a host crystal, transparent for VUV light will be investgated. The host crystal should have low absorptance effects and no luminescence at wavelengths about 160 nm. Possible host crystals could be CaF_2 and $LiCaAlF_6$.

In this diploma thesis CaF_2 crystal doped with ^{232}Th (as a test version for CaF_2 doped with ^{229}Th) and other possible host crystals like $LiCaAlF_6$ will be investigated. For realization of the first "solid-state nuclear clock" a sample characterization routine must be developed. Some samples will be manufactured by the Institute of Atomic and Subatomic Physics and some samples will be manufactured by collaborators. Established characterization methods like gamma spectroscopy, neutron activation analysis, atomic force microscopy, transmittance and luminescence measurements as well as surface preparation methods will be applied. The aim is the characterization of several material property correlations. Within this aim, we want to know, how extrinsic and intrinsic crystal defects (laser induced) affect optical properties of the crystal. For optical caracterization, a fluorine excimer laser with a wavelenth of 157 nm will be used.

The exploration of a more accurate atomic clock (nuclear clock) will have far-reaching consequences for science and technology, for example more accurate navigation systems. At the moment only initial steps can be made towards a "solid-state nuclear clock", but they could be the basis for new technologies.

2. Characterization Methods

This chapter gives a brief introduction to the methods employed in this thesis. Although all of them are established standard tools, for quantitative measurements, specific calibrations are needed.

2.1. Radiological Characterization

This subsection gives an overview of the radiological characterization methods used in this diploma thesis. The research focus is on the quantitative composition of the samples, especially doping concentration, and on possible unwanted crystal impurities.

2.1.1. Gamma Spectroscopy

Gamma spectroscopy is a method to record the energy-resolved gamma spectrum of a radioactive sample. In the present case a germanium semiconductor detector has been used. In brief the working principle of a semiconductor detector is based on the production of free charge-carriers as a result of the absorption of gamma radiation. If an electric field is applied to the semiconductor, the electrons and the holes are separated and collected at the electrodes. The resulting electrical pulse is proportional to the energy of the incident gamma photon [16].

There are three interaction mechanisms between the gamma photons and the semiconductor material that should be mentioned: photoelectric effect, pair production and Compton effect [11]. In figure 2.1 the dependence of the interaction cross sections on the radiation energy for the three mechanisms is shown.

Photoelectric effect: Matter absorbs the energy of electromagnetic radiation and emits electrons. The kinetic energy E_{kin} of the emitted electrons depends

on the frequency of the γ-quantum ν and the work function - the energy required to remove an electron from the electron shell W_W - and not on the intensity of the emitted electromagnetic radiation

$$E_{kin} = h \cdot \nu - W_W. \tag{2.1}$$

The cross section for the photoelectric effect is getting smaller with increasing gamma energy. The cross section depends also on the charge number Z of the semiconductor material and is proportional to Z^n with n between 4 and 5. It is mainly the photoelectric effect that is used to identify and quantify gamma quanta in gamma spectroscopy.

Pair production: Interaction of gamma photons with an energy E_γ above $1022 \, \text{keV}$ with the detector material can cause pair production, which is the creation of an electron and a positron. The sum of the rest mass of an electron and a positron is $1022 \, \text{keV}$. The resudal energy $\Delta E = E_\gamma$ - $1022 \, \text{keV}$ is transfered almost entirely to kinetic energy of the electron. This electron is detected the same way as an electron caused by photoelectric effect. Simultaneously the positron annihilates with an electron and emits two gamma quanta of each $511 \, \text{keV}$. If the kinetic energy and the momentum of the annihilation electron-positron system before annihilation are negligible then the angle between the two gamma quanta is $180°$.

If both of the gamma quanta escape from the detector volume, then only the resudal energy ΔE is measured. This causes a double escape peak in the gamma spectrum with the energy

$$E_{DEP} = E_\gamma - 1022 \, \text{keV}. \tag{2.2}$$

If only one of the annihilation gamma quanta escapes, then the detector detects the electron with the kinetic energy ΔE and one annihilation gamma photon with $511 \, \text{keV}$ simultaneously. This causes a single escape peak in the gamma spectrum with the energy

$$E_{SEP} = E_\gamma - 511 \, \text{keV}. \tag{2.3}$$

If both of the annihilation gamma photons are detected by the gamma detector, then the detected energy corresponds to the gamma ray energy E_γ. Pair production can also occur in air before the incident gamma photon with E_γ above $1022\,\text{keV}$ reaches the gamma detector. In this case the electron does not reach the detector, because it is absorbed in air. The positron annihilates with an electron and the two gamma quanta with $511\,\text{keV}$ can be detected with the gamma detector. This means that it is very probable to see a $511\,\text{keV}$ photo peak in the gamma spectrum.

The dependence of the pair production cross section on the charge number of the semiconductor material is proportional to Z^2.

Compton effect: This is the inelastic scattering of photons on matter as a consequence of the interaction with the electron shell. The result is a decrease in the energy of the photon. According to equation 2.4 the difference of the wavelength of the scattered gamma photon λ'_γ and the wavelength of the gamma photon λ_γ depends on the scattering angle θ

$$\lambda'_\gamma - \lambda_\gamma = \frac{h}{m_e \cdot c} \cdot (1 - \cos\theta). \tag{2.4}$$

The Compton effect is the reason for the backscattering peak and the continuous Compton background. The cross section is proportional to Z.

Because of these three effects described before, I expect an annihilation peak at $511\,\text{keV}$, peaks at the energy of the single escape peak E_{SEP} and the energy of the double escape peak E_{DEP}, backscattering peaks, a continuous Compton background and of course photo peaks. Natural radon abundant in the institute basement (where the gamma detectors are located) could cause peaks of ^{214}Pb or other decay products like ^{214}Bi. Peaks of ^{40}K are always detected, as ^{40}K is always abundant.

Gamma spectroscopy is useful to determine which radionuclides occur in a sample as long as they emit gamma radiation. For natural radionuclides such as ^{232}Th the dynamics of the decay chain has to be taken into account (until radioactive equilibrium is reached). Obviously, no statements can be made about non-radiating ingredients.
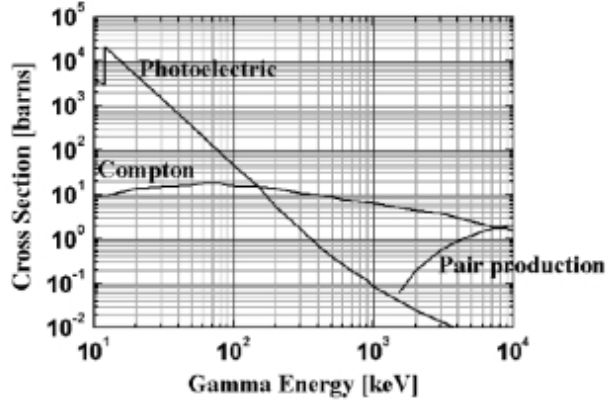
Figure 2.1.: Compton effect, photoelectric effect, and pair production cross section of Ge for high energy γ-rays [18].

2.1.2. Neutron Activation Analysis

Neutron activation analysis is a method for analyzing samples of unknown or little known composition. Activation means the captering of a neutron by a nucleus as a result of the interaction between the nucleus $_Z^A$X and a neutron at thermal energy n_{th}. The nucleus captures the neutron in dependence of the cross section at thermal neutron energy σ_{th}. The reaction product is the same nuclide X with the increased mass number A+1 and the same atomic number Z

$$_Z^A\text{X} + n_{th} \rightarrow \, _Z^{A+1}\text{X}. \tag{2.5}$$

$_Z^{A+1}$X in most cases is not stable and disintegrates. In this decay of nuclides $_Z^{A+1}$X gamma photons are emitted that can be detected with a gamma spectrometer. In its simplest version, this characterization method requires a device for thermal neutron irradiation with a neutron flux density of least $10^{11}\,\text{cm}^{-2}\text{s}^{-1}$. For calculation of the sample composition, a certified reference material, also called standard (sample of known composition) is required.

The sample to be analyzed must be prepared beforehand, because the geometric shape of sample and standard should be as identical as possible. The reason for this is the gamma spectroscopy employed later, where the detection efficiency for samples and standards must be identical. The standard is usually present as a

powder and can be filled in little plastic vials. In most of the cases the sample must therfore be crushed.

After the sample preparation, samples and standards are exposed to the neutron flux for the same time duration and at the same time. The reaction rate of the number of activation product nuclides N_B is the difference of the activation term and a decay term (see equation 2.6). The activation term is proportional to the number of interacting nuclides N_A and depends on the cross section at thermal neutron energy σ_{th} and the neutron flux density ϕ. The decay term is proportional to N_B and depends on the decay constant λ of the nuclide B

$$\frac{dN_B}{dt} = \sigma_{th} \cdot \phi \cdot N_A - \lambda \cdot N_B. \tag{2.6}$$

The solution to the differential equation 2.6 yields N_B with the irradiation time t

$$N_B(t) = \frac{\sigma_{th} \cdot \phi \cdot N_A}{\lambda} \cdot (1 - e^{-\lambda \cdot t}). \tag{2.7}$$

With equation 2.7 the activity of nuclide B, $A_B = \lambda \cdot N_B$ can be calculated (activation equation)

$$A_B(t) = \sigma_{th} \cdot \phi \cdot N_A \cdot (1 - e^{-\lambda \cdot t}). \tag{2.8}$$

If long-lived radionuclides are targeted, a two-week cooldown must be scheduled so that short-lived isotopes with very high activity, such as ^{49}Ca and ^{20}F, do not predominate the peaks which shall be observed.

The last step is gamma spectroscopy of activated samples. Standards and samples are measured each for the same time duration and the peaks of the standards and samples are evaluated and compared. From the relative activity of standards and samples together with the known composition of the standard, the composition of the sample can be derived.

In this diploma thesis the doping concentration of ^{232}Th implanted in CaF_2 crystals is studied. The cross section at thermal neutron energy is 7.37 barn (1 barn = 10^{-28} m^2), which is sufficient for activation. ^{232}Th activates to ^{233}Th (nuclide B). The half-life $t_{\frac{1}{2}}$ of ^{233}Th is 21.83 minutes. The irradiation duration for activation can be scheduled with two hours. After this time the factor $(1 - e^{-\lambda \cdot t})$ in equation 2.8 has a value of 0.978. After a two-week cooldown we can not measure the

decay of ^{233}Th because of that short half-life. What will be measured is the decay product ^{233}Pa with $t_{\frac{1}{2}} = 27$ days. The activity of ^{233}Pa is an indicator for the mass of ^{232}Th. With the activity of ^{233}Pa in a sample $A_{Pa_{sample}}$, the activity of ^{233}Pa in the standard $A_{Pa_{standard}}$ and the known mass ^{232}Th in the standard $m_{Th_{standard}}$, the mass of ^{232}Th in the sample $m_{Th_{sample}}$ can be calculated

$$m_{Th_{sample}} = \frac{A_{Pa_{sample}}}{A_{Pa_{standard}}} \cdot m_{Th_{standard}}. \tag{2.9}$$

Instead of the activities also the count rates can be used for calculation. For the calculation with count rates the requirements are that they are count rates of the same peak and the detection efficiency (geometry of the samples and reference materials) is the same for all measured samples and reference materials. It should be noted, that the characteristic peak should be in an energy range with high efficiency of the gamma detector.

The neutron activation analysis is not always suited to solve all analytical problems. Not every element responds to neutron irradiation the same way. It depends on the neutron cross section at thermal neutron energy σ_{th}. A look at the chart of nuclides before starting the analysis is useful. This assumes that the nuclides of interest are known. Furthermore the half-life of the isotope of interest is important. If the half-life is too short, no peak will be observed in the gamma spectroscopy. The big advantage of this method is that also non-active substances can be detected.

2.2. Surface Characterization

This chapter describes briefly the surface characterization method atomic force microscopy, which yields a roughness value for different crystal surface preparation methods.

2.2.1. Atomic Force Microscopy

Atomic force microscopy (AFM) is a surface scanning method with a very high resolution. A cantilever with a tip is guided within a defined area obove the surface
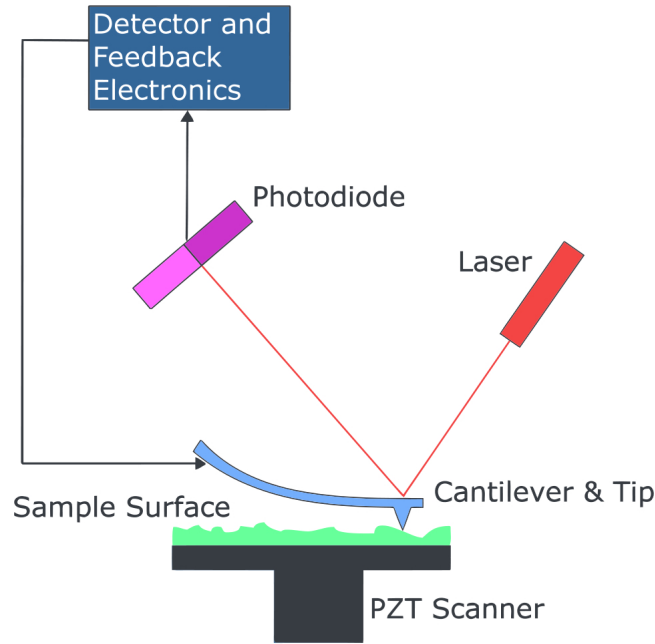
Figure 2.2.: Atomic force microscope

of the sample using a piezo scanner. Because of the surface structure and the forces between the tip and the surface (for example van der Waals forces, electrostatic forces, ...), the cantilever deflects. This deflection is measured with an optical sensor as a function of the tip position. The assembly is shown in figure 2.2.

After recording the deflections, a digital 2D image is generated. The possible spatial resolution of the image is determined by the radius of the tip. This is usually 10 to 20 nm. The possible height resolution is usually 0.1 to 10 nm [11]. A disadvantage of this method is the limit for the sample thickness imposed the AFM used in this thesis. Usually only samples with a thickness below 1 cm could be measured. It should be noted that electrostatic charge on the surface leads to errors in the measurement.
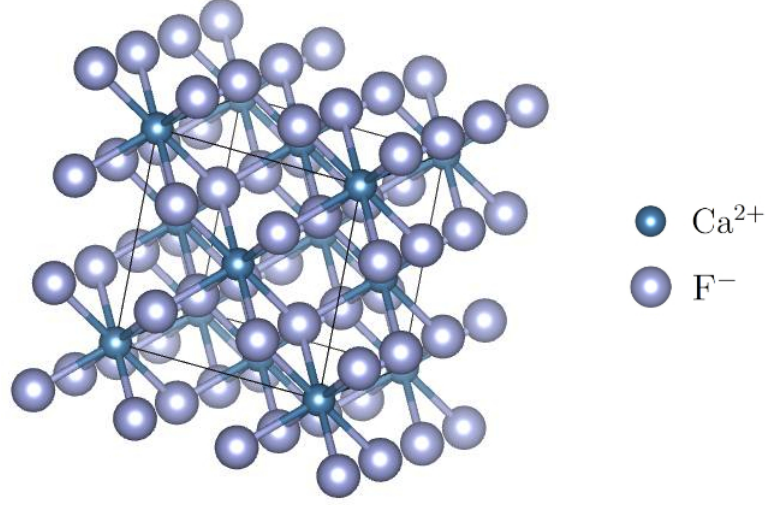
Figure 2.3.: Crystal lattice of CaF_2

2.3. Optical Characterization

This section gives an overview on the possible defect states of crystals, especially CaF_2, and the consequences for optical performance of VUV transparent crystals. The characterization methods used in this thesis for determining optical performance are transmittance and luminescence measurements.

2.3.1. Electronic Structure and Defect States of CaF_2

The interaction between VUV light and VUV transparent materials is one of the main issues of this diploma thesis. For this, the electronic structure of the crystal lattice and the defect states play a major role.

CaF_2 is an alkaline earth fluoride and crystallizes in a face-centered cubic lattice. The basis of the lattice is a Ca^{2+}-ion with the coordinates $\{0, 0, 0\}$ and two F^--ions with the coordinates $\{\frac{1}{4}, \frac{1}{4}, \frac{1}{4}\}$ and $\{\frac{1}{4}, -\frac{1}{4}, \frac{1}{4}\}$ with the experimentaly measured lattice constant $5.4630\,\mathring{A}$ (see figure 2.3). This crystal is a large-band-gap insulator. Two types of band-gaps are distinguished, direct and indirect band-gaps. The difference is due to the conservation of momentum. Direct band-gap means that the momentum of electrons and holes in the valence band and the conduction band is the same. This means that the k-vectors are the same and a photon can be emitted

Figure 2.4.: Colored Ce:CaF$_2$ after VUV irradiation

directly. This is impossible in an indirect band-gap, because the electron relaxes into an intermediate state and transfers momentum to the crystal lattice. Experimentally, the direct band-gap is 12.1 eV (corresponds to wavelength 102.5 nm) and the indirect band-gap is 11.8 eV (corresponds to wavelength 105.1 nm) in CaF$_2$ [27].

In theory, today mostly hybrid methods are used to calculate electronic energy values and other parameters, combining elements of the Hatree-Fock-Methode and density-functional theory [13] [14]. Within the duration of this thesis, such calculations were used to determine the band-gap of thorium-doped CaF$_2$ [8].

Crystallographic defects are the reason for binding and releasing electrons, which leads to electronic states within the band-gap. We distinguish intrinsic and extrinsic defects. Intrinsic defects are defects which even occur in a pure crystal in thermodynamic equilibrium (F-centers, self-trapped excitons,...). Extrinsic defects are caused by the presence of a second phase (impurities).

F-centers: The F-center is an anionic vacancy in a crystal lattice which is filled with one or more electrons. F-centers are also called color centers because the trapped electrons can absorb electromagnetic waves in the visible spectrum. This leads to coloring of the crystal.

In a previous project work I observed the coloration of Ce:CaF$_2$ after irradiation with a 157 nm fluorine laser, which is shown in figure 2.4. A trivalent cerium ion occupies a lattice site and fluor interstitials compensate the extra positive charge [17]. The absorbance of the 157 nm photons generates

2. Characterization Methods

F-centers which cause a red coloration. This effect depends on the intensity of the laser beam.

In the same project work I could not find any coloration of pure CaF_2 or $^{232}Th{:}CaF_2$ crystal. Obviously coloration of CaF_2 crystals depends on impurities and their concentration.

Excitons: An exciton is a bound state of an electron and a hole, an electrically neutral quasiparticle which is an elementary excitation of condensed matter. The attraction force between the electron and the hole is the Coulomb force. If a photon with an energy greater than the band-gap is absorbed, an electron is excited from the valence band into the conduction band and a bound state of an electron and a hole could be the result. In CaF_2 the excitons are strongly bound.

Beside the free excitons, there are also the self trapped excitons. If one or more photons are absorbed, a fluor ion F^- is neutralized. After that, a weak bond between the fluor atom and the neighbouring fluor ion, a so-called H-center, is the result. The F_2^- molecule rotates into the diagonal of the fluor cube and orientates in the [111] direction [15]. After trapping the free electron, an F-center is formed. This metastable system of F-center and H-center is called self-trapped exciton (STE). The systen is in a metastable triplet state $^3\Sigma_u$ and can relax to the ground state with or without radiation of a photon. This STE luminescence is a π-luminescence and is spin-forbidden. A rather long lifetime of microseconds to milliseconds is the result [24]. The second possibility of relaxation is the lattice relaxation or the formation of stable F and H-centers [25].

V$_k$-centers are as well as H-centers a molecule ion F_2^-. The difference is the orientation into the [100] direction. The reason for a V$_k$-center is that a fluor ion traps a hole. V$_k$-centers are unstable at room temperature and recombine with an electron or an F-center. The recombination in some cases causes luminescence, but we do not expect it for CaF_2 and at a wavelength of 157 nm.

Impurities: The periodicity of the crystal lattice is distorted. Depending on the

kind of impurities and their concentration they cause a change of all characteristics of the crystal (band-gap, defect states within the band-gap, ...).

Excitons and F-centers are often the reason for luminescence and reduced transmittance effects. Oxygen contamination could also affect the optical properties of CaF_2. According to the information from the manufacturers of the samples I used for my measurements there is no or only a negligible amount of oxygen in the samples.

2.3.2. Transmittance

Beside reflection and absorptance the transmittance value describes the behaviour of light when moving trough a crystal. The transmittance T is the fraction of incident light intensity I_{em} that passes through a sample with the thickness x, which is the optical path

$$T = \frac{I_{em}(x)}{I_{em}(0)}. \tag{2.10}$$

Absorptance A is the fraction of incident light intensity which is absorbed in a sample. Reflectance R is the fraction of incident light intensity which is reflected on the surface of a sample. The sum of T, A and R is 1. Transmittance depends on the wavelength of the light.
In the following we want to look at the possible absorptance and reflection effects and the dependence of T on absorption coeffiecents and refractive indices. We will mainly refer to CaF_2 in this section.

Bulk absorptance effects

First we take a look at the absorptance in the bulk, where the sum of transmittance and absorptance is 1:

$$T + A = 1. \tag{2.11}$$

Absorptance also includes scattering effects like Compton effect and Rayleigh scattering and absorbing effects like photoelectric effect and pair production. Because of the periodicity of the scattering centers of the measured samples (low impurity concentration) and the wavelength of the incident light (157 nm) the mentioned

scattering and absorbing effects affect the transmittance performance substantially less than one-photon or two-photon absorptance. So, they will not be discussed in this diploma thesis.

Linear Absorptance (One-Photon Absorptance): A photon with an energy greater than the energy of the band-gap of a crystal, can be absorbed and an electron is excited from the valence band to the conduction band. For this effect there is no dependence of the absorptance coefficient α on the intensity of the electromagnetic wave I_{em} and it is homogeneous trough the whole sample $\alpha(I_{em}) = \alpha_1$. The change of intensity of the electromagnetic wave I_{em} crossing an absorptive medium with the thickness x is proportional to I_{em}

$$\frac{dI_{em}}{dx} = -\alpha_1 \cdot I_{em}(x). \tag{2.12}$$

After solving this equation the integral form of the Labert-Beer-Law follows

$$I_{em}(x) = I_{em}(0) \cdot e^{-\alpha_1 \cdot x}. \tag{2.13}$$

If the density of the absorber material is homogeneous over the sample, then the transmittance T is independent of the incident intensity

$$T = \frac{I_{em}(x)}{I_{em}(0)} = e^{-\alpha_1 \cdot x}. \tag{2.14}$$

For linear absorptance we expect that $T(I_{em}) = const$ at a constant sample thickness x.

Non Linear Absorptance (Multiphoton absorptance): If the band-gap of a crystal is too large (greater than the energy of a incident photon), then the energy of more than one photon is needed to excite an electron from the valence band to the conduction band. Multiphoton absorptance is the simultaneous absorptance of two or more photons in the crystal. For higher intensities of the electromagnetic wave the absorptance coefficient α depends on the local intensity. The absorptance coefficient α is given by

$$\alpha(I_{em}) = \sum_n \alpha_n \cdot I_{em}{}^{n-1} \quad \text{with } n = 1, 2, ... \tag{2.15}$$

where α_n is the n-photon absorptance coefficient. Phenomenologically the multiphoton absorptance can be described by the generalized Lambert-Beer-Law

$$\frac{dI_{em}}{dx} = -\sum_n \alpha_n \cdot I_{em}{}^n \quad \text{with } n = 1, 2, \dots . \tag{2.16}$$

The theoretical background can be found in [19].

For CaF_2 (band-gap about $12\,\text{eV}$) and vacuum ultraviolet light about $157\,\text{nm}$ ($7.9\,\text{eV}$) two-photon absorptance is the only multiphoton absorptance that can occur. With the absorptance coefficient for two-photon-absorptance β and $n = 2$ the absorptance law is given by

$$\frac{dI_{em}}{dx} = -\beta \cdot I_{em}{}^2. \tag{2.17}$$

After solving this differential equation $I_{em}(x)$ is given by

$$I_{em}(x) = \frac{I_{em}(0)}{1 + \beta \cdot x \cdot I_{em}(0)}. \tag{2.18}$$

By dividing equation 2.18 through $I_{em}(0)$, we get the transmittance (see equation 2.10)

$$T = \frac{1}{1 + \beta \cdot x \cdot I_{em}(0)}. \tag{2.19}$$

The absorptance is given by equation 2.11. For constant sample thickness we expect a decreasing Transmittance with increasing I_{em}.

In most of the cases one and two-photon absorptance are present

$$\frac{dI_{em}}{dx} = -\alpha I_{em} = -(\alpha_1 + \beta I_{em})I_{em}. \tag{2.20}$$

After solving this differential equation, T can be calculated with equation 2.10

$$T = \frac{e^{-\alpha_1 \cdot x}}{1 + \beta \cdot I_{em}(0) \cdot \dfrac{1 - e^{-\alpha_1 \cdot x}}{\alpha_1}}. \tag{2.21}$$

Beside the two-photon absorptance there is also the linear two-step absorptance, which is a stepwise one-photon absorptance. This effect is possible in the presence

of excitation states within the band-gap. In transmittance measurements two-step absorptance behaves just like the two-photon absorptance. Depending on the energy of the photon, this two-step absorptance is possible directly or indirectly by relaxation into energetically lower states within the band-gap. The absorption coeffients of the linear two-step absorptance and the two-photon absorptance are sumed up to an effective two-photon absorptance coefficient β_{eff}. In this case β can be replaces by β_{eff} in equation 2.21.

The smaller β_{eff}, the more the function in 2.21 approaches a linear function for a fixed sample thickness (optical path).

Surface absorptance effects

The surface absorptance effects are the same as the bulk absorptance effects. The two-photon absorptance is usually a bulk effect. However, there are strong indications for two-photon absorptance at the surface caused by an absorbing interface layer [7]. The reason for two-photon or linear two-step absorptance could also be crystal defects on or near the surface which are caused by polishing the crystal surface. Additional surface defect states occur within the band-gap.

Transmittance performance depends strongly on the surface roughness. The reasons are more scattering and diffuse reflection effects, because of deeper grooves and more adsorbed particles. Absorptance effects decrease with lower roughness value. [22]

Reflection

Reflection describes what fraction of the incident light is reflected. Reflection depends on whether the interface reflection is specular or diffuse (surface roughness). If the roughness is much smaller than the wavelength of the light, then reflection is specular and the Fresnel equations, which are derived from the Maxwell equations, can be used to calculate the reflection.

The surface roughness of the CaF_2 sample "Hellma Disc" (root mean square surface deviation $R_{rms} \approx 1.3\,\text{nm}$) is much smaller than the wavelength of the 157 nm fluorine laser. Furthermore we know the absorptance per thickness (optical path) from the manufactuerer "Hellma Materials" ($>99{,}4\,\%$ per 10 mm for 157 nm) and
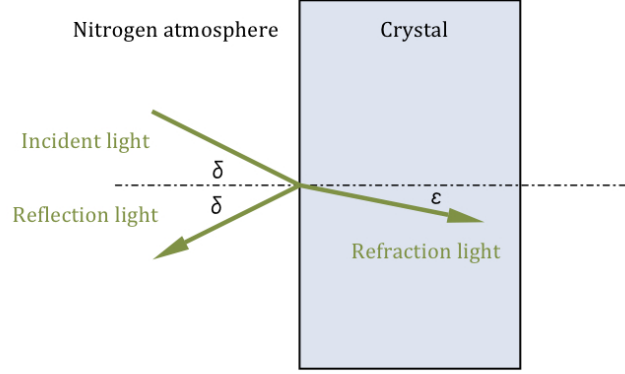
Figure 2.5.: Angle of incidence and of refraction

the sample thickness which is 10.3 mm. Thus the expected value for the total transmittance can be calculated with the Fresnel equations.

For normal incidence (angle of incidence light $\delta=0$) the Fresnel equation simplifies and the reflectance depends on the refractive indices $n_N \approx 1.003$ (transmittance will be measured in a nitrogen atmosphere) and $n_{CaF_2} \approx 1.559$

$$R(\delta = 0) = \left(\frac{n_N - n_{CaF_2}}{n_N + n_{CaF_2}} \right)^2. \tag{2.22}$$

The calculated value for the reflectance is $R = 4.7\%$ for one surface. The transmittance value for the bulk is 99.4%, the result for the total transmittance for normal incidence is $T = 90.2\%$ assuming no non-linear absorptance in the bulk.

It should be noted, that in experiments it is probable that the incidence is not perfectly normal. An angle of incidence light δ (see figure 2.5) should be considered. Assuming nitrogen atmosphere and the sample to be a perfect dialectric material, the transmittance coefficients for the vertical and parallel component of the amplitude vector on the incident plane are given by [10]

$$\tau_v = \frac{2 \cdot \sin(\epsilon) \cdot \cos(\delta)}{\sin(\delta + \epsilon)}, \tag{2.23}$$

$$\tau_p = \frac{2 \cdot \sin(\epsilon) \cdot \cos(\delta)}{\sin(\delta + \epsilon) \cdot \cos(\delta - \epsilon)}. \tag{2.24}$$

17

The transmittance T is given by

$$T_v = \tau_v{}^2 \tag{2.25}$$

and

$$T_p = \tau_p{}^2. \tag{2.26}$$

For an incidence deviation of $\delta = 5°$ the deviation of the transmittance is not greater than $0.3\,\%$. We expect a transmittance value $T \approx 90.2\,\% \pm 0.3\,\%$.

2.3.3. Photoluminescence

Photoluminescence (PL) is the emission of light by a substance. Simplified, this means that an electron is excited from the ground state into an excited electronic state. Thereafter the electron relaxes to the ground state and emits a luminescence photon.

The characteristics of photoluminescence (PL) are the spectrum of the photoluminescence peaks and the decay characteristics which are defined by the lifetime or decay time τ, the number of electrons or molecules in the excited state $N_{excited}$ and the time t

$$N_{excited}(t) = N_{excited}(0) \cdot e^{-\frac{t}{\tau}}. \tag{2.27}$$

In reality PL is more complicated. There are more than one possibilities how an excited electron can relax to the ground state. If the excited state is a singlet state, then the PL is called flourescence. The lifetime is typically 10^{-8} to 10^{-5} seconds. In CaF_2 crystals such short-lifetime luminescence is caused by electronic states of atoms or molecules (impurities) mostly. If the excited state is a triplet state, the relaxation to the ground state is quantum mechanically forbidden meaning the lifetime is typically 10^{-5} seconds up to hours. This is called phosphorescence and is caused in crystals by intrinsic defect states mostly.

Due to the defects in solids with a valence band, a band-gap, and a conduction band, the excited states are within the band-gap. If extrinsic defects cause the excited states, than there are three electron excitation processes.
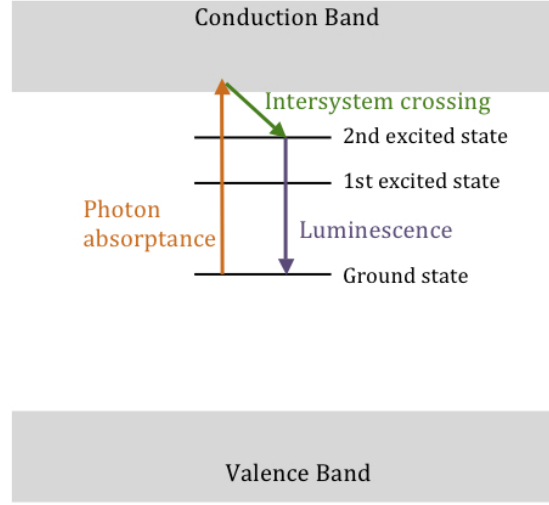
Figure 2.6.: Electron excitation in the electron shell of an impurity (schematically)

Intersystem crossing: Excited states of the electron shell of impurities near the conduction band enable a transition between the electronic state and the conduction band (intersystem crossing). This process is radiationless.

Excitation within the electron shell of the impurity: If an electron of the impurity electron shell is excited by a photon into the conduction band, it can relax radiationless to a excited state of the impurity electron shell (see figure 2.6). After that intersystem crossing process it can relax to the ground state of the impurity electron shell and emits an photon (PL).

Charge transfer is the excitation of an electron to a ground state of an impurity ion. The ion traps the electron and changes the charge state. After absorbing a photon, an electron can be excited to the conduction band and relax again to the ground state of the impurity ion. During the relaxation process a luminescence photon is emitted.

Excited states within the band-gap could be also caused by STE (intrinsic defects). This formation requires two-photon excitation [26]. As mentioned in subsection 2.3.1 STEs are in a metastable triplet state $^{3}\Sigma_{u}$ and can relax to the ground through STE luminescence (π-luminescence). Görling, Leinhos and Mann measured the STE luminescence of CaF_2 [6]. They report one STE luminescence peak at 285 nm.

The decay time of this STE is $0.9\,\mu$s. In [9] is shown, that the wavelength of this peak is the same for irradiation with a 157 nm laser. Cramer also measured the STE luminescence comparing cleaved and polished surfaces for irradiation with a 157 nm laser. Obviously polished surfaces cause a shift of the STE luminescence peak energy.

There is no luminescence in perfectrly pure CaF_2 caused by F-centers or other intrinsic defects.

3. Sample Preparation and Specification

In this chapter different sample preparation methods such as cutting, cleaving, etc. are described and all measured samples are specified.

3.1. Sample Preparation

The sample preparation is an important part of this diploma thesis. Each sample characterization method as described in the previous chapter 2 requires a separate sample preparation.

Grown crystals, in example the ones I got from Institut für Kristallzüchtung IKZ Berlin[1], first have to be cut to get a series of handy samples. Obviously during cutting the crystal must not crack or break which requires some skill and practise together with patience.

The requirement for transmittance and luminescence measurements is a smooth (optical quality) surface. A low quality surface would absorb nearly $100\,\%$ of the laser beam.

For neutron activation analysis and gamma spectroscopy the sample should be crushed. Otherwise the geometry of the sample could be unfitting. An exception is when the samples have a very similar geometry as the standards.

These are just a few reasons, why it is necessary to carefully look at some cutting, polishing and cleaving methods.

---

[1]http://www.ikz-berlin.de

3.1.1. Crystal Cleaving

The crystal cleaving is a controlled break along a crystal lattice plane. This method is a very quick one. Once the lattice plane is found, the crystal is easily prepared for transmittance measurements.

CaF_2 crystals were cleaved at the Institute for Applied Physics of the Vienna University of Technology[2] with a razor blade and a small hammer. I hold the razor blade in a lattice plane of the crystal in a way, such that the edge touched the crystal surface. A light tap with the hammer on the other edge of the razor blade is sufficient to cleave the crystal.

Advantages of this method are the quickness and the perfectly smooth surface. This advantages assume that the lattice plane is known. If the lattice plane is unknown it could take some time to find it. This requires a lot of razor blades, because the value of hardness of CaF_2 is higher than the one of the razor blade.

A disadvantage of cleaving are the typical atomic steps in the surface that could accur (see subsection 4.2.1). This atomic steps could cause reflaction effects and affect the transmittance performance.

As it is shown in section 4.3 crystal cleaving is not advisable, as this sample preparation method causes unwanted tranmittance and luminescence effects.

3.1.2. Crystal Cutting

The crystal cutting is a method which needs a saw. Two types of saws were used for cutting a crystal: an oscillating wire saw (see figure 3.1) and a circular saw with a diamond cutting disc (see figure 3.2).

The oscillating wire saw uses abrasion to cut, the abrasion material being a suspension, which contains the cutting grain. The suspension is a mixture of equal parts "Silicon Carbide Powder GRIT 400" and "Silicon Carbide Powder GRIT 1000" with glycerine ($C_3H_8O_3$).

One advantage of the circular saw is the quick cutting, up to $2\,cm$ diameter per hour. The disadvantage is the high mechanical stress for the crystal. The crystal may crack or cleave spontaneously. The wire saw on the other hand is a very gentle cutting method. It is unlikely to crack or destroy the crystal.

---

[2]http://www.iap.tuwien.ac.at/
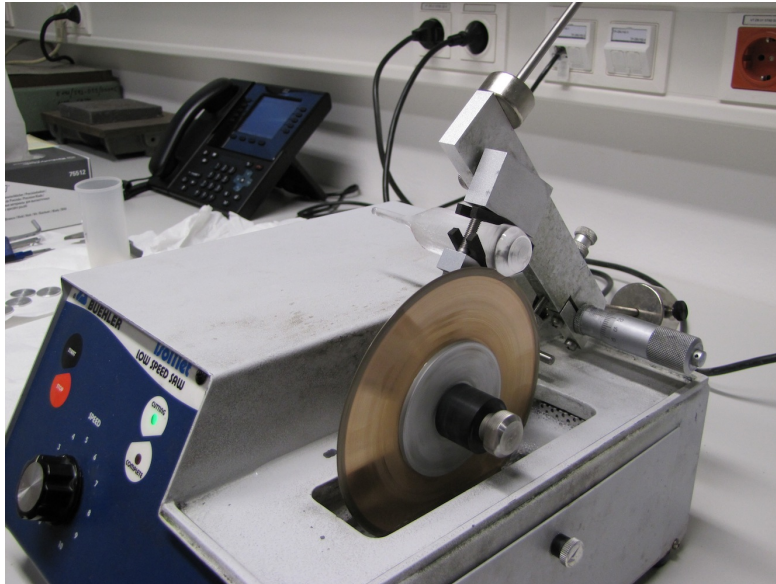
Figure 3.1.: Wire saw

Figure 3.2.: Crystal cutting with circular saw

Figure 3.3.: Polishing machine with rotating polishing disk

A second advantage of the wire saw is the sample mount. Samples are attached to the mount with wax. Cutting of every sample size and shape is possible.

However, the big disadvantages are the necessity to regulary retighten the cutting wire and the high temperature (about 80°C) required during sticking the sample. At temperatures about 100°C, samples with small cracks have shown to cleave spontaneously.

Some of the samples used for the measurements in my diploma thesis were cut and polished at the Institute for Atomic and Subatomic Physics in Vienna using the circular saw and, if necesary, polished with a polishing machine with rotating polishing disk. Samples cut at the Dipartimento di Fisica "E. Fermi", Universita' di Pisa [3] are cut with a wire saw.

3.1.3. Crystal Polishing

Some samples had to be polished for the transmittance and luminescence measurements. I polished the samples at the Institute of Atomic and Subatomic Physics Vienna with a polishing machine with rotating polishing disk (see figure 3.3). The

---

[3]http://www.df.unipi.it
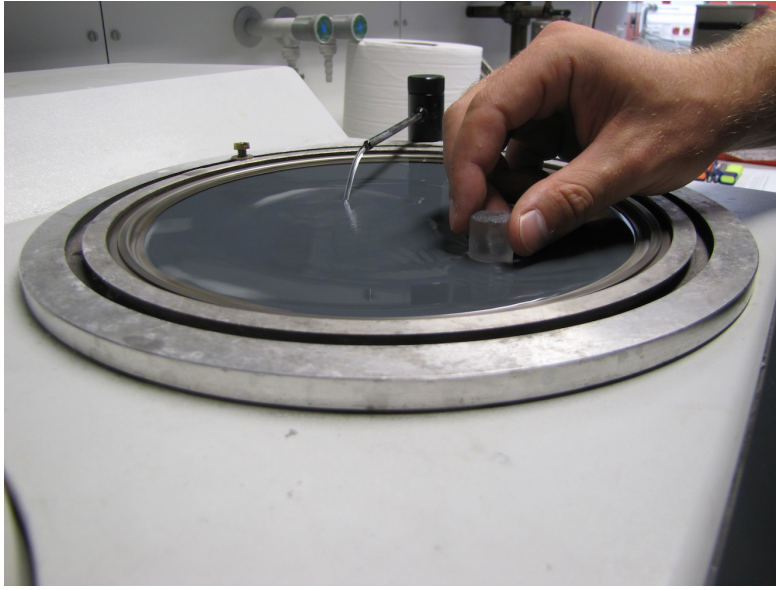
Figure 3.4.: Polishing the crystal

coarse polishing was with a sandpaper grain of 1000, 1200 and 2400, the fine polishing with a grain of 4000. The laser beam entry and exit surfaces should be parallel after polishing. That is not easily achived because I had to hold the samples by hand during polishing (see figure 3.4). If the force is not uniform over the surface the entry and exit surfaces may not be parallel. This could be a reason for deflection of the laser beam. To improve on this point, a simple sample holder was build (see figure 3.5). Unfortunately, the sample holder was used for samples that I have not measured.

This polishing method needs patience. Every sandpaper grain has a characteristic abrasive track which must be recognized. After the fine polishing these track are nearly invisible to the human eye, but still visible with an atomic force microscope. A sandpaper with a grain higher than 4000 will cause a smoother surface.

Some of the samples used for the measurements in my diploma thesis were cut and polished at the Dipartimento di Fisica "E. Fermi", Universita' di Pisa. They are polished with sandpaper but the fine polishig was done with diamond paste (size 1 micron).

Figure 3.5.: Polishing setup

3.2. Sample Specification

The tables in the following subsections describe the samples for gamma spectroscopy, neutron activation analysis, atomic force microscopy and transmittance and luminescence mesurements. The attribute "Material" contains the information about the state of matter and whether it is crushed or a powder. If not specified otherwise it is in crystaline form. There is no information about the exact age of all samples. Samples with the same name have been used in different characterization methods.

The doping concentrations of ^{232}Th:CaF$_2$ crystals and their melt is measured by Institut für Kristallzüchtung Berlin IKZ by inductively-coupled-plasma mass-spectrometry (ICP-MS).

3.2.1. Samples for Gamma Spectroscopy

For the quantitative analysis the geometry of the samples is very important. The attribute "Geometry" is not exactly a sample specification, but describes the relevant spatial geometry. In some cases it is a specification of the little plastic vials.

^{232}Th:CaF$_2$ Melt	
Material	^{232}Th:CaF$_2$ melt
Doping	$\sim 600 \left(\dfrac{\text{mg}}{\text{kg}} \right)$ Th
Manufacturer	Institut für Kristallzüchtung Berlin IKZ
Mass	20.8233 g
Measurement Geometry	Std A 15 ml Sand

Table 3.1.: Sample ^{232}Th:CaF$_2$ Melt

^{232}Th:CaF$_2$	
Material	^{232}Th:CaF$_2$
Doping	$\sim 200 \left(\dfrac{\text{mg}}{\text{kg}} \right)$ Th
Mechanism of crystal growth	Czochralski technique
Manufacturer	Institut für Kristallzüchtung Berlin IKZ
Preparation	cut and polished at Institute for Atomic and Subatomic Physics in Vienna
Mass	21.4012 g
Measurement Geometry	Std A 15 ml Sand

Table 3.2.: Sample ^{232}Th:CaF$_2$

ThF$_4$	
Material	ThF$_4$ powder
Certificate of Analysis	Buchem bv, Minden 60, 7327 AW Abeldoom, the Netherlands
Molecular Weight	308.03 g/mol
Mass	0.2701 g
Measurement Geometry	Std D 1 ml Sand

Table 3.3.: Sample ThF$_4$

3.2.2. Samples for Neutron Activation Analysis

The geometry of all samples is "Std D 1 ml Sand" because they have to be easily compareable.

CFA	
Material	coal fly ash (standard reference material 1633b) powder
Certificate of Analysis	National Institute of Standards & Technology, Department of Commerce, United States of America, 1993
Mass	0.10037 g
Certified Value of ^{232}Th	25.7 $\frac{mg}{kg}$ $\pm$ 1.3 $\frac{mg}{kg}$

Table 3.4.: Certified reference material CFA

SO1	
Material	soil powder
Certificate of Analysis	CANADIAN CERTIFIED REFERENCE MATERIAL PROJEKT, Canada Centre for Mineral and Energy Technology 555 Booth St., Ottawa, Ontario K1A 0G1
Mass	$0.08011\,g$
Certified Value of ^{232}Th	$12.4\,ppm$

Table 3.5.: Certified reference material SO1

GBW	
Material	rock powder
Certificate of Analysis	Institute of Rock and Mineral Analysis, Ministry of Geology and Minerals Ressources, Beijing, China, 1993
Mass	$0.07973\,g$

Table 3.6.: Certified reference material GBW

ThO$_2$	
Material	ThO$_2$ powder
Molecular Weight	$264.04\,u$ ($87.88\,\%$ Th, $12.12\,\%$ O)
Mass	$0.00144\,g$

Table 3.7.: Reference material ThO$_2$

ThF$_4$	
Material	ThF$_4$ powder
Certificate of Analysis	Buchem bv, Minden 60, 7327 AW Abeldoom, the Netherlands
Molecular Weight	308.03 g/mol
Mass	0.00598 g

Table 3.8.: Reference material ThF$_4$

^{232}Th:CaF$_2$ Melt 1	
Material	crushed ^{232}Th:CaF$_2$ melt
Doping	$\sim 600 \left(\dfrac{\text{mg}}{\text{kg}} \right)$ Th
Manufacturer	Institut für Kristallzüchtung Berlin IKZ
Mass	0.04368 g

Table 3.9.: Sample ^{232}Th:CaF$_2$ Melt 1

^{232}Th:CaF$_2$ Melt 2	
Material	crushed ^{232}Th:CaF$_2$ Melt
Doping	$\sim 600 \left(\dfrac{\text{mg}}{\text{kg}} \right)$ Th
Manufacturer	Institut für Kristallzüchtung Berlin IKZ
Mass	0.02450 g

Table 3.10.: Sample ^{232}Th:CaF$_2$ Melt 2

^{232}**Th:CaF$_2$ Melt 3**	
Material	crushed ^{232}Th:CaF$_2$ Melt
Doping	$\sim 600 \left(\dfrac{\text{mg}}{\text{kg}}\right)$ Th
Manufacturer	Institut für Kristallzüchtung Berlin IKZ
Mass	$0.04367\,\text{g}$

Table 3.11.: Sample ^{232}Th:CaF$_2$ Melt 3

^{232}**Th:CaF$_2$ 1**	
Material	crushed ^{232}Th:CaF$_2$
Doping	$\sim 200 \left(\dfrac{\text{mg}}{\text{kg}}\right)$ Th
Mechanism of crystal growth	Czochralski technique
Manufacturer	Institut für Kristallzüchtung Berlin IKZ
Mass	$0.02753\,\text{g}$

Table 3.12.: Sample ^{232}Th:CaF$_2$ 1

^{232}**Th:CaF$_2$ 2**	
Material	crushed ^{232}Th:CaF$_2$
Doping	$\sim 200 \left(\dfrac{\text{mg}}{\text{kg}}\right)$ Th
Mechanism of crystal growth	Czochralski technique
Manufacturer	Institut für Kristallzüchtung Berlin IKZ
Mass	$0.05483\,\text{g}$

Table 3.13.: Sample ^{232}Th:CaF$_2$ 2

^{232}Th:CaF$_2$ 3	
Material	crushed ^{232}Th:CaF$_2$
Doping	$\sim 200 \left(\dfrac{\text{mg}}{\text{kg}} \right)$ Th
Mechanism of crystal growth	Czochralski technique
Manufacturer	Institut für Kristallzüchtung Berlin IKZ
Mass	$0.04307\,\text{g}$

Table 3.14.: Sample ^{232}Th:CaF$_2$ 3

ThO$_2$ + Vit C	
Material	ThO$_2$ powder in liquid Vit C
Molecular Weight	$264.04\,\text{u}$ ($87.88\,\%$ Th, $12.12\,\%$ O
Mass	$0.00744\,\text{g}$

Table 3.15.: Reference material ThO$_2$ + Vit C

3.2.3. Samples for AFM

^{232}Th:CaF$_2$ Melt	
Material	^{232}Th:CaF$_2$ melt
Doping	$\sim 600 \left(\dfrac{\text{mg}}{\text{kg}} \right)$ Th
Manufacturer	Institut für Kristallzüchtung Berlin IKZ
Preparation	cut and polished at Institute for Atomic and Subatomic Physics in Vienna

Table 3.16.: Sample ^{232}Th:CaF$_2$ Melt

^{232}Th:CaF$_2$	
Material	^{232}Th:CaF$_2$
Doping	$\sim 200 \left(\dfrac{\text{mg}}{\text{kg}} \right)$ Th
Mechanism of crystal growth	Czochralski technique
Manufacturer	Institut für Kristallzüchtung Berlin IKZ
Preparation	cut and polished at Institute for Atomic and Subatomic Physics in Vienna

Table 3.17.: Sample ^{232}Th:CaF$_2$

CaF$_2$ sample "Hellma disc"	
Material	CaF$_2$
Mechanism of crystal growth	Bridgman-Stockbarger technique
Manufacturer	Hellma Materials[4]
Preparation	Hellma Materials

Table 3.18.: CaF$_2$ sample "Hellma disc"

3.2.4. Samples for Transmittance and Luminescence Measurements

The samples for transmittance and luminescence measurements are either cleaved or cut and polished. The figures in this subsection show the samples sticked on a fixture, which is needed for the measurement setup in section 4.3.

---

[4]http://www.hellma-materials.com
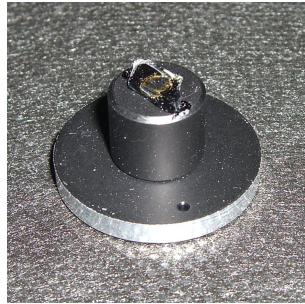
Figure 3.6.: CaF$_2$ sample "Small Chip"
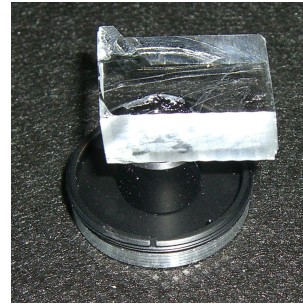
Figure 3.7.: CaF$_2$ sample "Big Boy"

CaF$_2$ sample "Small Chip"	
Material	CaF$_2$
Mechanism of crystal growth	Bridgman-Stockbarger technique
Manufacturer	Fraunhofer Institute for Integrated Systems and Device Technology IISB[5]
Preparation	Cleaved at the Institute for Applied Physics of the Vienna University of Technology
Thickness (optical path)	1.24 mm

Table 3.19.: CaF$_2$ sample "Small Chip"

---

[5]http://www.iisb.fraunhofer.de

CaF$_2$ sample "Big Boy"	
Material	CaF$_2$
Mechanism of crystal growth	Bridgman-Stockbarger technique
Manufacturer	Fraunhofer Institute for Integrated Systems and Device Technology IISB
Preparation	Cleaved at the Institute for Applied Physics of the Vienna University of Technology
Thickness (optical path)	6.28 mm

Table 3.20.: CaF$_2$ sample "Big Boy"

Figure 3.8.: Sample ^{232}Th:CaF$_2$

Figure 3.9.: CaF$_2$ sample "Hellma disc"

^{232}Th:CaF$_2$	
Material	^{232}Th:CaF$_2$
Doping	$\sim 200 \left(\dfrac{\text{mg}}{\text{kg}} \right)$ Th
Mechanism of crystal growth	Czochralski technique
Manufacturer	Institut für Kristallzüchtung Berlin IKZ
Preparation	cut and polished at Institute for Atomic and Subatomic Physics in Vienna
Thickness (optical path)	8.14 mm

Table 3.21.: Sample ^{232}Th:CaF$_2$

CaF$_2$ sample "Hellma disc"	
Material	CaF$_2$
Mechanism of crystal growth	Bridgman-Stockbarger technique
Manufacturer	Hellma Materials[6]
Preparation	Hellma Materials
Thickness (optical path)	10.3 mm

Table 3.22.: CaF$_2$ sample "Hellma disc"

---

[6]http://www.hellma-materials.com

Figure 3.10.: Sample YLF

Figure 3.11.: Sample LiF

YLF	
Material	$LiYF_4$
Mechanism of crystal growth	Czochralski technique
Manufacturer	Dipartimento di Fisica "E. Fermi", Universita' di Pisa
Preparation	cut and polished at Dipartimento di Fisica "E. Fermi", Universita' di Pisa
Thickness (optical path)	1.70 mm

Table 3.23.: Sample YLF

LiF	
Material	LiF
Mechanism of crystal growth	Czochralski technique
Manufacturer	Dipartimento di Fisica "E. Fermi", Universita' di Pisa
Preparation	cut and polished at Dipartimento di Fisica "E. Fermi", Universita' di Pisa
Thickness (optical path)	3.78 mm

Table 3.24.: Sample LiF
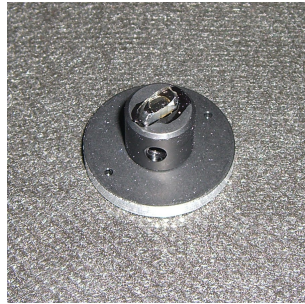
Figure 3.12.: Sample Nd:LiLuF$_4$
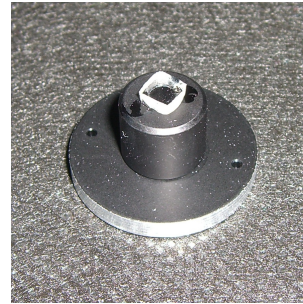
Figure 3.13.: Sample LiCaAlF$_6$

Nd:LiLuF$_4$	
Material	Nd:LiLuF$_4$
Doping	30 ppm Nd
Mechanism of crystal growth	Czochralski technique
Manufacturer	Dipartimento di Fisica "E. Fermi", Universita' di Pisa
Preparation	cut and polished at Dipartimento di Fisica "E. Fermi", Universita' di Pisa
Thickness (optical path)	2.41 mm

Table 3.25.: Sample Nd:LiLuF$_4$

LiCaAlF$_6$	
Material	LiCaAlF$_6$
Mechanism of crystal growth	Czochralski technique
Manufacturer	Dipartimento di Fisica "E. Fermi", Universita' di Pisa
Preparation	cut and polished at Dipartimento di Fisica "E. Fermi", Universita' di Pisa
Thickness (optical path)	1.88 mm

Table 3.26.: Sample LiCaAlF$_6$

4. Sample Characterization

This chapter is a summary of the specific calibrations of the characterization methods described in chapter 2. Furthermore the results of the radiological and optical characterization as well as surface measurements, especially for CaF_2 crystals, ^{232}Th:CaF_2 crystals and their melt, and their discussion are presented in this chapter.

4.1. Radiological Characterization

In this section, the investigation of possible unwanted impurities in ^{232}Th:CaF_2 crystals and their melt and the measurement of the quantitative concentration of ^{232}Th are presented and discussed.

4.1.1. Radiological Characterization: Gamma Spectroscopy

As described in section 2.1.1, gamma spectroscopy is useful to determine which radionuclides occur in a sample as long as they emit gamma radiation. The measurements were performed with a germanium semiconductor detector, a 151 cm^3 [1] (1.77 keV resolution at the 1332 keV ^{60}Co peak; 33 % relative efficiency), connected to a PC-based multi-channel analyzer with preloaded filter and loss-free counting system. The samples used for the gamma spectroscopy are described in subsection 3.2.1.

For analyzing the gamma spectroscopy measurements the efficiency of the gamma detector had to be callibrated. The efficiency depends on the geometry of the sample and material properties of the detector. For example the gamma spectrometer detects gamma rays with very high and very low energy less efficiently. Those with

---

[1] Ortec(TM) HPGe-gamma-detector

very low energy are absorbed in the detector cladding and those with very high energy pass through the detector without being detected.

The efficiency was measured with a calibration solution. The calibration solution is a liquid of known composition and certified gamma spectrum at a reference time. After the measurement of the solution the measured count rates of the peaks can be compared with the count rate they should have according to the certificate, taking into account a decay correction.

The efficiency curve was recorded with the calibration solution from GE Healthcare Limited, Radiation & Radioactivity, Calibration Laboratory, The Grove Centre[2]. It consists of ten radionuclides in a solution in 4M HCl. Their certified gamma ray energies $E_{\gamma C}$ and certified gamma ray count rates $CR_{\gamma C}$ are listed in table 4.1 (Product code: QCY48). The reference time for the certificate is 12:00 GMT on April, 1st 2011. The mass of the solution is 5.3928 g.

For the gamma spectroscopy measurements in this thesis two efficiency curves are relevant. One for the 1 ml and one for the 15 ml sample geometry. For the geometry with a volume of 1 ml, 0.10526 g of QCY48 solution were weighted. This geometry was used for the ThF_4 sample. For the geometry with a volume of 15 ml, 0.10595 g QCY48 solution were weighted. This geometry was used for the samples ThO_2:CaF_2 crystal and melt. Table 4.2 and table 4.3 list the decay-corrected certified gamma ray count rate $CR_{\gamma C}$ per gram. Equation 4.1 shows the decay correction.

The gamma count rate $CR_{\gamma M}$ was measured on the date indicated in the table. The efficiency is the measured gamma count rate divided by the time-corrected certified gamma ray count rate per 0.10526 g (August 25th 2011) or the certified gamma ray count rate per 0.10595 g (September 16th 2011) respectively in %. With a curve fitting tool the measurement points were fitted (see figures 4.1 and 4.2).

After recording the efficiency curve, the gamma spectra of the samples ^{232}Th:CaF_2 melt and crystal and ThF_4 could be analyzed. The measurement tables are in appendix A.2. The measurement time for the ^{232}Th:CaF_2 was 267033 s ($\sim$3 d), for the ^{232}Th:CaF_2 Melt 86380 s ($\sim$1 d) and for the ThF_4 215117 s ($\sim$2 d).

---

[2]GE Healthcare Limited, United Kingdom Accreditation Service: http://www.ukas.org/

Parent radionuclide	$E_{\gamma C}$ (keV)	$CR_{\gamma C}$ per g (γ-rays per gram)	Combined Type A uncertainty	Combined Type B uncertainty	Expanded uncertainty
Americium-241	59.54	1132	± 0.1 %	± 0.8 %	± 1.5 %
Cadmium-109	88.03	629	± 0.3 %	± 2.9 %	± 5.8 %
Cobalt-57	122.10	532	± 0.1 %	± 0.7 %	± 1.4 %
Cerium-139	165.90	690	± 0.1 %	± 0.8 %	± 1.6 %
Mercury-203	279.20	1943	± 0.2 %	± 0.8 %	± 1.6 %
Tin-113	391.70	2111	± 0.1 %	± 2.0 %	± 4.0 %
Strontium-85	514.00	3965	± 0.2 %	± 0.7 %	± 1.4 %
Caesium-137	661,70	2394	± 0.1 %	± 0.8 %	± 1.6 %
Yttrium-88	898.00	6182	± 0.1 %	± 0.9 %	± 1.7 %
Cobalt-60	1173.00	3397	± 0.1 %	± 0.8 %	± 1.5 %
Cobalt-60	1332.00	3402	± 0.1 %	± 0.8 %	± 1.5 %
Yttrium-88	1836.00	6539	± 0.1 %	± 0.8 %	± 1.6 %

Table 4.1.: Calibration solution April, 1st 2011

Radionuclide	$E_{\gamma C}$ (keV)	$CR_{\gamma C}$ per g (γ-rays per g)	$CR_{\gamma C}$ per 0.10526 g (γ-rays per g)	$CR_{\gamma M}$ (cps)	Efficiency (%)
Americium-241	59.54	1131,2734	119.0778	2.016	1.6930
Cadmium-109	88.03	505.3148	53.1894	2.646	4.9747
Cobalt-57	122.10	366.4933	38.5771	2.557	6.6283
Cerium-139	165.90	330.4979	34.7882	2.236	6.4275
Mercury-203	279.20	220.9640	23.2587	1059	4.5531
Tin-113	391.70	875.6209	92.1679	3.186	3.4567
Strontium-85	514.00	832.6488	87.6446	2.397	2.7349
Caesium-137	661,70	2372.0815	249.6853	5.616	2.2492
Yttrium-88	898.00	2390.4712	251.6210	4.116	1.6358
Cobalt-60	1173.00	3222.8202	339.2341	4.449	1.3115
Cobalt-60	1332.00	3227.5639	339.7334	3.970	1.1686
Yttrium-88	1836.00	2528.5168	266.1517	2.392	0.8987

Table 4.2.: Efficiency curve August 25th, 2011 Std D 1 ml
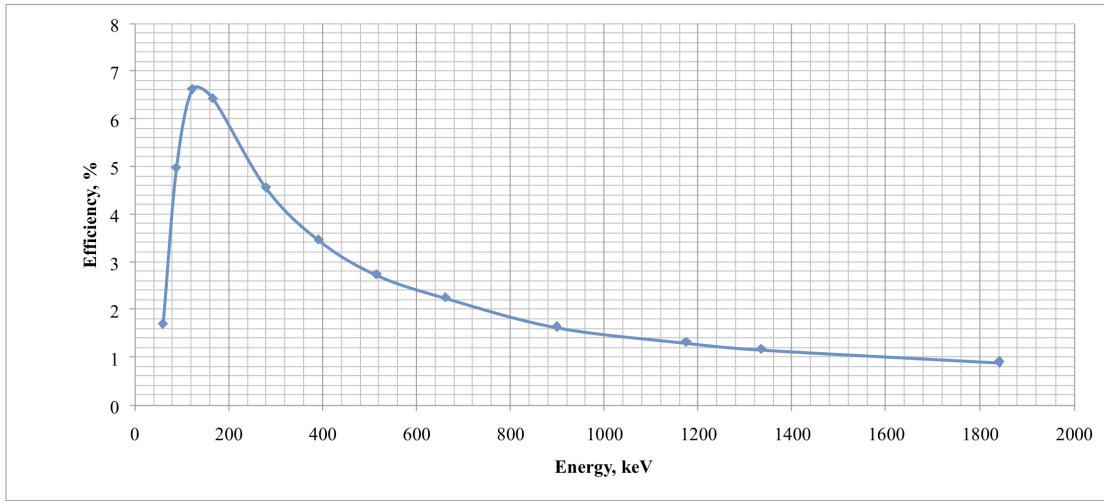
Figure 4.1.: Efficiency curve August 25th, 2011 Std D 1 ml

Radionuclide	$E_{\gamma C}$ (keV)	$CR_{\gamma C}$ per g (γ-rays per g)	$CR_{\gamma C}$ per 0.10595 g (γ-rays per g)	$CR_{\gamma M}$ (cps)	Efficiency (%)
Americium-241	59.54	1131.1604	119.8464	1.790	1.4936
Cadmium-109	88.03	488.3799	51.7438	2.521	4.8721
Cobalt-57	122.10	345.8347	36.6412	2.387	6.5145
Cerium-139	165.90	294.7123	31.2248	2.029	6.4980
Mercury-203	279.20	157.5172	16.6889	0.787	4.7139
Tin-113	391.70	763.5127	80.8941	2.803	3.4650
Strontium-85	514.00	653.0389	69.1895	1.943	2.8082
Caesium-137	661,70	2368.6872	250.9624	5.778	2.3023
Yttrium-88	898.00	2061.7657	218.4441	3.635	1.6640
Cobalt-60	1173.00	3196.5178	338.6711	4.471	1.3202
Cobalt-60	1332.00	3201.2227	339.1695	4.069	1.1997
Yttrium-88	1836.00	2180.8292	231.0588	2.150	0.9305

Table 4.3.: Efficiency curve September 16th, 2011 Std A 15 ml
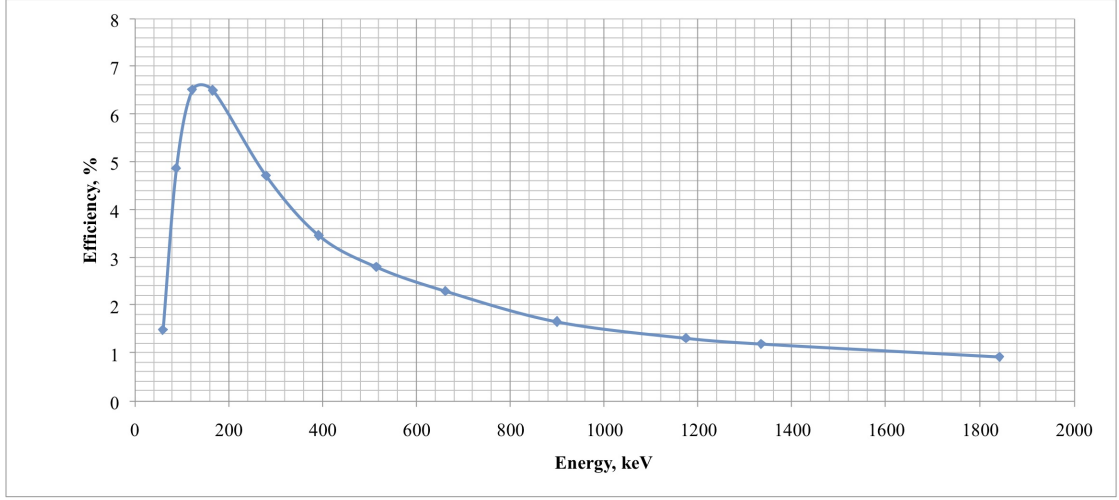
Figure 4.2.: Efficiency curve September 16th, 2011 Std D 15 ml

For better understanding of the following tables and calculations the decay chain of the radioactive nuclide ^{232}Th is needed (see figure 4.3). Beside the expected nuclides as argued in section 2.1.1 I expected all decay products of ^{232}Th to appear in gamma spectroscopy.

For calculating the activity of the samples, those peaks with the highest count rate and smallest error were analyzed. After the correction with the efficiency curve and a comparison of the energy values with the National Nuclear Data Center, Brookhaven National Laboratory [5], we could conclude which nuclides cause which peaks. It should be noted that the relative measured count rates of the different peaks of the same nuclide must be consistent with relativ intensities I_γ of the different peaks of the same nuclide.

In the tables 4.4, 4.5 all relevant values for calculating the activity A of the ^{232}Th:CaF$_2$ crystal and the ^{232}Th:CaF$_2$ melt are listed. To get the value of the activity, the measured gamma count rate corrected with the efficiency curve $CR_{\gamma E}$ must be divided by the intensity I_γ.

Table 4.7 is a comparison of the peaks with the highest count rate. The gamma ray energy E_γ and the intensity I_γ in this table is according to the National Nuclear Data Center, Brookhaven National Laboratory [5].

The ratio between the activity of the melt and the crystal is ∼3.4 for ^{208}Tl, ^{212}Pb and ^{224}Ra. The exception is ^{228}Ac. Here the ratio is ∼15.1. The difference
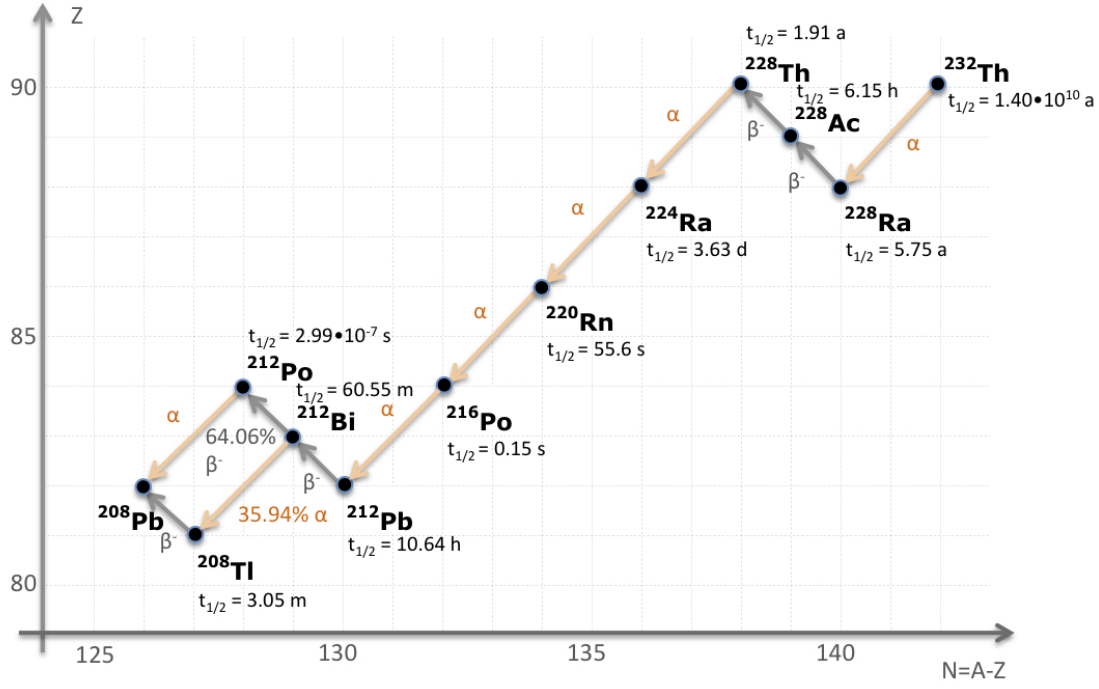
Figure 4.3.: Decay chain of ^{232}Th [5]

$E_{\gamma M}$ (keV)	$CR_{\gamma M}$ (cps)	Error (%)	Radio- nuclide	I_γ (%)	Efficiency (%)	$CR_{\gamma E}$ (cps)	A (Bq)
238.37	$3.66 \cdot 10^{-1}$	0.34	^{212}Pb	43.6	5.4534	6.71	15
240.75	$3.40 \cdot 10^{-2}$	1.37	^{224}Ra	4.1	5.4038	$6.29 \cdot 10^{-1}$	15
299.84	$2.08 \cdot 10^{-2}$	1.98	^{212}Pb	3.3	4.4465	$4.69 \cdot 10^{-1}$	14
337.96	$2.01 \cdot 10^{-2}$	1.94	^{228}Ac	11.3	3.9798	$5.05 \cdot 10^{-1}$	4.5
462.59	$5.70 \cdot 10^{-3}$	1.94	^{228}Ac	4.4	3.0405	$1.87 \cdot 10^{-1}$	4.3
582.68	$1.07 \cdot 10^{-1}$	0.62	^{208}Tl	85.0	2.5509	4.19	4.9
910.57	$2.22 \cdot 10^{-2}$	1.43	^{228}Ac	25.8	1.6427	1.35	5.2
968.35	$1.28 \cdot 10^{-2}$	1.97	^{228}Ac	15.8	1.5531	$8.25 \cdot 10^{-1}$	5.2

Table 4.4.: Activity of CaF$_2$ doped with ^{232}Th

$E_{\gamma M}$ (keV)	$CR_{\gamma M}$ (cps)	Error (%)	Radio-nuclide	I_γ (%)	Efficiency (%)	$CR_{\gamma E}$ (cps)	A (Bq)
238.37	1.24	0.32	^{212}Pb	43.6	5.4534	$2.27 \cdot 10^1$	52
240.74	$1.18 \cdot 10^{-1}$	1.24	^{224}Ra	4.1	5.4040	2.19	53
299.82	$7.04 \cdot 10^{-2}$	1.76	^{212}Pb	3.3	4.4468	1.58	48
337.99	$3.18 \cdot 10^{-1}$	0.67	^{228}Ac	11.3	3.9794	7.99	71
462.57	$8.87 \cdot 10^{-2}$	1.36	^{228}Ac	4.4	3.0406	2.92	66
582.69	$3.59 \cdot 10^{-1}$	0.60	^{208}Tl	85.0	2.5509	$1.41 \cdot 10^1$	16
910.56	$3.36 \cdot 10^{-1}$	0.60	^{228}Ac	25.8	1.6427	$2.05 \cdot 10^1$	79
968.33	$2.00 \cdot 10^{-1}$	0.78	^{228}Ac	15.8	1.5532	$1.29 \cdot 10^1$	13

Table 4.5.: Activity of CaF$_2$ doped with ^{232}Th melt

$E_{\gamma M}$ (keV)	$CR_{\gamma M}$ (cps)	Error (%)	Radio-nuclide	I_γ (%)	Efficiency (%)	$CR_{\gamma E}$ (cps)	A (Bq)
238.36	$1.687 \cdot 10^1$	0.05	^{212}Pb	43.6	5.2506	3.213	737
240.72	1.585	0.20	^{224}Ra	4.1	5.2035	3.046	743
299.82	1.034	0.28	^{212}Pb	3.3	4.3103	2.399	727
337.98	3.501	0.13	^{228}Ac	11.3	3.9118	8.950	794
462.57	1.022	0.25	^{228}Ac	4.4	2.9917	3.416	776
582.69	5.570	0.09	^{208}Tl	85.0	2.4836	2.243	264
910.56	3.825	0.11	^{228}Ac	25.8	1.6157	2.367	918
968.35	2.232	0.25	^{228}Ac	15.8	1.5327	1.456	922

Table 4.6.: Activity of ThF$_4$

Nuclide	E_γ (keV)	$A_{Th:CaF_2}$ (Bq)	A_{melt} (Bq)
^{208}Tl	583.187	4.9	17
^{212}Pb	238.632	15	52
^{228}Ac	911.204	5.2	79
^{224}Ra	240.986	15	53

Table 4.7.: Activity comparison of ^{232}Th:CaF$_2$ crystal and melt

between ^{228}Ac and the other nuclides in table 4.7 is that it is the parent nuclide of ^{228}Th and the other are daughter nuclides (see figure 4.3).

This behavior could be an indication of different ages of the ^{232}Th:CaF$_2$ crystal and the melt. However according to the information of IKZ Berlin this is not the case, the crystal has been grown from this melt. Hence they have nearly the same age. Nevertheless the measurement indicates that equilibrium in the decay chain is not achieved. Possibly, different isotopes are implanted into the crystal with a different probability (e.g. due to ionic radii). The composition of the crystal an the melt can therefore not be determined quantitatively using gamma spectroscopy, because it changes until equilibrium is reached. In the next subsection 4.1.2 we will show that this difficulty could be overcome using neutron activation analysis. The gamma spectroscopy is useful to see, if there is unexpected radiation. A disadvantage is that samples with unknown composition are very hard to analyze. Every energy peak in the spectrum must be compared to a nuclide database. All count rates must be corrected with the efficiency curve and the relative count rates of different peaks of the same nuclide must be consistent.

In the present case no unexpected nuclides could be found, e.g. to identify unwanted impurities. The energy value 1460.822 keV, which is a peak caused by background ^{40}K, could be measured. Every other peak, which is not caused by a decay product of ^{232}Th was expected as described in section 2.1.1.

4.1.2. Neutron Activation Analysis

According to subsection 2.1.2 and equation 2.9 the focus in this subsection is to measure the ^{232}Th concentration of the ^{232}Th:CaF$_2$ crystal and their melt. In addition we wanted to detect unexpected and non-radiating impurities.

For detecting non-radiating unexpected impurities, multi-element standards are needed. For this reason the certified reference materials CFA (coal fly ash), SO1(soil) and GBW (rocks) were activated togehter with the samples. For calculating the ^{232}Th concentration ThO$_2$ and ThF$_4$ are suitable because of their both high and precisely known Th-concentration. The samples "^{232}Th:CaF$_2$ Melt 1", "^{232}Th:CaF$_2$ Melt 2" and "^{232}Th:CaF$_2$ Melt 3" are pieces of a crushed ^{232}Th:CaF$_2$

4. Sample Characterization

Nr.	Sample	m (mg)
1	CFA	100.37 ± 0.01
2	SO1	80.11 ± 0.01
3	GBW	79.73 ± 0.01
4	ThO_2	1.44 ± 0.01
5	ThF_4	5.98 ± 0.01
6	Melt 1	43.68 ± 0.01
7	Melt 2	24.50 ± 0.01
8	Melt 3	43.67 ± 0.01
9	$^{232}Th:CaF_2$ 1	27.53 ± 0.01
10	$^{232}Th:CaF_2$ 2	54.83 ± 0.01
11	$^{232}Th:CaF_2$ 3	43.07 ± 0.01
12	ThO_2 + Vit C	7.44 ± 0.01

Table 4.8.: Table of masses

melt and the samples "$^{232}Th:CaF_2$ 1", "$^{232}Th:CaF_2$ 2" and "$^{232}Th:CaF_2$ 3" are pieces of a crushed $^{232}Th:CaF_2$ crystal. The specification of all used samples and reference materials can be found in subsection 3.2.2. The mass m of the samples and the reference materials are listed in table 4.8.

The neutron activation took place in the research reactor TRIGA Mark II Vienna with a neutron flux density of $3 \cdot 10^{12} \, cm^{-2}s^{-1}$. The activation date was the November, 16th 2011, the activation duration was three hours and the activation was finished at 4 p.m. on the same day. During activation, ^{232}Th activates to ^{233}Th. After a cooldown of $1288800 \, s$ (nearly two weeks), the samples were measured in the gamma spectrometer sequentially. The analysis was performed with a $222 \, cm^3$ Canberra(TM) HPGe-gamma-detector ($1.78 \, keV$ resolution at the $1332 \, keV$ ^{60}Co peak; $48.2 \, \%$ relative efficiency), connected to a PC-based multi-channel analyzer with preloaded filter and loss-free counting system. Each sample was measured for $20000 \, s$. The first measurement started on December, 1st 2011 at 2 p.m. Because of the short half-life $t_{\frac{1}{2}}$ of ^{233}Th (21.83 minutes), only the decay product ^{233}Pa ($t_{\frac{1}{2}}=27$ days) was detected after the two-week cooldown. The activity of ^{233}Pa is proportional to the mass of ^{232}Th in the activated samples and the reference materials.

A decay correction had to be applied, because the samples are measured with the

Nr.	Sample	t (s)	f_{cor}
1	CFA	0	1.0000
2	SO1	20000	0.9941
3	GBW	40000	0.9882
4	ThO_2	60000	0.9823
5	ThF_4	80000	0.9765
6	Melt 1	100000	0.9707
7	Melt 2	120000	0.9649
8	Melt 3	140000	0.9592
9	^{232}Th:CaF$_2$ 1	160000	0.9535
10	^{232}Th:CaF$_2$ 2	180000	0.9479
11	^{232}Th:CaF$_2$ 3	200000	0.9423
12	ThO_2 + Vit C	220000	0.9367

Table 4.9.: Decay correction factor

gamma spectrometer sequentially. With the measured gamma count rate $CR_{\gamma M}$, which is the count rate at the time t after starting gamma spectroscopy and the decay constant λ, the gamma count rate at time 0 $CR_{\gamma 0}$ after starting gamma spectroscopy can be calculated

$$CR_{\gamma M} = CR_{\gamma 0} \cdot e^{-\lambda \cdot t}. \tag{4.1}$$

The decay constant λ is connected to the half-life $t_{\frac{1}{2}}$ of ^{233}Pa

$$\lambda = \frac{ln(2)}{t_{\frac{1}{2}}}. \tag{4.2}$$

With the decay correction factor $f_{cor} = e^{-\lambda \cdot t}$, which is nothing else but the exponential factor in equation 4.1, $CR_{\gamma 0}$ can be calculated. The results are listed in table 4.9.

For the neutron activation analysis, peaks with a high count rate emerging in a gamma spectrometer range with good detection efficiency are interesting. The count rates of the ^{233}Pa peak at 311.904 keV with the highest intensity 38.5 % [5] were analyzed. With the measured gamma count rates (see appendix A.3) the decay corrected peaks (gamma count rate at time 0) were calculated and are listed

4. Sample Characterization

Nr.	Sample	$CR_{\gamma 0}$ (cps)	Error (%)
1	CFA	$9.2 \cdot 10^{-1}$	2.14
2	SO1	$3.39 \cdot 10^{-1}$	1.31
3	GBW	$7.39 \cdot 10^{-1}$	0.79
4	ThO_2	$4.367 \cdot 10^{2}$	0.06
5	ThF_4	$1.3805 \cdot 10^{3}$	0.04
6	Melt 1	8.68	0.34
7	Melt 2	8.74	0.34
8	Melt 3	9.09	0.22
9	^{232}Th:CaF_2 1	2.08	0.72
10	^{232}Th:CaF_2 2	3.97	0.33
11	^{232}Th:CaF_2 3	3.27	0.60
12	ThO_2 + Vit C	$2.1854 \cdot 10^{3}$	0.03

Table 4.10.: Count rates of ^{233}Pa peak at 311.904 keV - decay corrected

Nr.	Sample	m_{Th} (mg)
5	ThF_4	4.13 ± 0.03
6	Melt 1	$(2.60 \pm 0.02) \cdot 10^{-2}$
7	Melt 2	$(2.53 \pm 0.02) \cdot 10^{-2}$
8	Melt 3	$(2.64 \pm 0.2) \cdot 10^{-2}$
9	^{232}Th:CaF_2 1	$(6.02 \pm 0.07) \cdot 10^{-3}$
10	^{232}Th:CaF_2 2	$(1.15 \pm 0.010) \cdot 10^{-2}$
11	^{232}Th:CaF_2 3	$(9.48 \pm 0.10) \cdot 10^{-3}$

Table 4.11.: Mass of ^{232}Th, calculated by using the 311.904 keV γ-peak

in table 4.10. We chose ThO_2 + Vit C as reference material because of the very small error of the peak at 311.904 keV (see table 4.10). As mentioned before, the ^{232}Th concentration in ThO_2 is very high, so that the error is minimized. After dividing $CR_{\gamma 0}$ of the samples by $CR_{\gamma 0}$ of the reference material and multiplying with the Th mass of the reference materials (see equation 2.9) we get the mass of ^{232}Th in the sample. It should be noted, that the fraction of count rates equals the fraction of activities. In table 4.11 the arithmetic mean and the standard deviation (calculated with error prapagation) of the mass of ^{232}Th m_{Th} are listed.

The mass fraction $q_m = \dfrac{m_{Th}}{m}$ can be calculated with the values of table 4.11 and table 4.8. Additionaly the number of particles per volume $n_{Th} = \dfrac{N_{Th}}{N_{CaF_2}} \cdot n_V$ can

Nr.	Sample	$q_m \left(\dfrac{\text{mg}}{\text{kg}} \right)$	n_{Th} $(10^{18}\,\text{cm}^{-3})$
6	Melt 1	595 ± 5	4.91 ± 0.04
8	Melt 3	603 ± 5	4.89 ± 0.04
9	^{232}Th:CaF$_2$ 1	219 ± 2	1.80 ± 0.02
10	^{232}Th:CaF$_2$ 2	210 ± 2	1.73 ± 0.01
11	^{232}Th:CaF$_2$ 3	220 ± 2	1.82 ± 0.02

Table 4.12.: ^{232}Th mass fraction and n_{Th} at $311.904\,\text{keV}$

be calculated. The number of ^{232}Th particles N_{Th}, the number of CaF$_2$ particles N_{CaF_2} and the number of particles per volume n_V can be calculated with atomic mass of ^{232}Th and CaF$_2$ and the density of the CaF$_2$ crystal and melt $\rho{=}3.18\,\dfrac{\text{g}}{\text{cm}^3}$. q_m for ThF$_4$ should be $75.33\,\%$ but it is $67.89\,\%$ at $311.904\,\text{keV}$. The fact that it deviates so strongly suggests a non-stoichiometric composition.

It was suspected, that the value for melt 2 is wrong. We figured out that the count rate values in the data file of melt 2 equal the count rate values in the data file of melt 1, which is improbable. Both data files have even the same time stamp. We have not figured out why this error happend, but the measuring data file of melt 2 contains obviously not the data for sample melt 2.

The results for q_m and the number of ^{232}Th particles per volume of matter at $311.904\,\text{keV}$ except those for ThF$_4$ and melt 2 are listed in table 4.12.

The activation products of the decay products of ^{232}Th are too short-lived to be detected. Lanthanides like Cerium and Europium, which could be possible unexpected impurities, as well as other impurities could not be identified. The results for the numbers of particles match with the mass spectrometry data we got from IKZ Berlin. The maximum deviation of the mass fraction of the ^{232}Th:CaF$_2$ crystal in table 4.12 is an indicator for a rather homogenous doping of ^{232}Th.

4.2. Surface Analysis

This section is an overview on the surface analysis by atomic force microscopy. We then discuss how optical properties depend on the surface roughness of the

measured samples.

4.2.1. Atomic Force Microscopy

As mentioned in 2.2.1, an atomic force microscope (AFM) measures the height deviation of a tip caused by the roughness of the sample surface as a function of the tip position. In the present case the analysis was performed with a MFP-3D-BIO AFM, Asylum Research [21] at the Institut for Applied Physics of the Vienna University of Technology[3].

After fixing the sample in the sample holder, the AFM scaned three or four defined areas of the sample surface (square with a side length of 5 - 20 μm). The measured samples are a ^{232}Th:CaF$_2$ crystal and a ^{232}Th:CaF$_2$ melt. Both were polished at the Institute for Atomic and Subatomic Physics in Vienna (finest sandpaper grain 4000). For comparison, we measured a CaF$_2$ sample "Hellma Disc", with a surface prepared by Hellma-materials. The sample specifications can be found in subsection 3.2.3.

The accuracy of the measurement depends on the scan speed. The faster the scan, the less accurate the result. This is the reason why the values of the sample "Hellma Disc" are accurate to two decimal places and the other samples to one.

For surface analysis there are two types of parameters: profile roughness parameters and amplitude parameters. An amplitude parameter is the surface characterization based on the vertical deviation of the roughness profile from the mean line, for example minima or maxima of the deviation. Profile parameters are for example the arithmetic mean of the roughness amplitude or the root mean squared roughness amplitude. They give information about the surface profile. In table 4.13 both types of parameters are listed, the minimum, maximum, median, arithmetic mean and the root mean square roughness deviation.

In this diploma thesis only the root mean square surface deviation R_{rms}, which is a profile parameter, is used for surface characterization. The reason is that root mean square surface deviation R_{rms} is the most meaningful roughness parameter because it includes the arithmetic mean and the standard deviation of the amplitude. Beside that, it is often used in publication. This makes the comparison with
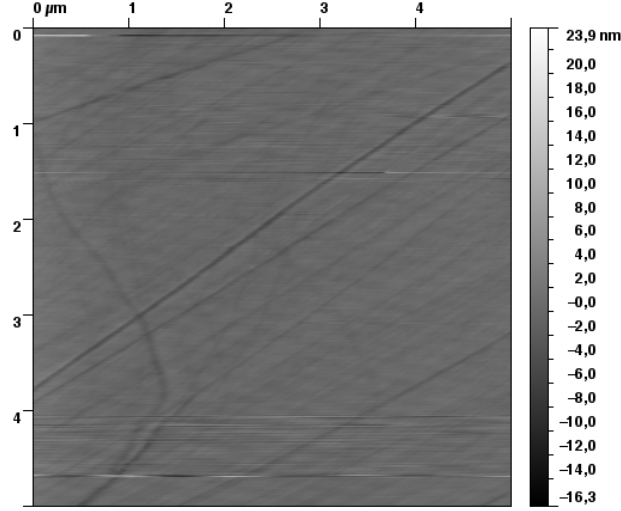
---

[3]http://www.iap.tuwien.ac.at/

Figure 4.4.: AFM image CaF_2 sample "Hellma Disc" (polished by Hellma-materials)

values from other measurements very easily.

The images that were taken with the AFM are shown in the figures 4.4, 4.5 and 4.6. According to [22] the surface of the sample "Hellma disc" is presumably prepared by a multi-step polishing protocol. The surface roughness of the polished CaF_2 sample "Hellma disc" is $R_{rms} \approx 1.3$ nm. The ^{232}Th:CaF_2 crystal, which was polished at the Institut for Atomic and Subatomic Physics in Vienna (sandpaper grain 4000) has a root mean square surface deviation that is one order of magnitude larger $R_{rms} \approx 12$ nm. For comparison (see figure 4.7(a)) the local roughness of a cleaved CaF_2 crystal is $R_{rms} \approx 0.3$ nm, which is even better than the polished CaF_2 sample "Hellma disc". The disadvantage are typical atomic steps after cleaving which can affect the transmittance performance (see figures 4.7(b) and 3.7).

Noting that the Hellma disc has the best transmittance performance and almost no luminescence (see section 4.3), it should be the aim to reach the roughness of the Hellma disc. This can only be achieved with a finer sandpaper than a grain 4000 or other polishing methods. Despite a small R_{rms}, the transmittance and luminescence performance of the cleaved CaF_2 crystal is undesirable.

(a)   (b)
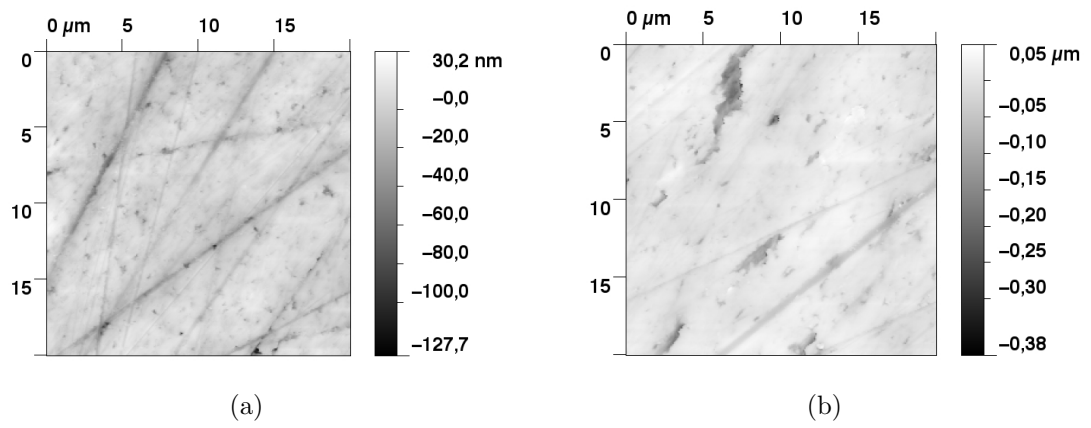
Figure 4.5.: AFM Images ^{232}Th:CaF$_2$ Melt (polished with sandpaper grain 4000)
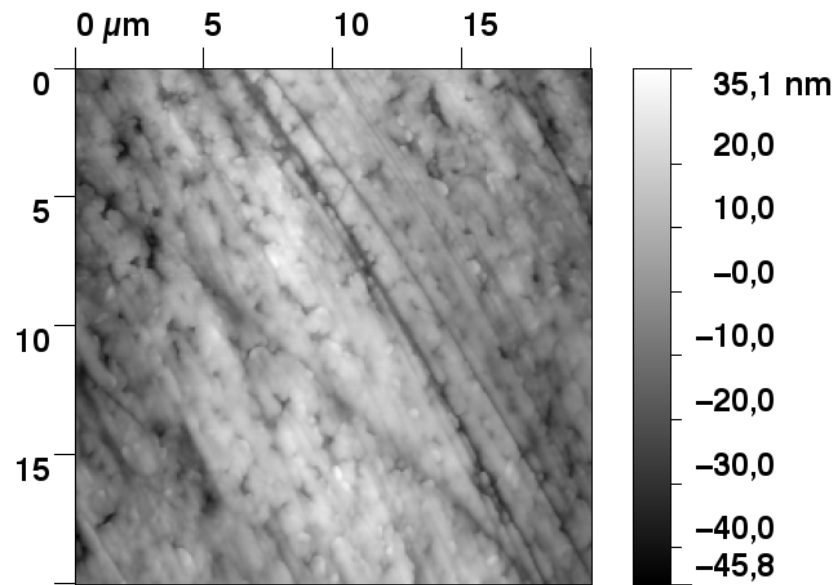
Figure 4.6.: AFM Image ^{232}Th:CaF$_2$ crystal (polished with sandpaper grain 4000)

	Min (nm)	Max (nm)	Median (nm)	R_a (nm)	R_{rms} (nm)
^{232}Th:CaF$_2$ area 1	-63.6	40.2	0.8	9.9	12.3
^{232}Th:CaF$_2$ area 2	-79.1	36.7	1.2	9.0	11.6
^{232}Th:CaF$_2$ area 3	-45.82	35.09	-0.04	10.02	12.09
^{232}Th:CaF$_2$ Melt area 1	-127.7	30.2	2.1	7.4	10.4
^{232}Th:CaF$_2$ Melt area 2	-377.7	50.4	4.6	15.8	25.6
^{232}Th:CaF$_2$ Melt area 3	-83.8	25.0	1.0	6.0	8.4
^{232}Th:CaF$_2$ Melt area 4	-91.9	25.7	0.7	4.6	6.5
Hellma disc area 1	-30.44	34.53	0.02	0.95	2.31
Hellma disc area 2	-6.73	3.72	0.00	0.35	0.46
Hellma disc area 3	-16.31	23.89	0.03	0.70	1.12

Table 4.13.: Surface roughness

(a) Cleaved surface of the CaF$_2$ crystal - roughness $R_{rms} \approx 0.3\,\mathrm{nm}$

(b) Typical atomic steps after cleaving CaF$_2$ crystals

Figure 4.7.: Cleaved CaF$_2$ crystal
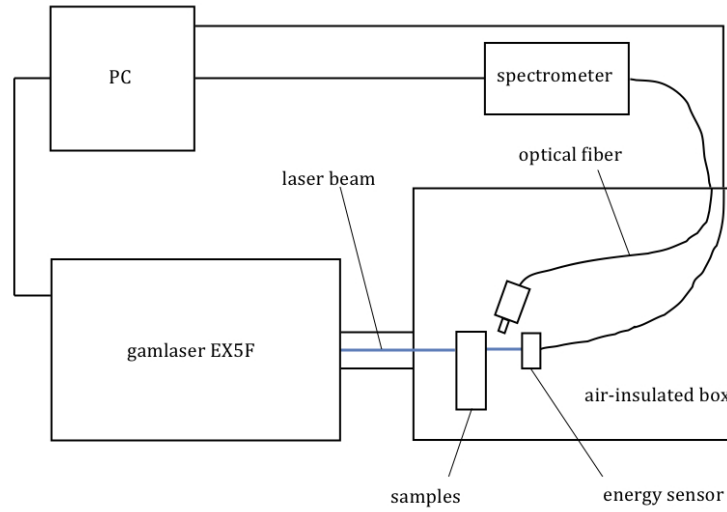
Figure 4.8.: Measurement assembly for transmittance spectrally resolved lumines-
cence measurement

4.3. Optical Characterization

In this section the optical characteristic of the ^{232}Th:CaF$_2$ crystal and of possi-
ble host crystals for ^{229}Th was investigated. The optical characterization contains
transmittance and luminescence measurements. The luminescence measurements
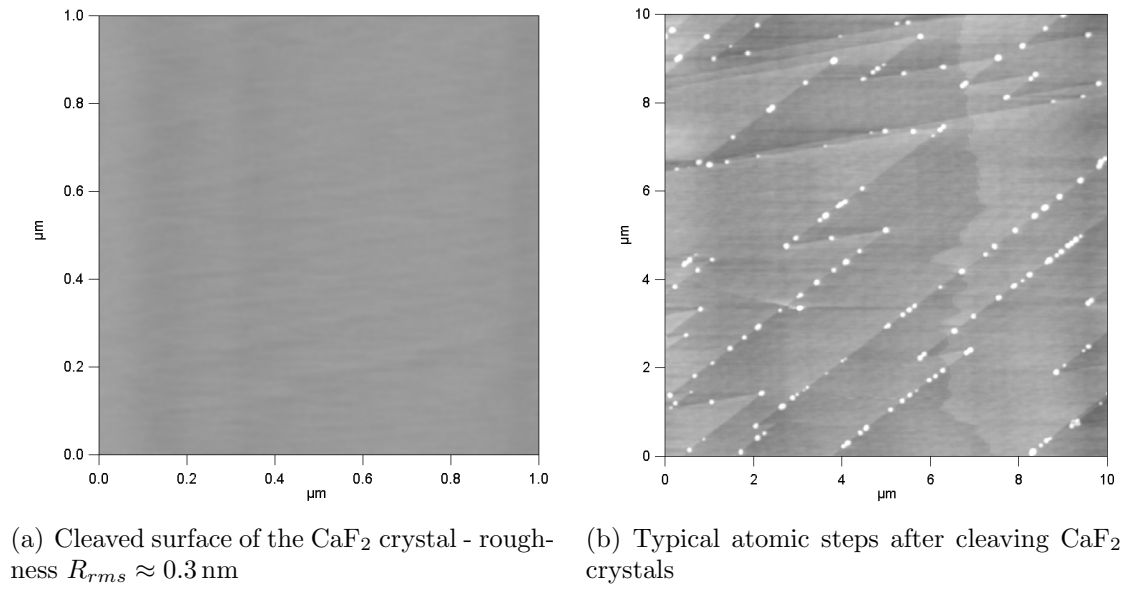include the the spectrally resolved luminescence measurements for wavelengths
above 180 nm and the time resolved luminescence measurements. As discussed in
section 2.3, the aim is to figure out which defect states within the band-gap affect
the luminescence and transmittance performance.

The measurement setup for the transmittance measurement in section 4.3.1 and
the luminescence measurement above 180 nm in section 4.3.2 is shown in figure 4.8.
For the time-resolved luminescence measurements below 180 nm the spectrometer
in figure 4.8 would be replaced by a photo multiplier (see figure 4.11).

Because the laser beam we need for irradiating the samples has a wavelength in
a VUV spectral range, where the laser beam would be absorbed in air (157 nm),
every measurement assembly has to be in a nitrogen atmosphere or under vac-
uum. For the optical characterization in this diploma thesis we chose the nitrogen
atmosphere. Figure 4.9 shows the measurement assembly for the optical charace-
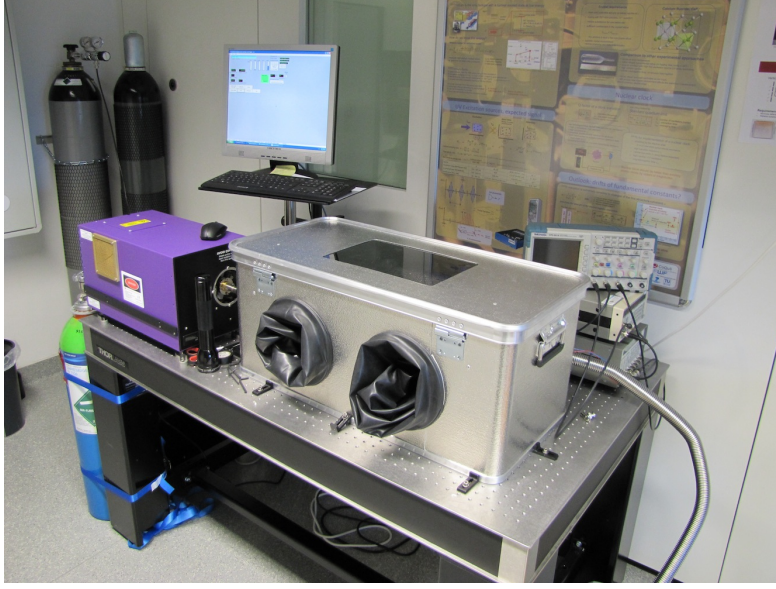
Figure 4.9.: Measurement setup

terization measurements.

The laser we used for the sample irradiation is an excimer laser: Gamlaser EX5F, VUV 157 nm Fluorine Laser [12]. The repetition rate is adjustable from 20 to 250 Hz, but it should be noted, that the power decreases from 150 Hz to 250 Hz. The maximum energy per pulse is 1.5 mJ. The pulse width w is 8 ns. The laser beam cross section has a rectangular shape with the dimensions of around 3 mm × 6 mm.

The samples are fixed in a holder that looks and acts like two cylinders of a revolver. One cylinder is placed behind the other and they can be rotated independent from each other. On each of the cylinders six samples can be fixed. The cylinder, which is closer to the laser beam output is suitable for intensity filters. The samples for measurement are positioned in the second cylinder (see figure 4.10).

The cross-section of the laser beam should be the same for every measurement. For this the samples are glued on a small fixture. This limits the laser beam to a circular cross section with a diameter of 3.6 mm. To be able to measure the intensity of the laser beam one fixture should stay empty. The intensity of the laser beam was measured with a pyroelectric energy sensor, Ophir probe PE25-C, Computer-Interface Juno [23]. The spectrally-resolved luminescence was measured

Figure 4.10.: Sample holder

with an AvaSpec spectrometer, 3648-USB-2-10 (10 μm enter slot) [3].

 The transmittance and luminescence performance was measured for cleaved and polished CaF_2 crystals and for a polished $^{232}Th:CaF_2$, YLF, LiF, $Nd:LiLuF_4$ and $LiCaAlF_6$ crystals. The sample specification can be found in subsection 3.2.4. The energy values per pulse of the laser beam are summerized in appendix A.2 in the tables A.16 to A.23. Assuming that the laser pulse has a rectangular shape, the peak intensity of the laser beam I can be calculated with the energy per pulse of the incident laser beam E_p, the pulse width w and the cross section area A_{cs}

$$I \approx \frac{E_p}{w \cdot A_{cs}}. \tag{4.3}$$

All measurements were performed at room temperature (296 K).

4.3.1. Transmittance

According to equation 2.10 in subsection 2.3.2 the transmittance T is the fraction of incident light intensity that passes through a sample with the thickness x, which is the optical path and constant for every sample measured in the following. In the
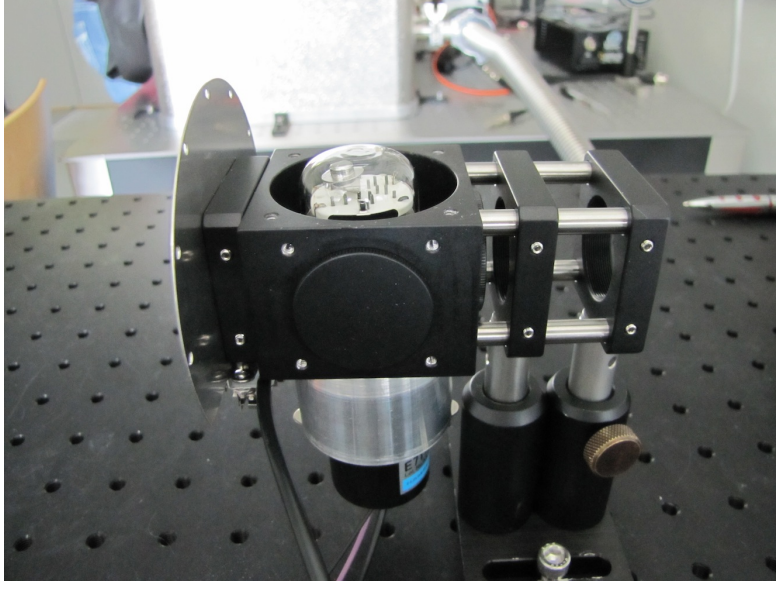
Figure 4.11.: Photomultiplyer

present case the transmittance can also be calculated with the energy per pulse of the incident laser light E_p and the energy per pulse after passing through the sample E_{pc}

$$T = \frac{E_{pc}}{E_p}. \tag{4.4}$$

The values in equation 4.4 are arithmetic mean values. The standard deviation of the transmittance ΔT was calculated using error propagation

$$\Delta T^2 = \left(\frac{\partial T}{\partial E_{pc}} \cdot \Delta E_{pc} \right)^2 + \left(\frac{\partial T}{\partial E_p} \cdot \Delta E_p \right)^2. \tag{4.5}$$

In the tables 4.14 to 4.21 the calculated mean transmittance T values and the standard deviation of the transmittance ΔT are listed in dependence on the mean intensity of the laser beam I and the standard deviation of the intensity of laser beam ΔI. The source data can be found in appendix A.4. In the figures 4.12 to 4.19, the graphical representation of this dependence is shown.

The transmittance measurement points of the samples "Hellma disc", ^{232}Th:CaF$_2$, YLF, LiF and LiCaAlF$_6$ seem to have a linear dependence on the intensity of the laser beam I, which indicates a small two-photon and two-step absorption

$I\left(\dfrac{\text{W}}{\text{mm}^2}\right)$	$\Delta I\left(\dfrac{\text{W}}{\text{mm}^2}\right)$	T (%)	ΔT (%)
150	14	75	9.4
350	21	54	4.7
500	17	47	2.8
510	40	49	4.5
570	17	46	2.5
750	68	52	5.4
960	82	46	5.3
1110	83	52	4.5
1520	52	45	2.3
2500	100	42	2.8

Table 4.14.: Transmittance of the CaF_2 sample "Small Chip" (cleaved)

$I\left(\dfrac{\text{W}}{\text{mm}^2}\right)$	$\Delta I\left(\dfrac{\text{W}}{\text{mm}^2}\right)$	T (%)	ΔT (%)
340	24	35	3.7
460	16	27	2.3
510	40	29	2.6
1460	55	10.7	0.68
1520	52	8.5	0.70
2500	100	6.9	0.55

Table 4.15.: Transmittance of the CaF_2 sample "Big Boy" (cleaved)

coefficient as expected in subsection 2.3.2. This possible linear dependence can be approached by a linear regression curve. The linear regression curves for the samples mentioned before are listed in table 4.22.

Görling, Leinhos and Mann measured the linear dependence of the transmittance on the laser beam intensity for polished CaF_2 samples before [7]. According to their measurements the linear transmittance value is the intercept of the linear regression curve with the ordinate and the slope of the regression curve gives the information about non linear effects.

In the present case the linear regression curve for the transmittance measurement of the CaF_2 sample "Hellma disc" is $T = 84\%$ (see table 4.22). This means that
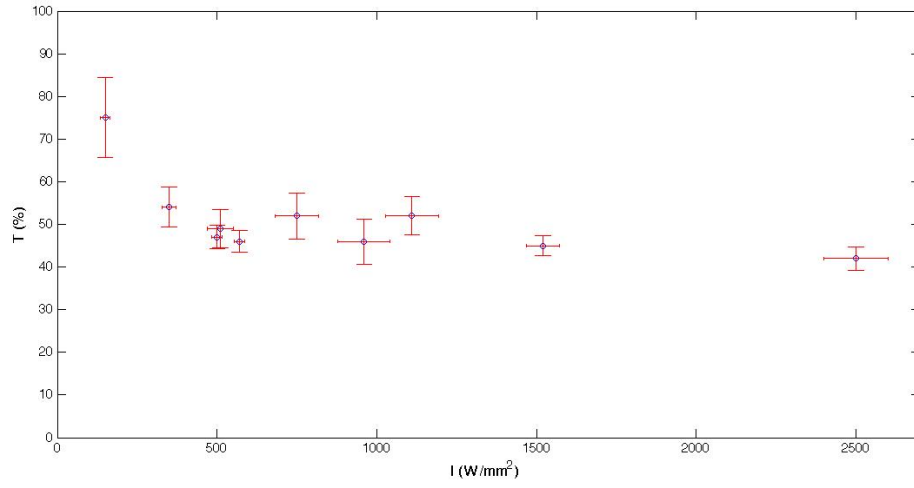
Figure 4.12.: Transmittance of the CaF$_2$ sample "Small Chip" (cleaved)
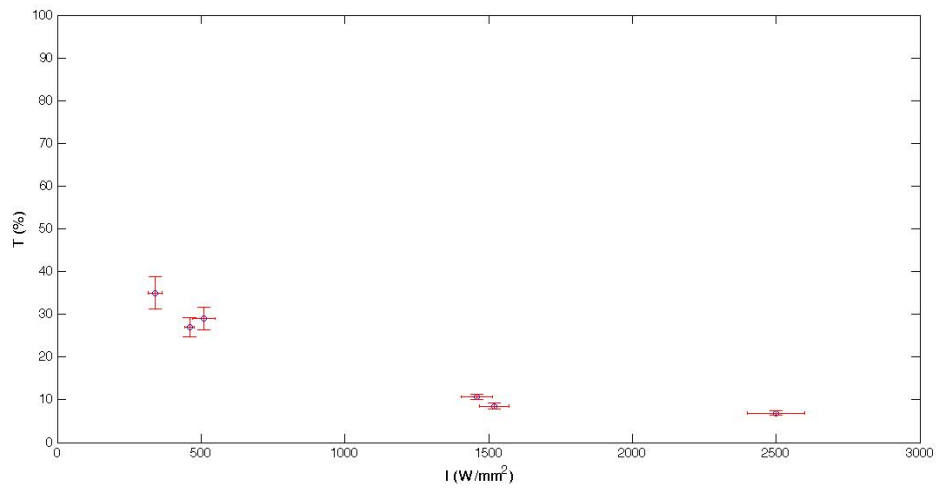
Figure 4.13.: Transmittance of the CaF$_2$ sample "Big Boy" (cleaved)

$I \left(\dfrac{\text{W}}{\text{mm}^2} \right)$	$\Delta I \left(\dfrac{\text{W}}{\text{mm}^2} \right)$	T (%)	ΔT (%)
190	11	89	8.1
290	14	76	5.4
480	22	84	5.5
490	42	90	12
660	18	80	3.4
1000	59	88	7.6
1340	64	83	5.5
1640	52	88	3.8
2320	72	84	3.8

Table 4.16.: Transmittance of the CaF$_2$ sample "Hellma disc" (polished)
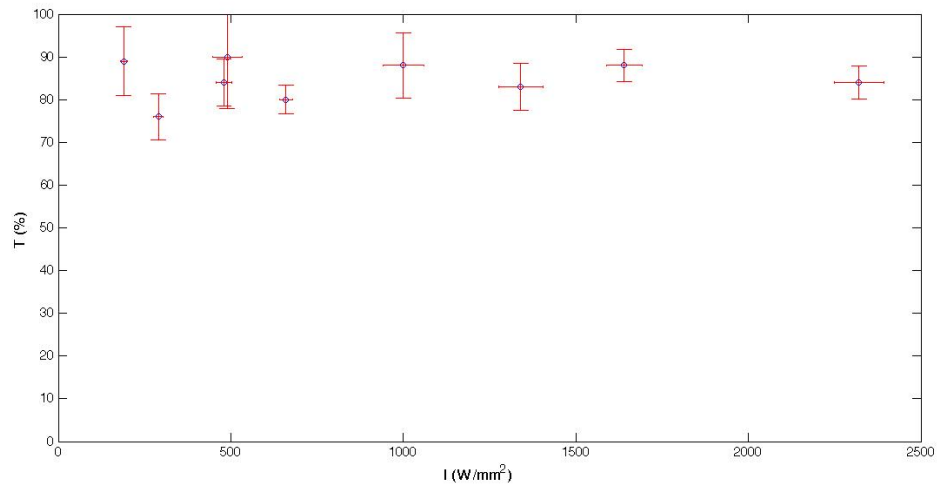
Figure 4.14.: Transmittance of the CaF$_2$ sample "Hellma disc" (polished)

the absorptance coefficient for effective two-photon-absorptance β_{eff} is too small to be measured.

The measured linear transmittance value of the sample "Hellma disc" is smaller than the calculated transmittance $90.2\,\% \pm 0.3\,\%$ in subsection 2.3.2. One reason for this deviation of calculated and measured transmittance could be the roughness $R_{rms} \approx 1.3\,\text{nm}$ of the CaF_2 sample "Hellma disc". A second reason could be measurement points which are outliers, most probably because of a not-homogeneous nitrogen atmosphere. The measurement points at $290\,\dfrac{\text{W}}{\text{mm}^2}$ and $660\,\dfrac{\text{W}}{\text{mm}^2}$ could be outliers (see table 4.16. The third possible reason are adsorbed particles on the surface of the sample.

Compared with all other samples measured in this diploma thesis "Hellma disc" has the best transmission performance, almost no non linear absorptance effects and a very low linear absorptance.

The transmittance behavior of the cleaved CaF_2 samples "Big Boy" and "Small Chip" (see figures 4.13 and 4.12) shows the expected non-linear transmittance behavior (see equation 2.21). This points to a large absorptance coefficient for effective two-photon-absorptance β_{eff}. The difference between the transmittance performance of "Small Chip" and the one of "Big Boy" could due to the bigger sample thickness (optical path) of the sample "Big Boy" $6.28\,\text{mm}$ ("Small Chip": $1.24\,\text{mm}$) - according to equation 2.21. Manufacturer and mechanism of crystal growth are the same for "Small Chip" and "Big Boy".

As described in subsection 2.3.2 the non-linear absorptance could be caused by an absorbing interface layer [7]. Intrinsic defects could also affect the transmission performance. Especially the CaF_2 sample "Big Boy" is, as we will also see in subsection 4.3.2, interesting. The energy of the laser beam after passing the crystal E_{pc} has a nearly constant value for every energy of the laser pulse E_p (see table A.17).

Obviously polishing is the better surface preparation for the transmittance performance. It should be noted, that the samples have to be cleaned before measuring, because dust particles or other surface impurities reduce the transmittance value.

The transmittance curve for the polished crystal ^{232}Th:CaF_2 (see figure 4.15) is obviously linear. The data points at $690\,\dfrac{\text{W}}{\text{mm}^2}$, $1100\,\dfrac{\text{W}}{\text{mm}^2}$ and $1520\,\dfrac{\text{W}}{\text{mm}^2}$ are

$I \left(\dfrac{\text{W}}{\text{mm}^2} \right)$	$\Delta I \left(\dfrac{\text{W}}{\text{mm}^2} \right)$	T (%)	ΔT (%)
150	14	90	11
340	21	82	7.4
480	38	87	9.1
500	17	84	4.1
610	91	97	25
690	68	51	5.8
960	82	78	8.4
1100	49	62	4.2
1300	110	77	8.9
1520	52	60	4.6
2000	96	77	5.0
2310	43	77	2.4
2400	94	84	4.3

Table 4.17.: Transmittance of the sample ^{232}Th:CaF$_2$ (polished)

Figure 4.15.: Transmittance of the sample ^{232}Th:CaF$_2$ (polished)

$I \left(\dfrac{\mathrm{W}}{\mathrm{mm}^2} \right)$	$\Delta I \left(\dfrac{\mathrm{W}}{\mathrm{mm}^2} \right)$	T (%)	ΔT (%)
150	11	90	9.2
350	13	71	4.2
690	22	72	3.1
970	23	73	2.5
1470	46	61	2.4
1920	79	53	2.7
2370	46	67	1.9

Table 4.18.: Transmittance of the sample YLF (polished

$I \left(\dfrac{\mathrm{W}}{\mathrm{mm}^2} \right)$	$\Delta I \left(\dfrac{\mathrm{W}}{\mathrm{mm}^2} \right)$	T (%)	ΔT (%)
120	10	90	12
200	40	80	22
530	85	80	16
600	37	77	7.0
1020	35	74	3.6
1590	70	75	4.2
2020	56	61	2.1

Table 4.19.: Transmittance of the sample LiF (polished)

outliers, most probably the nitrogen distribution with in the box was not homogeneous. The linear regression curve is $T = -0.004 \, \dfrac{\mathrm{mm}^2}{\mathrm{W}} \cdot I_{em} + 87.72 \,\%$ (see table 4.22). The behavior of the linear regression curve is an indicator for a small absorptance coefficient for effective two-photon-absorptance β_{eff} and a small linear absorptance. The transmittance performance of the ^{232}Th:CaF$_2$ crystal is quite comparable to the transmittance performance of the CaF$_2$ sample "Hellma disc".

The transmittance curves for the samples YLF (figure 4.16), LiF (figure 4.17) and LiCaAlF$_6$ (figure 4.19) are linear. The regression curves can be found in table 4.22. The slopes are an indicator for a larger non-linear absorptance than those of the samples "Hellma disc" and ^{232}Th:CaF$_2$. The intercept of the linear regression curves with the ordinate are indicators for a small linear absorptance.
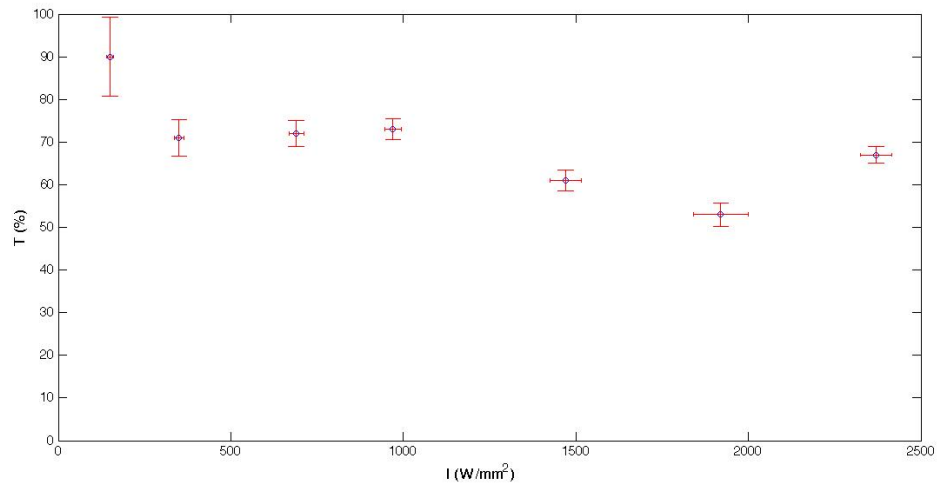
Figure 4.16.: Transmittance of the sample YLF (polished)
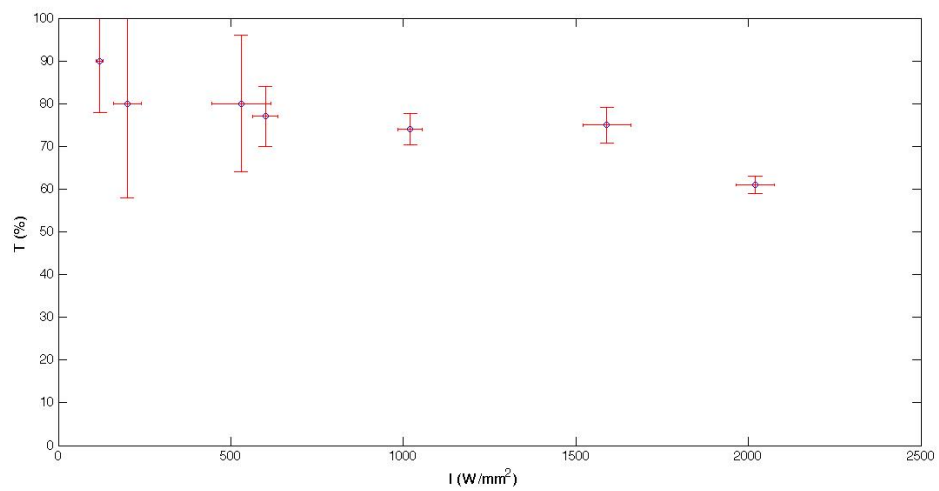
Figure 4.17.: Transmittance of the sample LiF (polished)

$I\left(\dfrac{\text{W}}{\text{mm}^2}\right)$	$\Delta I\left(\dfrac{\text{W}}{\text{mm}^2}\right)$	$T\ (\%)$	$\Delta T\ (\%)$
130	11	80	11
300	44	39	7.1
590	63	44	5.8
740	30	34	2.2
1060	28	33	1.5
1650	61	32	1.8
2250	75	23	1.1

Table 4.20.: Transmittance of th sample Nd:LiLuF$_4$ (polished)
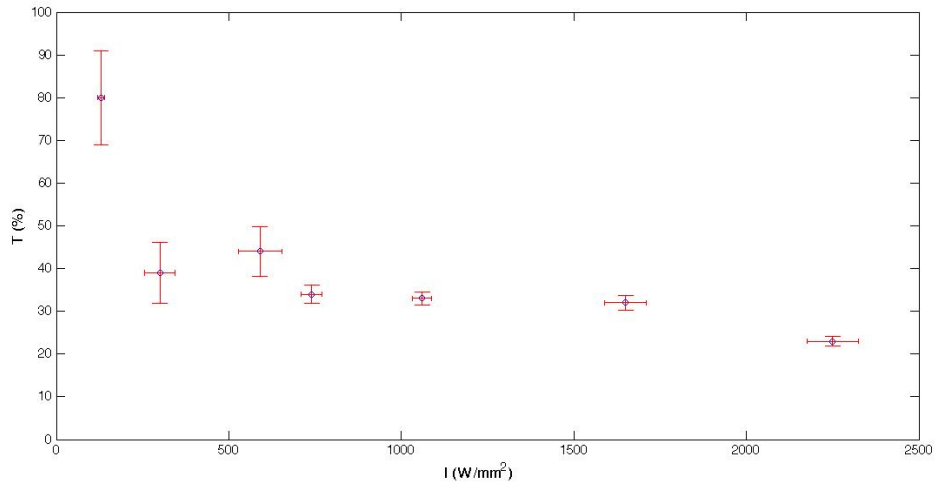
Figure 4.18.: Transmittance of the sample Nd:LiLuF$_4$ (polished)

$I\left(\dfrac{\mathrm{W}}{\mathrm{mm}^2}\right)$	$\Delta I\left(\dfrac{\mathrm{W}}{\mathrm{mm}^2}\right)$	$T\ (\%)$	$\Delta T\ (\%)$
130	11	90	11
300	44	80	16
590	63	90	11
740	30	75	4.3
1060	28	79	3.0
1650	61	69	4.0
2250	75	59	2.9

Table 4.21.: Transmittance of the sample LiCaAlF$_6$ (polished)
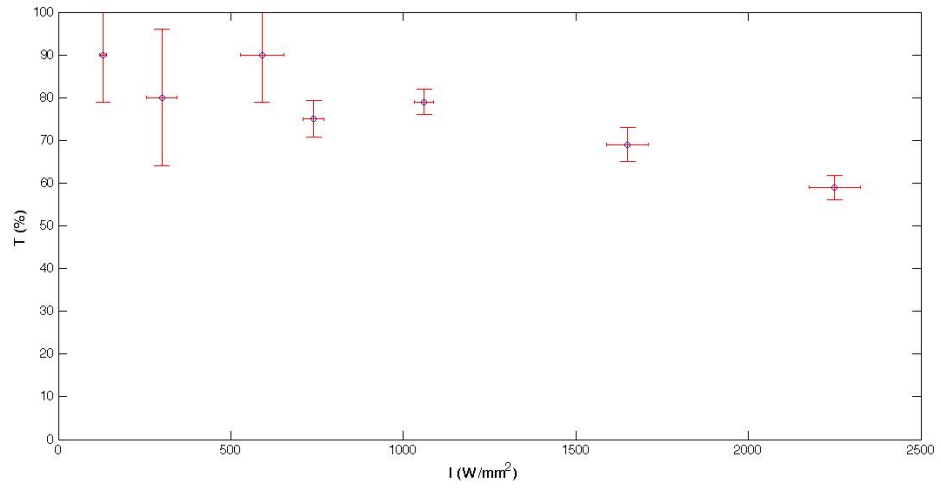
Figure 4.19.: Transmittance of the sample LiCaAlF$_6$ (polished)

Sample	Linear regression curve
Hellma disc	$T = 84\%$
^{232}Th:CaF$_2$	$T = -0.004 \frac{\text{mm}^2}{\text{W}} \cdot I_{em} + 87.72\%$
YLF	$T = -0.01 \frac{\text{mm}^2}{\text{W}} \cdot I_{em} + 81\%$
LiF	$T = -0.01 \frac{\text{mm}^2}{\text{W}} \cdot I_{em} + 86\%$
LiCaAlF$_6$	$T = -0.01 \frac{\text{mm}^2}{\text{W}} \cdot I_{em} + 90\%$

Table 4.22.: Linear regression curves of the samples Hellma disc, ^{232}Th:CaF$_2$, YLF, LiF and LiCaAlF$_6$

The absorptance coefficient for effective two-photon-absorptance β_{eff} is large for the sample Nd:LiLuF$_4$ and causes a non-linear transmittance curve (see figure 4.18). As shown in the next subsection the luminescence of this sample has very high count rates.

We found no noteworthy dependence of the transmittance on the pulse repetition rate of the laser. This could be because the intensity of the laser beam decreases slightly for higher repetition rates (about $200\,\text{Hz}$). Less incident intensity means less absorptance effects. It could be that this effect compensates a possible increasing of absoptance because of higher repetition rates.

In summary we can conclude that polishing is the best surface preparation method for transparency of VUV-transparent materials. A further conclusion is that the CaF$_2$ sample "Hellma disc" and the samples LiF, YLF, LiCaAlF$_6$ and ^{232}Th:CaF$_2$ have a desirable transmittance performance (small linear and non linear absorptance). The small linear and non-linear absorptance for the sample ^{232}Th:CaF$_2$ could be an indicator for a high transparancy of a ^{229}Th:CaF$_2$ crystal.

4.3.2. Luminescence

According to subsection 2.3.3 the nature of photoluminescence depends on the defect states within the band-gap of the measured samples. In this diploma thesis the spectraly resolved photoluminescence for wavelengths above $180\,\text{nm}$ was measured. The time-resolved photoluminescence was planed to be measured. Why it

Figure 4.20.: Spectrally resolved luminescence of the cleaved CaF$_2$ sample "Small Chip" at a laser repetition rate of 200 Hz and a intensity of 962 $\frac{\text{W}}{\text{mm}^2}$. Integration time: 100 s

has not been measured will be discussed later.

Spectraly Resolved

The luminescence peak counts in the following measurements depend on the repetition rate of the laser, on the incident laser light intensity and on the integration time of the measurement. For most of the samples no luminescence could be measured for a laser repetition rates smaller than 100 Hz and for small incident laser light intensity. The integration time is for most of the luminescence measurements very large (about 50 s or more).

No spectraly resolved luminescence for the wavelength range 180 nm - 700 nm was measured for the cleaved CaF$_2$ sample "Small Chip" (see figure 4.20).

It is surprising that the luminescence performance of the cleaved CaF$_2$ sample "Big Boy" (see figure 4.21) is that different to the one of "Small Chip", because manufacturer and mechanism of crystal growth are the same for both. The only difference is the thickness of the samples. No publications which point to a dependence of the luminescence performance on the sample thickness were found, but we can not exclude such a dependence. However, if non-linear absorption effects

Figure 4.21.: Spectrally resolved luminescence of the cleaved CaF$_2$ sample "Big Boy" at a laser repetition rate of 200 Hz and a intensity of 962 $\frac{W}{mm^2}$. Integration time: 1 s

are caused by surface effects, the curvature of the curve would be independent of the thickness.

The photoluminescence peak of the CaF$_2$ sample "Big Boy" is at 226 nm. First the peak seems to be the expected self-trapped excitons peak [6] as described in subsection 2.3.3, but this expected peak should be at 285 nm. Thus we can not conclude with certainty that self-trapped excitons cause the peak at 226 nm.

We found the same photoluminescence peak at 226 nm in the spectraly resolved luminescence measurement of the polished CaF$_2$ sample "Hellma disc" (see figure 4.22), but with less counts as the one of the CaF$_2$ sample "Big Boy" (see figure 4.21). The reason for this could be the different surface preparation. A second peak, which is very broad, is at 315 nm. We could not figure out what causes this peak.

The luminescence performance of the polished sample ^{232}Th:CaF$_2$ crystal is shown in figure 4.23. The luminescence peaks could be caused by ^{232}Th. They have very small count rates and it is not easy to figure out how many peaks are visible in the figure. We could identify peaks at ~ 235 nm, ~ 270 nm, ~ 285 nm, ~ 315 nm, ~ 330 nm, ~ 355 nm, ~ 377 nm, ~ 410 nm, ~ 488 nm, ~ 513 nm, ~ 377 nm, $\sim$

Figure 4.22.: Spectrally resolved luminescence of the polished CaF$_2$ sample "Hellma disc" at a laser repetition rate of 200 Hz and a intensity of 2256 $\frac{\text{W}}{\text{mm}^2}$. Integration time: 50 s

Figure 4.23.: Spectrally resolved luminescence of the polished sample ^{232}Th:CaF$_2$ at a laser repetition rate of 200 Hz and a intensity of 2138 $\frac{\text{W}}{\text{mm}^2}$. Integration time: 50 s
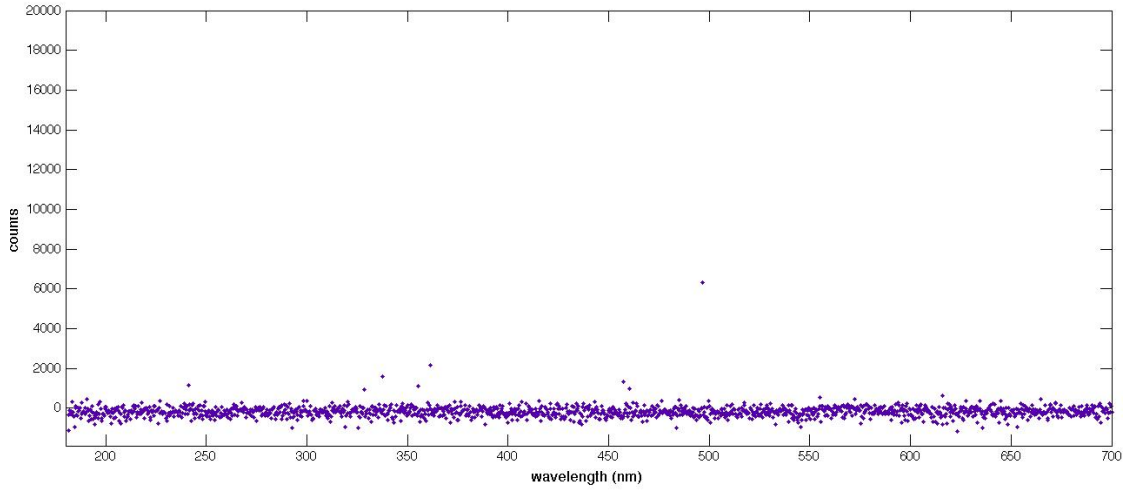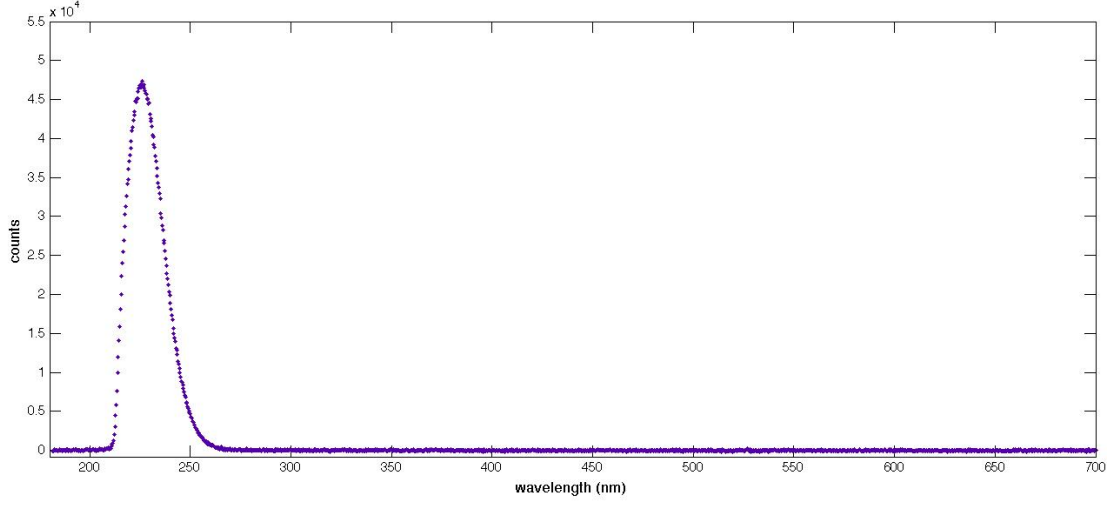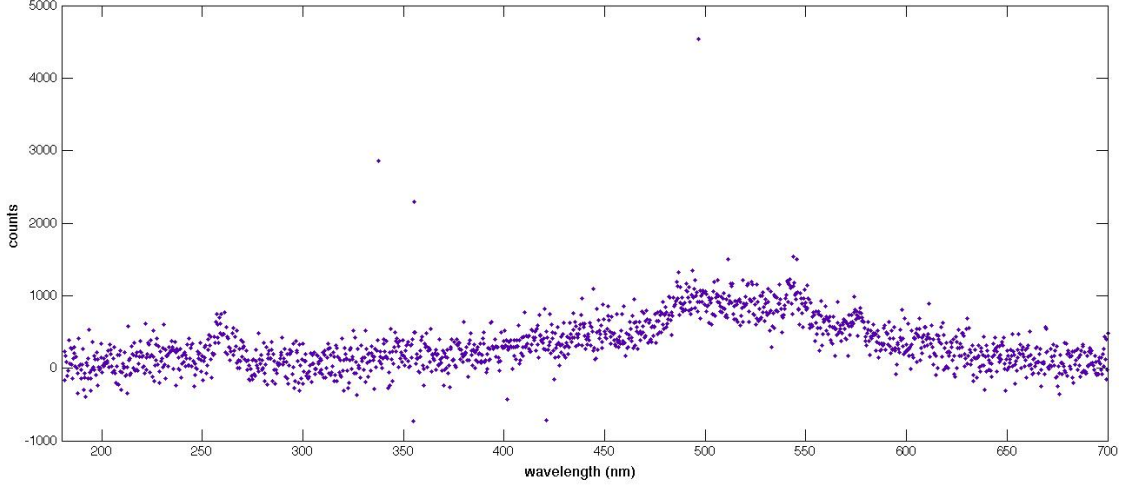
Figure 4.24.: Spectrally resolved luminescence of the polished sample YLF at a laser repetition rate of 200 Hz and a intensity of 1587 $\frac{W}{mm^2}$. Integration time: 50 s

545 nm, $\sim$ 580 nm. Maybe some of them consist of two or more peaks which can not be resolved. No publications could be found which describe the luminescence performance of thorium implanted in CaF_2. This is definetly a field of research that should be explored.

There is nearly no luminescence of the polished sample YLF (see figure 4.24). The peak structures at $\sim$ 260 nm and $\sim$ 500 nm are not clearly identifiable. According to [1] the peak at 260 nm could be caused by a small amount neodymium.

The luminescence performance of the polished sample LiF shows three peaks (see figure 4.25). They are at the wavelengths 286 nm, 390 nm and 490 nm.

The figures 4.26 and 4.27 show the luminescence performance of the polished sample Nd:LiLuF$_4$ at different repetition rates and integration times and nearly constant incident laser beam intensity. This is the only crystal that show such a luminescence even at a repetition rate of 20 Hz. On the basis of this figures, we see the obvious dependence of the luminescence peaks on the repetition rate of the laser. The peaks are at the wavelengths $\sim$ 188 nm, $\sim$ 227 nm, $\sim$ 260 (right next to this peak is a second one that can not be resolved), 374 nm, $\sim$ 413 nm, $\sim$ 478 nm, $\sim$ 488 nm, $\sim$ 568 nm, $\sim$ 574 nm, $\sim$ 577 nm, $\sim$ 580. In [2] and [1] are indications
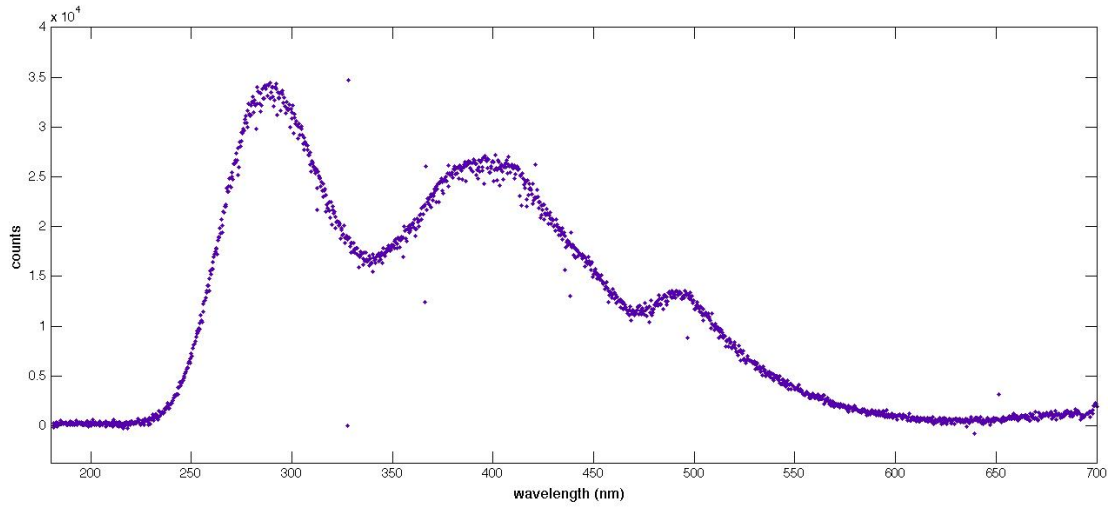
Figure 4.25.: Spectrally resolved luminescence of the polished sample LiF at a laser repetition rate of $200\,\mathrm{Hz}$ and a intensity of $2151\,\dfrac{\mathrm{W}}{\mathrm{mm}^2}$. Integration time: $50\,\mathrm{s}$
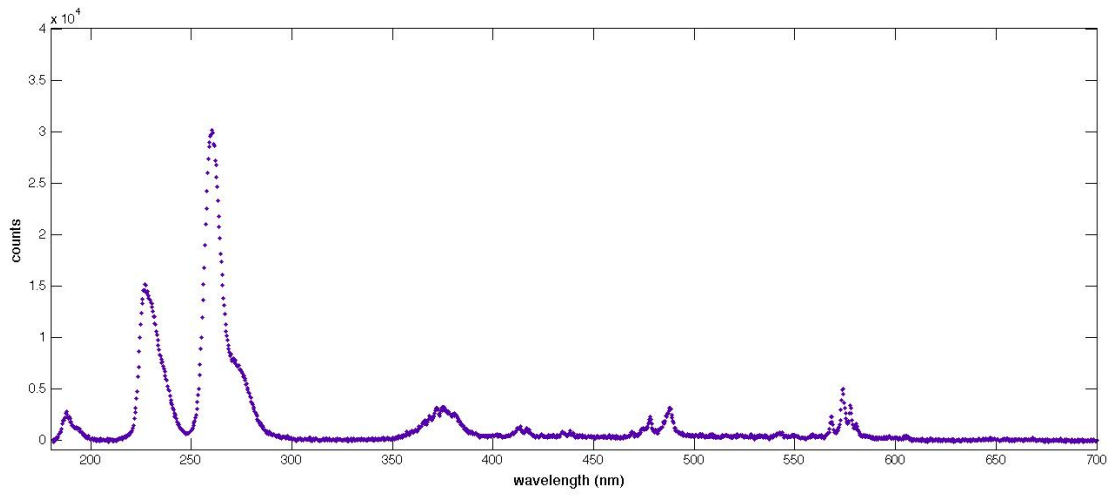
Figure 4.26.: Spectrally resolved luminescence of the polished sample Nd doped $\mathrm{LiLuF_4}$ at a laser repetition rate of $200\,\mathrm{Hz}$ and a intensity of $2350\,\dfrac{\mathrm{W}}{\mathrm{mm}^2}$. Integration time: $1\,\mathrm{s}$
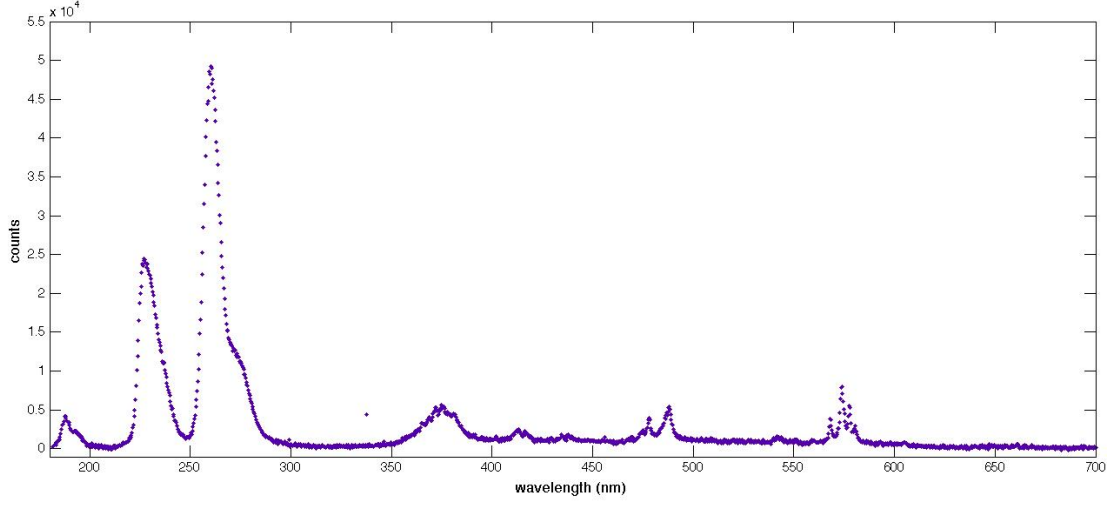
Figure 4.27.: Spectrally resolved luminescence of the polished sample Nd doped LiLuF$_4$ at a laser repetition rate of 20 Hz and a intensity of 2255 $\dfrac{\text{W}}{\text{mm}^2}$. Integration time: 20 s

that the peaks at 227 nm and 260 nm could be caused by Nd^{3+}.

The polished sample LiCaAlF$_6$ shows nearly no luminescence. In figure 4.28 there is one peak at ~ 515 nm, which is broad and has a very small count rate. In figure 4.29, which is a luminescence measurement of LiCaAlF$_6$ at a smaller incident laser beam intensity, are two peaks visible at ~ 542 nm and ~ 611 nm. Both have a very small count rate. We have not figured out what causes this peaks.

If we take a look at the transmittance and luminescence performance of the measured samples, we finally can conclude that there could be a context between a polished surface, which shows less non-linear absorptance effectes, and a smaller luminescence peak counts. Furthermore, we can conclude that polished CaF$_2$, YLF and LiCaAlF$_6$ have the best transmittance and luminescence perfomance, because of very low non-linear effects.

No statement could be made about the luminescence effects below 180 nm with the spectrally resolved luminescence measurements. Luminescence emissions with a wavelength about 160 nm should be subject of further investigation, because this is the spectral range where the isomer transition in the nucleus of ^{229}Th is expected (7.6 eV $\pm$ 0.5 eV).
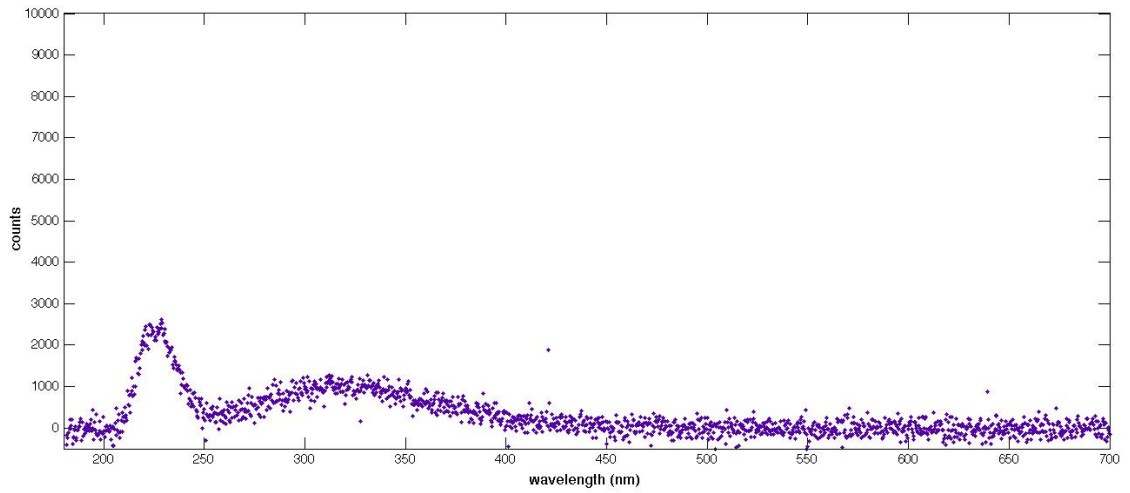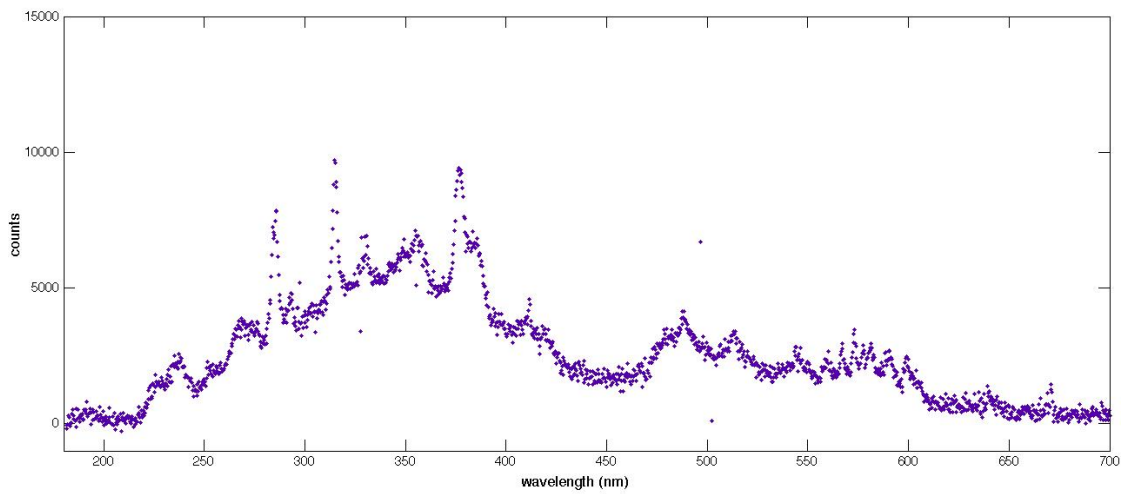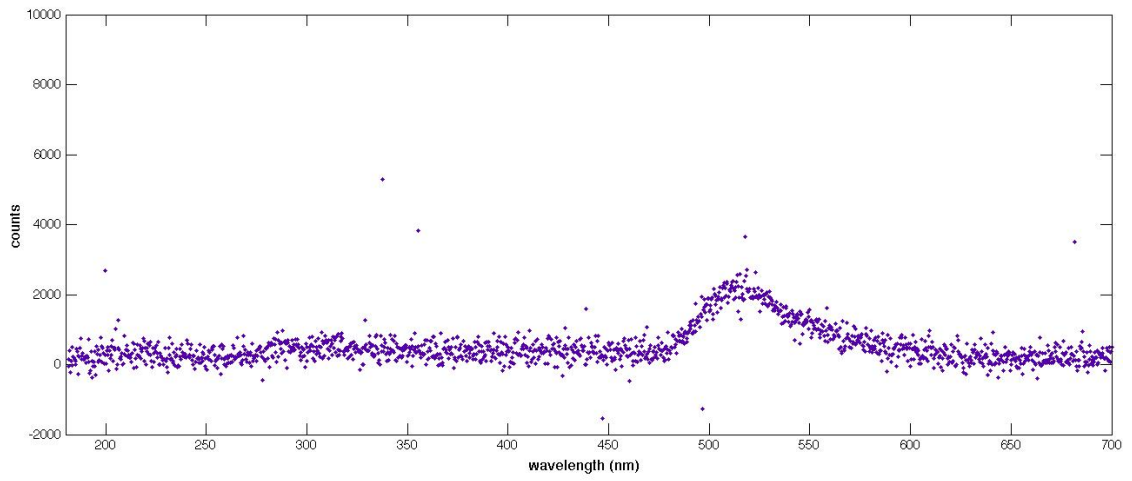
Figure 4.28.: Spectrally resolved luminescence of the polished sample LiCaAlF$_6$ at a laser repetition rate of $200\,\text{Hz}$ and a intensity of $3703\,\dfrac{\text{W}}{\text{mm}^2}$. Integration time: $100\,\text{s}$
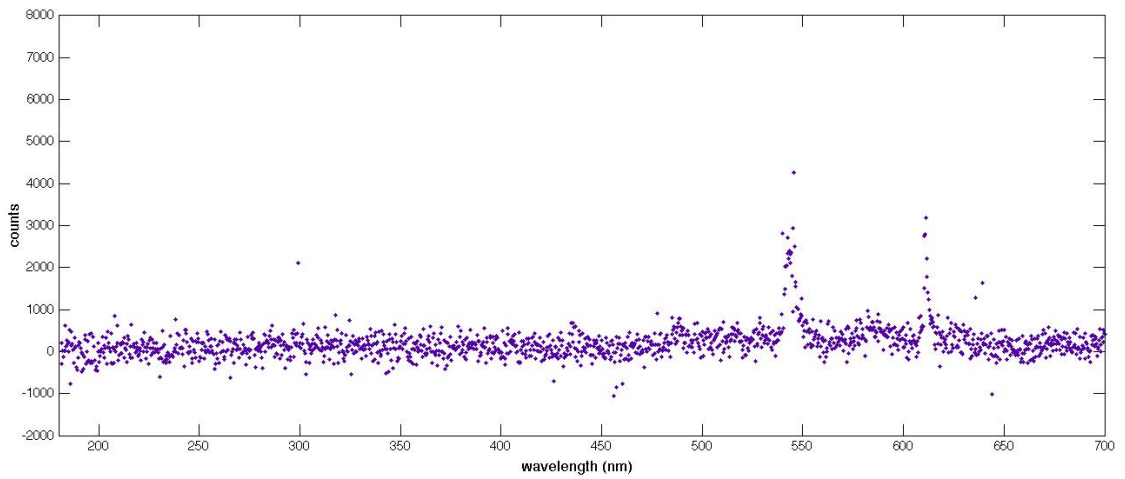
Figure 4.29.: Spectrally resolved luminescence of LiCaAlF$_6$ at a laser repetition rate of $200\,\text{Hz}$ and a intensity of $962\,\dfrac{W}{mm^2}$. Integration time: $100\,\text{s}$

Time-resolved

For the time-resolved luminescence above 80 nm a little adaption of the measurement setup shown in figure 4.8 is needed. The principle of the time-resolved luminescence measurement above 180 nm is that we change at a fix integration the start time of recording of the spectrometer. For this we need a photo diode to know when the laser is pulsed exactly. With a delay generator the start time of recording of the spectrometer can be changed and moved thus along the time scale of the time-resolved luminescence measurement.

The time-resolved luminescence above 180 nm could not be measured, because the luminescence peak counts are too small. As mentioned in this section before, luminescence effects depend on the repetition rate of the incident laser light and are only visible for repetition rates above 100 Hz (for most of the measured samples). For recording of a time-resolved luminescence curve more than one measurement points within a period have to be recorded. This results an integration time of 2 ms or 3 ms. Such a short integration time is not enough to see luminescence peaks.

The time-resolved luminescence below 180 nm should have been measured with a photomultiplier. It could not be measured because the shilding of the photomultiplier was insufficient. External electromagnetic fields affected the photomultiplier signal. The Thorium group at the Institute for Atomic and Subatomic Physics in Vienna measured the time-resolved luminescence with a photomultiplier at Berlin. The results will not be publicated in this diploma thesis.

5. Conclusion and Outlook

The purpose of this diploma thesis was the characterization of material property correlations of possible host crystals for ^{229}Th. The material properties included possible crystal impurities, doping concentration of CaF_2 doped with ^{232}Th, surface roughness, transmittance and luminescence. The methods employed in this thesis are established standard tools, for quantitative measurements, where specific calibrations were needed. This methods were gamma spectroscopy, neutron activation analysis, atomic force microscopy, transmittance and spectral-resolved luminescence. In chapter 2 the expected results are described and in chapter 4 the measured results are discussed. The sample preparation methods and the sample characterization are described in chapter 3.

Impurities: After perfoming gamma spectroscopy and neutron activation analysis no unwanted or unexpected impurities could be found for the ^{232}Th:CaF_2 crystal and the melt manufactured at the Institut für Kristallzüchtung Berlin IKZ. There is still a chance for impurities if they are non-radiation and their cross section at thermal neutron energy is too small for activation in the research reactor. Impurities could also be visible for spectral-resolved luminescence measurements. In subsection 4.3.2 the luminescence performance for the sample ^{232}Th:CaF_2 is shown in figure 4.23. The peaks that are visible could be caused by ^{232}Th or by unwanted impurities. We could not conclude what causes the peaks. For that the excited states within the band-gap of CaF_2 caused by implanting ^{232}Th must be calculated or measured for comparing the measurements in this diploma thesis with the luminescence peaks caused by ^{232}Th.

Doping concentration: Performing neutron activation analysis the doping concentration of sample ^{232}Th:CaF$_2$ crystal and the melt could be measured. The doping concentration of the crystal is about $(1.80 \pm 0.0198) \cdot 10^{18}\,\mathrm{cm^{-3}}$ and the doping concentration of the melt is about $(4.91 \pm 0.0419) \cdot 10^{18}\,\mathrm{cm^{-3}}$. The small deviation of the mass fraction and volume fraction of ^{232}Th in different pieces of one crystal is an indicator for a rather homogeneous doping of ^{232}Th.

Surface roughness: The surface roughness (root mean square deviation) of the polished ^{232}Th:CaF$_2$ crystal is $R_{rms} \approx 12\,\mathrm{nm}$. This crystal was polished at the Institute for Atomic and Subatomic Physics in Vienna with a sandpaper grain of 4000. The CaF$_2$ sample "Hellma disc" has a roughness that is one order of magnitude smaller $R_{rms} \approx 1.3\,\mathrm{nm}$. This sample was polished from the manufacturer Hellma-materials. For comparison, a cleaved CaF$_2$ has a local surface roughness about $R_{rms} \approx 0.3\,\mathrm{nm}$ and typical atomic steps (see figure 4.7). We expected lower transmittance for the ^{232}Th:CaF$_2$ crystal because of more diffuse reflection due to the roughness. We also expected, that a cleaved crystal should have least absorbtance because of a specular interface. After transmittance and luminescence measurements we figured out that the transmittance and luminescence performance for ^{232}Th:CaF$_2$ and "Hellma disc" are very similar (hardly no non-lineaer absorptance effects, small linear absorptance and small luminescence count rates). We also figured out that claved crystals show obviously more absorptance effects (small transmittance) and higher luminescence count rates than polished crystals. This effect could be caused by an absorbing interface layer [7] on the cleaved surface. We could conclude that polishing of the crystal surface is a very good surface preparation method, even with the sandpaper grain of 4000.

Transmittance and luminescence performance: Possible host crystals (CaF$_2$, LiF, YLF, Nd:LiLuF$_4$ and LiCaAlF$_6$) for ^{229}Th and the ^{232}Th:CaF$_2$ were characterized optically. In table 4.22 the linear regression curves for the crystals with a linear dependence of the transmittance on the laser light intensity

(crystals with small non-linear absorptance effects and small linear absorptance) are listed. In 4.3.2 the luminescence performance of the crystals mentioned before is shown. With this informations we could conclude that CaF_2, $LiCaAlF_6$ and YLF could be the best host crystals for ^{229}Th because of small absorbtance and nearly no luminescence. The optical characterization of the ^{232}Th:CaF_2 crystal is satisfactory. The linear regression curve $T = -0.004 \frac{mm^2}{W} \cdot I_{em} + 87.72\%$ of ^{232}Th:CaF_2 indicates a very small linear and non-linear absorptance at $157\,nm$. There is nearly no laser induced luminescence for the ^{232}Th:CaF_2 crystal. Luminescence could be measured only for very high laser repetition rates ($200\,Hz$), high laser light intensity ($2138 \frac{W}{mm^2}$) and a long integration time ($50\,s$). In figure 4.23 the luminescence performance of ^{232}Th:CaF_2 is shown. So there could be good chance to measure the low-energy isomer transition in the nucleus of ^{229}Th if it is implanted in CaF_2.

In this diploma thesis the time-resolved luminescence could not be measured. Further characterization steps should focus on the characteristic parameters of luminescence, like the decay time for different wavelength to unambiguously identify the microscopic processes. At this stage, ^{232}Th-doped CaF_2 seems to be a promising candidate for precision spectroscopy of the ^{229}Th isomer state. With this knowledge, we are closer to the "solid state nuclear clock".

A. Appendix

A.1. Acronyms

$E_{\gamma M}$ measured gamma ray energy

E_γ gamma ray energy

$E_{\gamma C}$ certified gamma ray energy

E_γ gamma ray energy

$CR_{\gamma C}$ certified gamma ray count rate

$CR_{\gamma M}$ measured gamma count rate

$CR_{\gamma E}$ measured gamma count rate corrected with the efficiency curve

A activity

I intensity of the laser beam

ΔI standard deviation of the intensity of laser beam

E_p energy per pulse of the incident laser beam

ΔE_p standard deviation of the energy per pulse of the laser beam

E_{pc} energy per pulse of the laser beam after passing the crystal

ΔE_{pc} standard deviation of the energy per pulse of the laser beam after passing the crystal

w pulse width

A_{cs} cross section area

T transmittance

t time

$CR_{\gamma 0}$ gamma count rate at time 0

λ decay constant

$t_{\frac{1}{2}}$ half-life

f_{cor} decay correction factor

$A_{Pa_{sample}}$ activity of ^{233}Pa in a sample

A. Appendix

$A_{Pa_{standard}}$ activity of ^{233}Pa in the standard

$m_{Th_{sample}}$ mass of ^{232}Th in the sample

$m_{Th_{standard}}$ mass ^{232}Th in the standard

m_{Th} mass of ^{232}Th

m mass

q_m mass fraction

N_{Th} number of ^{232}Th particles

N_{CaF_2} number of CaF_2 particles

n_V number of particles per volume

n_{Th} number of ^{232}Th particles per volume of matter

ρ density

E_{kin} kinetic energy

ν frequency of the γ-quantum

λ_γ wavelength of the gamma photon

λ'_γ wavelength of the scattered gamma photon

W_W work function - the energy required to remove an electron from the electron shell

h Planck constant

E_{SEP} energy of the single escape peak

E_{DEP} energy of the double escape peak

m_e mass of the electron

c velocity of light

θ scattering angle

Z charge number

I_γ intensity

N_A number of with thermal neutrons interacting nuclides

N_B number of activation product nuclides

σ_{th} cross section at thermal neutron energy

ϕ neutron flux density

$^A_Z X$ nuclide X with the mass number A and the atomic number Z

$^{A+1}_Z X$ nuclide X with the mass number A+1 and the atomic number Z

n_{th} neutron at thermal energy

A_B activity of activation product nuclide B

ΔT	standard deviation of the transmittance
α	absorptance coefficient
α_n	n-photon absorptance coefficient
α_1	absorptance coefficient for linear absorptance
I_{em}	intensity of the electromagnetic wave
x	thickness
β	absorptance coefficient for two-photon-absorptance
β_{eff}	absorptance coefficient for effective two-photon-absorptance
R_{rms}	root mean square surface deviation
R_a	arithmetic average of the surface deviation
A	absorptance
δ	angle of incidence light
ϵ	angle of refraction light
τ_v	transmittance coefficient for the vertical component of the amplitude vector on the incident plane
τ_p	transmittance coefficient for the parallel component of the amplitude vector on the incident plane
R	reflectance
n_N	refractive index of nitrogen
n_{CaF_2}	refractive index of CaF_2
$N_{excited}$	number of electrons or molecules in the excited state
τ	decay time
ICP-MS	inductively-coupled-plasma mass-spectrometry
VUV	vacuum ultraviolet
STE	self-trapped exciton
AFM	Atomic force microscopy
PL	photoluminescence

A.2. Gamma Spectroscopy

All errors quoted at 1.00 sigma.

Sample ^{232}Th:CaF$_2$ Single Crystal

Peak Nr.	$E_{\gamma M}$ (keV)	Net Peak Area (cts)	Bkgnd (cts)	FWHM (keV)	$CR_{\gamma M}$ (cps)	Error (%)
M 1	73.04	3984	16952	1.182	1.492E-002	2.91
m 2	75.06	19265	16708	1.187	7.215E-002	0.90
m 3	77.27	23352	16308	1.192	8.745E-002	0.80
M 4	84.54	5651	16142	1.313	2.116E-002	2.25
m 5	87.16	11403	17390	1.318	4.270E-002	1.34
m 6	89.84	4560	17024	1.324	1.708E-002	2.63
m 7	93.08	3356	16707	1.330	1.257E-002	3.40
F 8	115.10	1402	17667	1.263	5.249E-003	8.56
F 9	128.96	1534	20778	1.283	5.746E-003	8.21
F 10	185.47	1424	16862	1.497	5.334E-003	8.59
F 11	209.02	2119	16960	1.085	7.935E-003	5.03
F 12	215.71	551	16465	0.939	2.064E-003	16.47
M 13	238.37	97739	11532	1.279	3.660E-001	0.34
m 14	240.75	9077	9997	1.282	3.399E-002	1.37
F 15	252.68	593	8438	1.363	2.220E-003	14.22
F 16	269.92	1877	11381	1.476	7.030E-003	5.10
F 17	277.08	3848	11810	1.351	1.441E-002	2.65
M 18	287.90	708	7867	1.326	2.651E-003	10.11
m 19	294.87	598	7663	1.334	2.241E-003	11.07
m 20	299.84	5564	7478	1.339	2.084E-002	1.98
F 21	327.66	1460	8842	1.413	5.466E-003	5.87
F 22	337.96	5364	9949	1.399	2.009E-002	1.94
Continued on next page						

Table A.1.: Gamma spectroscopy of the sample ^{232}Th:CaF$_2$

Peak Nr.	$E_{\gamma M}$ (keV)	Net Peak Area (cts)	Bkgnd (cts)	FWHM (keV)	$CR_{\gamma M}$ (cps)	Error (%)
F 23	351.53	1369	7811	1.646	5.126E-003	6.10
F 24	409.16	735	6209	1.522	2.751E-003	9.48
F 25	462.59	1521	5710	1.556	5.696E-003	4.54
F 26	510.34	13491	5356	2.010	5.052E-002	0.98
F 27	582.68	28540	3852	1.610	1.069E-001	0.62
F 28	608.78	1346	3420	1.632	5.042E-003	4.41
F 29	726.72	6023	2377	1.732	2.255E-002	1.47
M 30	762.74	436	2213	1.880	1.634E-003	10.25
m 31	771.66	274	1750	1.886	1.027E-003	14.46
F 32	785.00	826	2066	1.753	3.092E-003	5.87
F 33	794.35	930	2021	1.764	3.483E-003	5.30
F 34	834.95	257	1430	1.480	9.606E-004	14.67
F 35	859.94	3475	1964	1.820	1.301E-002	1.97
F 36	910.57	5934	1938	1.909	2.222E-002	1.43
M 37	964.22	1053	1433	1.946	3.944E-003	4.20
m 38	968.35	3424	1364	1.949	1.282E-002	1.97
F 39	1078.26	424	1170	2.489	1.588E-003	9.06
F 40	1093.19	389	1714	2.388	1.457E-003	10.37
F 41	1119.76	576	1521	2.262	2.159E-003	7.24
F 42	1460.49	5498	960	2.329	2.059E-002	1.43
M 43	1588.04	465	756	2.727	1.742E-003	7.00
m 44	1592.19	1014	765	2.729	3.796E-003	4.03
M 45	1620.50	745	573	2.474	2.790E-003	4.77
m 46	1630.68	290	582	2.479	1.086E-003	8.87
F 47	1764.45	771	683	2.323	2.889E-003	4.65
F 48	2103.50	1564	726	3.936	5.857E-003	3.08
F 49	2615.06	10513	341	3.298	3.937E-002	0.99

Table A.1.: Gamma spectroscopy of the sample ^{232}Th:CaF$_2$

Sample ^{232}Th:CaF$_2$ Melt

Peak Nr.	$E_{\gamma M}$ (keV)	Net Peak Area (cts)	Bkgnd (cts)	FWHM (keV)	$CR_{\gamma M}$ (cps)	Error (%)
M 1	75.05	17532	17864	1.158	2.030E-001	0.97
m 2	77.27	25125	16587	1.163	2.909E-001	0.76
M 3	84.48	5037	16916	1.325	5.831E-002	2.42
m 4	87.16	12360	16497	1.330	1.431E-001	1.22
m 5	89.89	10685	16030	1.336	1.237E-001	1.35
m 6	93.28	12028	16939	1.343	1.392E-001	1.25
F 7	99.46	3204	16773	1.376	3.709E-002	3.93
M 8	105.37	4723	18365	1.554	5.468E-002	2.86
m 9	108.71	1682	18265	1.560	1.947E-002	6.51
F 10	115.06	1509	17930	1.255	1.747E-002	7.47
F 11	128.94	7785	21062	1.176	9.013E-002	1.80
F 12	153.79	2536	19029	1.123	2.936E-002	4.40
F 13	199.09	589	18274	1.112	6.822E-003	16.40
F 14	209.00	12511	15194	1.237	1.448E-001	1.20
F 15	215.79	648	11045	1.010	7.504E-003	13.57
M 16	238.37	106840	10235	1.284	1.237E+000	0.32
m 17	240.74	10203	8550	1.288	1.181E-001	1.24
F 18	252.49	521	8755	1.141	6.032E-003	14.75
F 19	269.95	8977	9587	1.302	1.039E-001	1.36
F 20	277.08	4120	8812	1.341	4.770E-002	2.44
F 21	287.79	791	6915	1.256	9.155E-003	9.76
F 22	299.82	6080	9095	1.321	7.039E-002	1.76
M 23	321.30	383	5166	1.346	4.435E-003	16.45
m 24	327.66	6581	6759	1.353	7.619E-002	1.55
m 25	331.96	784	6654	1.357	9.075E-003	7.55
m 26	337.99	27451	5879	1.363	3.178E-001	0.67

Table A.2.: Gamma spectroscopy of the sample ^{232}Th:CaF$_2$ Melt

Peak Nr.	$E_{\gamma M}$ (keV)	Net Peak Area (cts)	Bkgnd (cts)	FWHM (keV)	$CR_{\gamma M}$ (cps)	Error (%)
F 27	351.52	632	5924	1.487	7.316E-003	11.24
F 28	409.03	3527	6659	1.427	4.083E-002	2.42
F 29	452.55	501	2946	1.328	5.796E-003	11.41
F 30	462.57	7658	5395	1.482	8.865E-002	1.36
F 31	510.25	11018	5375	1.853	1.276E-001	1.10
F 32	562.04	1202	4666	1.470	1.392E-002	5.19
F 33	582.69	31000	4647	1.581	3.589E-001	0.60
F 34	608.85	638	3621	1.526	7.383E-003	8.69
F 35	726.71	7239	3871	1.725	8.380E-002	1.36
M 36	754.78	1179	2490	1.800	1.365E-002	4.69
m 37	762.75	528	2661	1.806	6.107E-003	8.50
m 38	771.71	1652	2421	1.812	1.913E-002	3.53
M 39	781.65	644	1883	1.795	7.451E-003	6.85
m 40	784.88	970	2001	1.798	1.122E-002	5.07
F 41	794.33	4707	2514	1.804	5.449E-002	1.71
M 42	829.84	510	1645	1.715	5.903E-003	7.61
m 43	835.12	1804	1516	1.718	2.088E-002	3.03
m 44	839.76	968	1383	1.721	1.120E-002	4.49
F 45	859.93	3884	1409	1.859	4.497E-002	1.84
F 46	892.80	288	1558	1.749	3.330E-003	12.47
M 47	903.47	718	1323	1.875	8.311E-003	5.51
m 48	910.56	29013	1183	1.879	3.359E-001	0.60
M 49	957.92	253	1098	1.912	2.931E-003	12.10
m 50	964.15	5043	1157	1.916	5.838E-002	1.52
m 51	968.33	17274	1112	1.918	2.000E-001	0.78
F 52	1064.48	302	1019	1.435	3.497E-003	9.85
F 53	1078.26	394	958	2.253	4.566E-003	8.80
F 54	1093.70	524	1063	2.804	6.069E-003	7.33
Continued on next page						

Table A.2.: Gamma spectroscopy of the sample ^{232}Th:CaF$_2$ Melt

Peak Nr.	$E_{\gamma M}$ (keV)	Net Peak Area (cts)	Bkgnd (cts)	FWHM (keV)	$CR_{\gamma M}$ (cps)	Error (%)
F 55	1109.93	476	993	1.997	5.512E-003	7.13
F 56	1246.44	514	1133	3.453	5.955E-003	7.82
F 57	1460.16	2208	757	2.711	2.556E-002	2.41
M 58	1495.63	668	460	2.205	7.728E-003	4.81
m 59	1501.23	360	453	2.208	4.167E-003	7.14
F 60	1512.50	240	428	2.653	2.780E-003	10.24
M 61	1580.25	415	421	2.551	4.809E-003	6.43
m 62	1587.97	2394	516	2.555	2.771E-002	2.24
m 63	1592.21	933	510	2.557	1.080E-002	3.98
M 64	1620.68	880	421	2.601	1.019E-002	3.94
m 65	1630.48	1219	401	2.605	1.411E-002	3.22
m 66	1638.13	371	357	2.609	4.295E-003	6.64
F 67	1764.53	227	493	2.395	2.624E-003	10.83
F 68	2103.64	1552	604	3.885	1.797E-002	3.00
F 69	2615.04	11062	302	3.307	1.281E-001	0.96

Table A.2.: Gamma spectroscopy of the sample ^{232}Th:CaF$_2$ Melt

Sample ThF$_4$

Peak Nr.	$E_{\gamma M}$ (keV)	Net Peak Area (cts)	Bkgnd (cts)	FWHM (keV)	$CR_{\gamma M}$ (cps)	Error (%)
M 1	72.99	65472	366229	1.238	3.044E-001	0.80
m 2	75.04	554703	362533	1.243	2.579E+000	0.18
m 3	77.27	508031	355623	1.248	2.362E+000	0.18
m 4	81.43	20277	384108	1.256	9.426E-002	2.09
m 5	84.44	130407	380582	1.263	6.062E-001	0.41
m 6	87.15	366592	375688	1.269	1.704E+000	0.20
m 7	89.89	664656	368391	1.274	3.090E+000	0.14
					Continued on next page	

Table A.3.: Gamma spectroscopy of the sample ThF$_4$

Peak Nr.	$E_{\gamma M}$ (keV)	Net Peak Area (cts)	Bkgnd (cts)	FWHM (keV)	$CR_{\gamma M}$ (cps)	Error (%)
m 8	93.28	962100	357504	1.281	4.472E+000	0.11
F 9	99.46	78420	392003	1.180	3.645E-001	0.74
M 10	105.30	434976	397465	1.586	2.022E+000	0.20
m 11	108.67	158848	372869	1.592	7.384E-001	0.39
F 12	115.10	31086	340805	1.259	1.445E-001	1.59
M 13	128.94	134300	264878	1.186	6.243E-001	0.43
m 14	131.48	8512	266157	1.190	3.957E-002	4.52
M 15	140.87	2055	235616	1.151	9.551E-003	18.05
m 16	145.66	9141	255272	1.159	4.249E-002	4.88
F 17	153.78	53373	345337	1.248	2.481E-001	0.95
F 18	166.21	8762	330392	1.128	4.073E-002	4.85
F 19	176.61	3501	259764	1.156	1.628E-002	12.08
F 20	184.46	8308	327304	2.525	3.862E-002	7.15
F 21	191.09	7527	321021	1.265	3.499E-002	5.86
M 22	199.15	20636	247123	1.249	9.593E-002	1.87
m 23	203.77	9572	243981	1.255	4.450E-002	3.86
m 24	208.98	319606	239039	1.262	1.486E+000	0.22
F 25	215.71	22760	276247	1.280	1.058E-001	1.96
F 26	223.57	2557	187148	0.851	1.188E-002	12.88
M 27	233.11	9107	224637	1.281	4.234E-002	3.96
m 28	238.36	3629618	194586	1.287	1.687E+001	0.05
m 29	240.72	341055	168136	1.290	1.585E+000	0.20
F 30	252.35	17274	187360	1.301	8.030E-002	2.16
M 31	263.35	3277	152168	1.306	1.523E-002	8.83
m 32	269.95	245207	149542	1.314	1.140E+000	0.25
M 33	277.10	150674	158828	1.344	7.004E-001	0.35
m 34	281.70	2733	143265	1.350	1.271E-002	8.18
m 35	287.86	25322	141092	1.357	1.177E-001	1.24
Continued on next page						

Table A.3.: Gamma spectroscopy of the sample ThF_4

Peak Nr.	$E_{\gamma M}$ (keV)	Net Peak Area (cts)	Bkgnd (cts)	FWHM (keV)	$CR_{\gamma M}$ (cps)	Error (%)
m 36	294.88	2070	138698	1.364	9.624E-003	8.78
m 37	299.82	222488	135920	1.370	1.034E+000	0.28
M 38	321.33	12915	106291	1.360	6.004E-002	2.29
m 39	327.66	191856	140973	1.367	8.919E-001	0.27
m 40	332.03	21452	140354	1.371	9.972E-002	1.28
m 41	337.98	753163	127307	1.378	3.501E+000	0.13
F 42	351.65	5111	102075	1.254	2.376E-002	5.71
F 43	377.22	1797	92542	0.977	8.353E-003	14.33
F 44	409.07	107218	141287	1.418	4.984E-001	0.41
F 45	440.04	6843	118009	1.471	3.181E-002	4.07
F 46	452.41	18987	94798	1.387	8.826E-002	1.54
F 47	462.57	219831	126002	1.481	1.022E+000	0.25
F 48	477.85	8797	88060	1.400	4.089E-002	3.01
M 49	503.36	5898	59519	1.026	2.742E-002	0.33
m 50	510.23	367743	102644	1.848	1.710E+000	0.02
M 51	519.63	2236	79165	1.562	1.039E-002	10.02
m 52	522.68	4604	85009	1.565	2.140E-002	5.49
M 53	546.00	8001	68937	1.503	3.719E-002	2.86
m 54	549.21	5910	75535	1.506	2.747E-002	3.78
m 55	554.71	1579	76100	1.510	7.339E-003	13.05
m 56	562.01	36954	83351	1.516	1.718E-001	0.86
F 57	571.01	12481	113340	2.461	5.802E-002	2.69
F 58	582.69	1198299	111079	1.588	5.570E+000	0.09
M 59	608.94	4952	85179	1.726	2.302E-002	5.00
m 60	615.66	2842	79160	1.731	1.321E-002	7.86
m 61	619.87	3036	84596	1.735	1.411E-002	7.48
F 62	639.75	1625	67997	1.541	7.556E-003	14.60
F 63	650.15	4429	90659	3.337	2.059E-002	7.25
						Continued on next page

Table A.3.: Gamma spectroscopy of the sample ThF_4

Peak Nr.	$E_{\gamma M}$ (keV)	Net Peak Area (cts)	Bkgnd (cts)	FWHM (keV)	$CR_{\gamma M}$ (cps)	Error (%)
M 64	673.84	3920	97370	2.032	1.822E-002	6.46
m 65	676.41	4028	91875	2.034	1.872E-002	6.35
F 66	687.49	2748	93381	1.510	1.278E-002	8.94
M 67	701.19	8686	122079	2.672	4.038E-002	3.46
m 68	706.87	8970	112403	2.676	4.170E-002	3.34
M 69	721.66	1685	60587	1.723	7.834E-003	12.01
m 70	726.71	260969	72489	1.726	1.213E+000	0.22
M 71	754.74	35115	65644	1.788	1.632E-001	0.80
m 72	762.77	21128	60481	1.794	9.822E-002	1.13
m 73	771.72	48385	55127	1.800	2.249E-001	0.62
M 74	781.55	16280	45886	1.736	7.568E-002	1.30
m 75	784.93	33954	44429	1.738	1.578E-001	0.76
F 76	794.35	136751	57590	1.786	6.357E-001	0.30
M 77	816.05	1204	34792	1.782	5.597E-003	12.18
m 78	824.53	1370	33477	1.788	6.369E-003	9.88
m 79	829.90	19373	34777	1.791	9.006E-002	1.19
m 80	835.10	46685	32935	1.795	2.170E-001	0.67
m 81	839.76	28342	31147	1.798	1.318E-001	0.78
F 82	859.93	140103	33639	1.823	6.513E-001	0.29
F 83	873.64	1507	29637	1.624	7.005E-003	9.65
M 84	887.08	1130	26978	1.898	5.252E-003	10.92
m 85	892.79	10592	24802	1.901	4.924E-002	1.68
M 86	903.57	20693	24112	1.877	9.619E-002	0.92
m 87	910.56	822909	22498	1.881	3.825E+000	0.11
F 88	927.26	1001	18961	1.751	4.655E-003	12.15
M 89	943.65	2643	15935	1.931	1.229E-002	1.61
m 90	947.37	2263	21170	1.933	1.052E-002	1.86
m 91	951.52	4242	21063	1.935	1.972E-002	1.05
					Continued on next page	

Table A.3.: Gamma spectroscopy of the sample ThF_4

Peak Nr.	$E_{\gamma M}$ (keV)	Net Peak Area (cts)	Bkgnd (cts)	FWHM (keV)	$CR_{\gamma M}$ (cps)	Error (%)
m 92	957.97	8157	20901	1.939	3.792E-002	0.61
m 93	964.17	147692	20296	1.943	6.866E-001	0.26
m 94	968.35	480079	18307	1.946	2.232E+000	0.25
m 95	975.21	1670	16739	1.950	7.761E-003	2.37
m 96	981.77	2546	16620	1.954	1.183E-002	1.59
m 97	987.56	5033	16499	1.957	2.340E-002	0.87
M 98	1000.64	1229	16107	1.933	5.714E-003	8.44
m 99	1003.84	2321	15786	1.935	1.079E-002	5.07
M100	1032.62	5755	16569	2.120	2.675E-002	2.36
m101	1039.64	2952	16615	2.124	1.372E-002	3.92
M102	1053.42	1152	16711	2.095	5.354E-003	8.89
m103	1057.89	1112	17019	2.098	5.168E-003	9.16
m104	1064.50	9082	16520	2.102	4.222E-002	1.69
F105	1078.15	13291	20456	1.978	6.178E-002	1.24
F106	1093.58	17380	20285	2.485	8.079E-002	1.05
M107	1110.02	11789	15859	2.151	5.480E-002	1.33
m108	1117.91	1800	15901	2.155	8.368E-003	5.72
m109	1122.23	4350	16862	2.158	2.022E-002	2.76
F110	1153.01	3877	20561	2.064	1.802E-002	3.31
M111	1164.11	1180	13514	2.036	5.484E-003	8.84
m112	1167.99	1323	16274	2.038	6.149E-003	8.14
F113	1246.27	14470	22531	3.322	6.727E-002	1.30
F114	1286.65	2389	19750	2.569	1.111E-002	5.75
F115	1373.84	4372	16719	2.058	2.032E-002	2.98
F116	1431.61	2450	14014	2.538	1.139E-002	4.87
F117	1459.13	20154	16240	2.833	9.369E-002	0.91
F118	1473.45	446	6956	1.261	2.073E-003	16.73
M119	1495.66	18738	10881	2.388	8.711E-002	0.88
Continued on next page						

Table A.3.: Gamma spectroscopy of the sample ThF_4

Peak Nr.	$E_{\gamma M}$ (keV)	Net Peak Area (cts)	Bkgnd (cts)	FWHM (keV)	$CR_{\gamma M}$ (cps)	Error (%)
m120	1501.31	9964	10587	2.390	4.632E-002	1.31
m121	1512.51	7684	10251	2.396	3.572E-002	1.57
M122	1528.89	1281	10416	2.411	5.956E-003	7.24
m123	1537.59	976	10368	2.415	4.537E-003	8.91
F124	1556.84	3930	12760	2.770	1.827E-002	2.93
M125	1580.28	11667	11935	2.583	5.424E-002	1.20
m126	1587.98	66403	12090	2.587	3.087E-001	0.42
m127	1592.19	36121	12250	2.589	1.679E-001	0.60
M128	1620.56	29759	12382	2.469	1.383E-001	0.66
m129	1624.88	5231	11614	2.471	2.432E-002	2.10
m130	1630.45	32662	11407	2.474	1.518E-001	0.62
m131	1638.10	9255	11166	2.478	4.302E-002	1.39
F132	1666.33	3797	10753	2.382	1.765E-002	2.96
M133	1678.64	2828	13972	3.717	1.315E-002	4.06
m134	1685.64	2695	15001	3.721	1.253E-002	4.24
F135	1702.16	1218	12925	3.338	5.664E-003	9.42
F136	1723.88	750	7972	2.459	3.485E-003	12.73
M137	1758.25	506	9284	2.008	2.351E-003	15.57
m138	1764.57	984	9444	2.011	4.575E-003	9.24
F139	1806.01	2129	11927	2.711	9.896E-003	5.29
F140	1823.17	745	12605	2.364	3.462E-003	13.40
F141	1887.23	1246	11737	2.160	5.792E-003	8.20
F142	2103.67	55170	20594	3.783	2.565E-001	0.50
F143	2615.07	381481	8109	3.277	1.773E+000	0.16
F144	2687.65	2112	3903	4.707	9.819E-003	3.69
F145	2892.66	1011	2429	2.979	4.699E-003	5.38
F146	3126.01	2970	677	3.486	1.381E-002	2.01

Table A.3.: Gamma spectroscopy of the sample ThF_4

A.3. Neutron Activating Analysis

All errors quoted at 1.00 sigma

Cerfied Reference Material CFA

Peak Nr.	$E_{\gamma M}$ (keV)	Net Peak Area (cts)	Bkgnd (cts)	FWHM (keV)	$CR_{\gamma M}$ (cps)	Error (%)
F1	4.75	13204	15752	1.268	6.602E-001	0.91
F2	49.78	1106	18686	1.339	5.529E-002	9.06
M3	62.34	1683	20507	1.087	8.417E-002	5.74
m4	67.05	1254	20732	1.096	6.272E-002	7.40
F5	74.33	2501	25129	1.313	1.250E-001	18.20
M6	85.92	3311	27187	1.546	1.655E-001	4.50
m7	90.49	3518	33338	1.553	1.759E-001	4.35
m8	93.89	5809	31644	1.559	2.904E-001	3.47
m9	97.78	10027	31997	1.565	5.014E-001	3.00
m10	102.55	16158	34518	1.572	8.079E-001	2.81
m11	109.84	3044	35200	1.582	1.522E-001	4.89
m12	112.57	4360	35438	1.587	2.180E-001	3.89
F13	121.29	11476	32666	1.534	5.738E-001	1.26
M14	132.55	3557	28072	1.408	1.778E-001	4.60
m15	135.73	1458	29928	1.412	7.292E-002	7.98
m16	141.92	2527	29630	1.420	1.264E-001	5.92
m17	144.93	18029	29419	1.424	9.014E-001	3.26
m18	151.91	868	29018	1.433	4.338E-002	12.26
m19	158.99	1515	30613	1.442	7.575E-002	7.74
F20	176.79	2214	26203	1.372	1.107E-001	23.09
M21	191.94	4846	26201	1.334	2.423E-001	2.44
m22	197.49	3519	30035	1.340	1.760E-001	3.27
M23	208.05	5588	34161	1.705	2.794E-001	9.21
						Continued on next page

Table A.4.: Neutron activation analysis of the certified reference material CFA

Peak Nr.	$E_{\gamma M}$ (keV)	Net Peak Area (cts)	Bkgnd (cts)	FWHM (keV)	$CR_{\gamma M}$ (cps)	Error (%)
m24	215.47	2296	34754	1.713	1.148E-001	10.29
F25	244.35	1820	16664	1.288	9.101E-002	5.31
F26	264.31	910	10637	1.582	4.548E-002	9.26
F27	282.31	1616	15759	1.334	8.082E-002	20.30
F28	299.17	6287	16497	2.118	3.144E-001	1.70
M29	307.64	753	11181	1.551	3.766E-002	11.57
m30	311.60	18470	11702	1.555	9.235E-001	2.14
m31	319.77	10204	10954	1.562	5.102E-001	2.35
F32	328.52	2196	12300	1.494	1.098E-001	3.72
M33	340.20	1965	11969	1.620	9.825E-002	3.98
m34	344.01	7224	14056	1.623	3.612E-001	1.43
F35	396.11	3145	11827	1.495	1.572E-001	2.67
M36	411.22	807	9817	1.492	4.036E-002	8.53
m37	415.63	643	11101	1.495	3.213E-002	10.51
F38	443.80	571	10783	1.251	2.855E-002	50.22
M39	481.89	3549	9318	1.589	1.774E-001	2.35
m40	486.72	4024	11270	1.592	2.012E-001	2.15
F41	496.02	1426	7427	1.557	7.130E-002	5.11
F42	513.66	690	11504	1.444	3.452E-002	10.30
F43	530.84	998	11797	2.024	4.991E-002	35.09
M44	563.63	2042	10101	1.695	1.021E-001	3.94
m45	569.10	708	12842	1.698	3.542E-002	9.96
F46	604.39	6279	12987	1.585	3.140E-001	8.84
F47	722.98	545	9553	1.472	2.723E-002	12.69
F48	778.66	1970	10108	2.044	9.852E-002	19.44
F49	795.53	3410	9817	1.791	1.705E-001	8.31
F50	815.44	1189	7267	1.635	5.945E-002	5.96
F51	834.55	2154	10961	1.889	1.077E-001	14.58
Continued on next page						

Table A.4.: Neutron activation analysis of the certified reference material CFA

Peak Nr.	$E_{\gamma M}$ (keV)	Net Peak Area (cts)	Bkgnd (cts)	FWHM (keV)	$CR_{\gamma M}$ (cps)	Error (%)
F52	867.14	893	11428	2.021	4.464E-002	35.89
M53	879.14	1780	10738	1.860	8.901E-002	4.93
m54	888.97	196870	10260	1.865	9.843E+000	0.35
F55	964.68	3628	7089	3.611	1.814E-001	2.11
M56	1076.59	1534	2988	1.774	7.670E-002	3.43
m57	1085.60	922	2878	1.778	4.609E-002	5.02
F58	1099.08	34922	3125	1.891	1.746E+000	0.51
M59	1111.88	1346	2124	1.995	6.729E-002	3.96
m60	1115.37	1569	2393	1.997	7.846E-002	3.57
m61	1120.38	168416	1944	1.999	8.421E+000	0.34
M62	1173.12	10830	1157	1.914	5.415E-001	0.93
m63	1177.82	817	966	1.916	4.087E-002	4.15
m64	1188.92	391	902	1.921	1.957E-002	7.05
M65	1221.33	598	813	1.981	2.990E-002	5.07
m66	1230.92	232	821	1.985	1.160E-002	10.22
F67	1291.62	23925	794	2.097	1.196E+000	0.91
F68	1312.52	113	450	1.561	5.663E-003	16.82
F69	1332.60	9671	615	2.023	4.835E-001	0.97
F70	1408.20	1921	409	2.123	9.606E-002	5.41
F71	1461.07	1968	318	2.252	9.840E-002	5.31
F72	1596.61	3528	226	2.225	1.764E-001	2.85
F73	1691.56	467	167	2.382	2.333E-002	13.17
F74	1765.23	336	151	2.315	1.678E-002	16.81
F75	2010.68	1096	68	2.347	5.479E-002	5.30
F76	2523.24	86	7	2.422	4.308E-003	31.12
F77	2616.21	354	7	2.512	1.770E-002	10.69

Table A.4.: Neutron activation analysis of the certified reference material CFA

Cerfied Reference Material SO1

Peak Nr.	$E_{\gamma M}$ (keV)	Net Peak Area (cts)	Bkgnd (cts)	FWHM (keV)	$CR_{\gamma M}$ (cps)	Error (%)
F1	3.90	7895	7436	1.050	3.948E-001	1.19
F2	62.32	518	8937	1.125	2.589E-002	12.06
F3	74.41	1120	12168	0.838	5.601E-002	27.30
M4	90.56	1116	9959	1.362	5.580E-002	6.41
m5	93.83	1962	13501	1.368	9.811E-002	3.85
m6	97.74	3322	14246	1.374	1.661E-001	2.50
m7	102.56	5034	14060	1.381	2.517E-001	1.85
F8	109.92	642	11662	1.241	3.210E-002	11.68
M9	121.19	3633	13224	1.435	1.817E-001	2.54
m10	123.09	2261	14873	1.438	1.131E-001	3.70
F11	132.53	1171	12551	1.185	5.853E-002	23.09
M12	142.11	1089	9788	1.333	5.447E-002	6.62
m13	144.97	8391	13203	1.337	4.195E-001	1.29
F14	158.92	1001	11895	1.435	5.006E-002	90.66
M15	191.95	2974	9797	1.313	1.487E-001	2.78
m16	197.47	857	12700	1.319	4.284E-002	8.09
M17	208.07	1207	10013	1.526	6.035E-002	6.28
m18	215.57	1261	15710	1.534	6.305E-002	6.37
F19	244.35	495	7127	1.010	2.476E-002	25.07
F20	282.41	320	5825	1.191	1.601E-002	15.96
F21	299.66	1700	6823	1.533	8.500E-002	17.48
M22	311.63	6733	5853	1.414	3.366E-001	1.31
m23	319.83	7237	5688	1.421	3.618E-001	1.24
F24	328.49	1028	4522	1.543	5.142E-002	5.17
M25	340.21	714	4172	1.456	3.572E-002	6.93
m26	343.99	2145	5546	1.459	1.073E-001	2.88
F27	373.08	592	4961	1.531	2.961E-002	8.27
						Continued on next page

Table A.5.: Neutron activation analysis of the certified reference material SO1

Peak Nr.	$E_{\gamma M}$ (keV)	Net Peak Area (cts)	Bkgnd (cts)	FWHM (keV)	$CR_{\gamma M}$ (cps)	Error (%)
F28	396.14	849	5400	1.815	4.244E-002	6.17
M29	481.82	1176	4104	1.676	5.879E-002	11.82
m30	486.73	1763	4126	1.679	8.815E-002	11.31
F31	496.01	1467	5459	1.553	7.337E-002	51.56
F32	604.42	1704	5101	1.569	8.518E-002	12.91
F33	778.57	470	4025	1.540	2.350E-002	9.66
F34	795.52	1336	3550	1.650	6.680E-002	4.03
F35	815.54	639	2868	1.682	3.194E-002	7.47
F36	834.61	1396	4080	1.684	6.979E-002	4.00
M37	879.24	502	4544	1.851	2.509E-002	10.83
m38	889.01	69086	4258	1.856	3.454E+000	0.65
F39	964.24	957	3323	3.068	4.783E-002	4.95
M40	1076.59	1182	1340	1.823	5.908E-002	3.58
m41	1085.69	305	1464	1.827	1.523E-002	10.00
F42	1099.12	21603	1442	1.882	1.080E+000	0.65
M43	1111.99	490	1031	1.989	2.448E-002	7.07
m44	1115.44	876	1094	1.991	4.382E-002	4.64
m45	1120.41	60121	947	1.993	3.006E+000	0.57
F46	1173.14	4987	1018	1.873	2.493E-001	1.40
F47	1221.25	218	356	2.336	1.091E-002	9.11
F48	1291.65	14700	510	2.050	7.350E-001	1.44
F49	1332.63	4704	385	2.058	2.352E-001	2.64
F50	1408.21	653	261	2.020	3.267E-002	4.09
F51	1461.11	1916	172	2.055	9.581E-002	2.23
F52	1596.66	1500	147	2.253	7.501E-002	2.50
F53	1765.33	269	125	1.990	1.343E-002	17.94
F54	2010.94	417	39	2.307	2.085E-002	6.04
F55	2205.21	90	33	2.280	4.477E-003	11.79
Continued on next page						

Table A.5.: Neutron activation analysis of the certified reference material SO1

Peak Nr.	$E_{\gamma M}$ (keV)	Net Peak Area (cts)	Bkgnd (cts)	FWHM (keV)	$CR_{\gamma M}$ (cps)	Error (%)
F56	2616.31	356	12	2.771	1.778E-002	5.15

Table A.5.: Neutron activation analysis of the certified reference material SO1

Cerfied Reference Material GBW

Peak Nr.	$E_{\gamma M}$ (keV)	Net Peak Area (cts)	Bkgnd (cts)	FWHM (keV)	$CR_{\gamma M}$ (cps)	Error (%)
M1	62.39	690	6087	1.146	3.449E-002	7.90
m2	66.95	1402	7320	1.154	7.012E-002	4.49
F3	74.44	1391	8851	1.489	6.955E-002	22.19
M4	85.99	1680	9475	1.599	8.402E-002	5.55
m5	90.52	2184	11527	1.606	1.092E-001	4.90
m6	93.95	4484	11548	1.612	2.242E-001	3.81
m7	97.77	7669	11578	1.618	3.834E-001	3.45
m8	102.56	6727	11614	1.625	3.364E-001	3.48
M9	110.16	2489	11051	1.870	1.245E-001	3.43
m10	112.84	2777	15633	1.874	1.389E-001	3.18
F11	121.41	2441	8319	1.796	1.220E-001	3.00
F12	132.54	4183	9622	1.270	2.091E-001	7.48
F13	144.94	12337	10008	1.452	6.169E-001	2.74
F14	176.80	1240	8316	1.352	6.202E-002	19.19
M15	185.33	453	5143	1.460	2.265E-002	16.26
m16	192.01	1144	6489	1.467	5.721E-002	11.24
m17	197.54	2090	6888	1.473	1.045E-001	10.35
M18	208.06	2404	6781	1.529	1.202E-001	10.00
m19	215.61	811	6848	1.537	4.057E-002	12.12
F20	244.42	318	4206	1.041	1.590E-002	70.29
F21	282.26	803	3218	1.402	4.013E-002	5.61
						Continued on next page

Table A.6.: Neutron activation analysis of the certified reference material GBW

Peak Nr.	$E_{\gamma M}$ (keV)	Net Peak Area (cts)	Bkgnd (cts)	FWHM (keV)	$CR_{\gamma M}$ (cps)	Error (%)
F22	299.56	3793	4442	1.996	1.896E-001	1.76
F23	311.66	14603	4025	1.408	7.302E-001	0.79
F24	328.55	1369	2739	1.407	6.847E-002	3.40
M25	340.14	1708	3125	2.071	8.538E-002	3.07
m26	344.29	2841	4349	2.075	1.420E-001	2.07
F27	396.18	1513	2595	1.573	7.567E-002	3.09
F28	415.58	404	1676	1.398	2.022E-002	8.45
M29	481.90	4297	1776	1.639	2.148E-001	3.49
m30	486.74	2448	1716	1.642	1.224E-001	3.83
F31	496.01	783	2015	1.591	3.917E-002	21.90
F32	510.66	819	2149	2.458	4.097E-002	4.73
F33	530.70	571	2104	1.946	2.855E-002	6.36
F34	563.10	245	1487	1.501	1.223E-002	12.51
M35	604.42	1167	2131	1.660	5.836E-002	12.92
m36	609.10	383	2360	1.663	1.915E-002	14.59
F37	723.73	166	1447	1.182	8.323E-003	17.61
F38	756.52	232	1157	1.549	1.158E-002	12.79
F39	778.78	310	1517	1.395	1.548E-002	34.12
F40	795.55	890	1992	1.759	4.450E-002	13.93
F41	815.47	795	1241	1.761	3.977E-002	4.68
F42	834.56	365	1086	1.756	1.823E-002	18.77
F43	867.53	273	1390	1.453	1.365E-002	11.63
M44	879.07	781	1625	1.845	3.905E-002	5.47
m45	889.01	19562	1662	1.850	9.781E-001	1.25
F46	924.91	189	930	1.485	9.433E-003	14.61
F47	965.49	1173	1370	3.370	5.867E-002	26.39
M48	1076.63	1907	735	1.804	9.533E-002	2.36
m49	1085.75	244	648	1.809	1.219E-002	9.22
					Continued on next page	

Table A.6.: Neutron activation analysis of the certified reference material GBW

Peak Nr.	$E_{\gamma M}$ (keV)	Net Peak Area (cts)	Bkgnd (cts)	FWHM (keV)	$CR_{\gamma M}$ (cps)	Error (%)
F50	1099.12	7933	722	1.892	3.967E-001	1.07
M51	1111.97	333	520	2.014	1.666E-002	7.75
m52	1115.42	571	515	2.016	2.857E-002	5.53
m53	1120.44	17348	461	2.018	8.674E-001	1.45
M54	1173.12	386	369	1.910	1.929E-002	6.05
m55	1177.92	271	429	1.912	1.354E-002	7.58
F56	1189.08	356	364	1.775	1.778E-002	21.54
M57	1221.36	573	323	1.971	2.864E-002	4.52
m58	1231.04	232	364	1.975	1.161E-002	8.26
F59	1291.67	5362	359	1.969	2.681E-001	1.31
F60	1332.79	372	248	2.048	1.861E-002	17.37
F61	1408.22	433	229	1.924	2.165E-002	5.09
F62	1461.10	2073	147	2.103	1.037E-001	4.50
F63	1596.70	2143	86	2.170	1.071E-001	4.24
F64	1730.17	73	48	1.073	3.654E-003	35.52
F65	1765.35	302	72	2.156	1.510E-002	5.89
F66	2010.91	118	36	2.055	5.922E-003	9.79
F67	2205.68	81	33	1.567	4.035E-003	41.32
F68	2523.07	60	12	1.862	2.998E-003	40.33
F69	2616.26	341	6	2.722	1.705E-002	5.26

Table A.6.: Neutron activation analysis of the certified reference material GBW

Reference Material ThO$_2$

Peak Nr.	$E_{\gamma M}$ (keV)	Net Peak Area (cts)	Bkgnd (cts)	FWHM (keV)	$CR_{\gamma M}$ (cps)	Error (%)
F1	6.24	246033	330880	1.288	1.230E+001	0.21
M2	71.40	85715	750709	1.407	4.286E+000	1.40
					Continued on next page	

Table A.7.: Neutron activation analysis of the reference material ThO$_2$

Peak Nr.	$E_{\gamma M}$ (keV)	Net Peak Area (cts)	Bkgnd (cts)	FWHM (keV)	$CR_{\gamma M}$ (cps)	Error (%)
m3	74.44	402843	1206103	1.412	2.014E+001	0.93
F4	85.79	464611	1129360	1.373	2.323E+001	0.71
M5	93.88	2397617	1035053	1.552	1.199E+002	0.12
m6	97.67	3894016	907440	1.558	1.947E+002	0.11
m7	103.14	217590	736015	1.566	1.088E+001	0.34
m8	110.33	1414444	689276	1.577	7.072E+001	0.13
m9	113.93	505377	567014	1.582	2.527E+001	0.19
F10	142.19	94885	1033500	4.413	4.744E+000	1.28
F11	228.00	1700	164097	0.983	8.498E-002	15.35
F12	247.92	15134	209612	1.505	7.567E-001	7.86
F13	258.09	8438	218900	1.606	4.219E-001	13.72
F14	271.18	80703	210961	1.486	4.035E+000	0.46
M15	279.85	2083	159166	1.269	1.041E-001	11.93
m16	287.82	3277	171743	1.277	1.638E-001	8.05
F17	299.75	1521400	211831	1.584	7.607E+001	0.17
F18	311.54	8580054	132343	1.583	4.290E+002	0.06
F19	320.51	1370	19262	1.317	6.851E-002	7.52
F20	340.13	938457	23553	1.600	4.692E+001	0.18
F21	364.08	636	7951	1.568	3.182E-002	10.46
M22	375.07	133916	9439	1.607	6.696E+000	0.51
m23	380.00	635	8517	1.611	3.176E-002	10.69
m24	386.93	1108	8392	1.617	5.539E-002	6.49
M25	398.14	265888	7103	1.628	1.329E+001	0.26
m26	406.19	570	5437	1.634	2.849E-002	9.67
m27	409.98	1344	5390	1.637	6.719E-002	4.57
m28	415.41	322297	3888	1.641	1.611E+001	0.25
m29	422.82	364	1440	1.647	1.820E-002	9.49
F30	455.30	180	1097	1.168	9.015E-003	14.05
						Continued on next page

Table A.7.: Neutron activation analysis of the reference material ThO_2

Peak Nr.	$E_{\gamma M}$ (keV)	Net Peak Area (cts)	Bkgnd (cts)	FWHM (keV)	$CR_{\gamma M}$ (cps)	Error (%)
F31	486.69	1230	1129	1.573	6.152E-002	9.46
F32	510.57	755	1123	2.230	3.777E-002	4.20
F33	537.00	431	624	1.596	2.154E-002	5.92
F34	582.75	342	704	1.508	1.712E-002	7.09
M35	608.97	425	632	1.650	2.125E-002	6.19
m36	611.41	515	741	1.652	2.574E-002	5.40
F37	623.19	1665	747	1.733	8.327E-002	6.85
F38	651.61	306	489	1.691	1.532E-002	35.71
F39	667.28	162	576	1.395	8.118E-003	40.17
F40	727.20	125	468	1.349	6.230E-003	15.22
M41	756.35	194	423	1.394	9.714E-003	10.04
m42	765.70	106	356	1.399	5.279E-003	15.11
m43	772.40	155	306	1.403	7.761E-003	10.97
F44	815.51	381	375	1.851	1.904E-002	5.72
F45	911.02	292	354	1.650	1.459E-002	24.00
F46	968.61	153	236	1.300	7.645E-003	11.11
F47	1120.01	260	281	1.830	1.298E-002	7.50
F48	1377.56	83	130	1.665	4.141E-003	14.78
F49	1460.99	1981	140	2.126	9.906E-002	4.66
F50	1596.59	1036	96	2.323	5.178E-002	5.91
F51	1729.95	59	36	1.850	2.949E-003	15.43
F52	1765.04	345	48	2.345	1.723E-002	13.46
F53	2205.38	97	27	2.513	4.853E-003	10.70
F54	2616.08	452	16	2.629	2.258E-002	8.79

Table A.7.: Neutron activation analysis of the reference material ThO_2

Reference Material ThF$_4$

Peak Nr.	$E_{\gamma M}$ (keV)	Net Peak Area (cts)	Bkgnd (cts)	FWHM (keV)	$CR_{\gamma M}$ (cps)	Error (%)
F1	7.43	813566	1110486	1.506	4.068E+001	0.12
M2	71.40	261508	2445515	1.441	1.308E+001	0.89
m3	74.37	1178595	3911746	1.446	5.893E+001	0.59
M4	85.74	1556425	3135289	1.610	7.782E+001	0.12
m5	89.32	508192	4131715	1.616	2.541E+001	0.26
m6	93.78	7775726	3634451	1.623	3.888E+002	0.07
m7	97.62	11963070	3144901	1.629	5.982E+002	0.07
m8	103.18	832684	2791671	1.638	4.163E+001	0.16
m9	110.27	4066447	2556048	1.648	2.033E+002	0.08
m10	113.87	1475575	2240562	1.654	7.378E+001	0.11
F11	142.14	266536	3224010	4.848	1.333E+001	9.44
F12	228.01	4203	532949	1.052	2.102E-001	11.11
F13	247.83	47409	726775	1.572	2.370E+000	4.86
F14	258.05	21784	632177	1.409	1.089E+000	2.30
F15	271.11	245118	731934	1.584	1.226E+001	1.01
M16	279.91	8360	520360	1.414	4.180E-001	5.59
m17	287.79	11021	601138	1.421	5.510E-001	4.43
F18	299.70	4760062	707521	1.639	2.380E+002	0.11
F19	311.49	26958968	497422	1.647	1.348E+003	0.04
F20	320.45	2927	95526	1.362	1.463E-001	7.11
F21	340.08	2954228	96993	1.660	1.477E+002	0.11
F22	364.18	1576	42840	1.387	7.881E-002	32.70
M23	375.01	423235	37513	1.670	2.116E+001	0.34
m24	379.87	2411	35430	1.674	1.206E-001	5.27
m25	386.62	3827	32706	1.680	1.914E-001	3.47
M26	398.09	843705	33101	1.692	4.219E+001	0.16
m27	405.92	6951	24784	1.698	3.476E-001	1.82

Table A.8.: Neutron activation analysis of the reference material ThF$_4$

Peak Nr.	$E_{\gamma M}$ (keV)	Net Peak Area (cts)	Bkgnd (cts)	FWHM (keV)	$CR_{\gamma M}$ (cps)	Error (%)
m28	409.86	12263	24405	1.701	6.132E-001	1.17
m29	415.36	1020064	16560	1.705	5.100E+001	0.15
m30	422.35	4941	7243	1.710	2.470E-001	1.74
m31	426.00	1787	7126	1.713	8.933E-002	3.76
m32	434.45	785	6947	1.719	3.927E-002	7.64
m33	438.27	1273	6866	1.722	6.363E-002	5.00
F34	455.52	871	7298	1.467	4.357E-002	6.80
F35	486.60	3194	5156	1.637	1.597E-001	7.16
36	496.38	150	2941	1.367	7.501E-003	54.53
F37	510.32	558	3100	0.922	2.789E-002	29.36
F38	536.84	1382	2524	1.709	6.910E-002	12.08
F39	582.86	794	2066	1.341	3.969E-002	19.19
F40	599.48	485	1900	1.646	2.426E-002	7.17
F41	611.33	6462	2091	1.912	3.231E-001	3.71
F42	623.11	16990	1668	1.887	8.495E-001	1.67
F43	639.93	614	1055	1.956	3.072E-002	18.01
F44	651.69	3747	917	1.941	1.874E-001	4.33
F45	667.28	535	808	1.687	2.677E-002	7.79
M46	680.59	174	490	1.378	8.676E-003	21.63
m47	686.82	551	934	1.382	2.754E-002	13.47
F48	698.06	124	461	1.331	6.201E-003	15.81
M49	709.63	1057	655	1.848	5.286E-002	7.37
m50	715.09	298	812	1.851	1.491E-002	9.45
m51	723.82	579	750	1.856	2.893E-002	8.92
m52	726.96	1472	730	1.858	7.358E-002	6.75
M53	751.03	231	491	1.953	1.156E-002	12.18
m54	756.20	885	479	1.955	4.423E-002	8.24
m55	765.44	396	461	1.961	1.979E-002	9.74
Continued on next page						

Table A.8.: Neutron activation analysis of the reference material ThF$_4$

Peak Nr.	$E_{\gamma M}$ (keV)	Net Peak Area (cts)	Bkgnd (cts)	FWHM (keV)	$CR_{\gamma M}$ (cps)	Error (%)
m56	772.27	462	475	1.964	2.308E-002	9.28
F57	815.38	1301	507	1.892	6.505E-002	8.14
F58	867.51	284	385	1.907	1.422E-002	7.19
F59	910.96	188	294	1.762	9.414E-003	37.79
F60	924.87	265	397	1.764	1.324E-002	10.17
F61	1120.14	193	362	1.676	9.644E-003	9.53
F62	1460.96	1997	174	2.146	9.986E-002	2.16
F63	1596.55	2970	137	2.318	1.485E-001	3.79
F64	1764.96	270	59	2.065	1.352E-002	6.26
F65	2205.34	102	36	2.384	5.113E-003	38.61
F66	2449.44	40	20	1.400	2.003E-003	18.92
F67	2616.10	539	14	2.658	2.697E-002	8.74

Table A.8.: Neutron activation analysis of the reference material ThF$_4$

Sample ^{232}Th:CaF$_2$ Melt 1

Peak Nr.	$E_{\gamma M}$ (keV)	Net Peak Area (cts)	Bkgnd (cts)	FWHM (keV)	$CR_{\gamma M}$ (cps)	Error (%)
F1	4.83	8850	9751	1.301	4.425E-001	1.08
F2	74.52	6938	23224	1.310	3.469E-001	6.92
F3	85.90	9375	23902	1.288	4.687E-001	4.66
M4	93.95	45721	23556	1.466	2.286E+000	0.90
m5	97.74	75224	21494	1.472	3.761E+000	0.82
m6	103.18	4334	18147	1.480	2.167E-001	2.58
M7	110.39	29321	16332	1.814	1.466E+000	2.08
m8	114.03	10382	16845	1.819	5.191E-001	2.31
F9	158.96	8761	20531	1.337	4.380E-001	1.35
F10	271.28	1456	5244	1.350	7.281E-002	3.86
						Continued on next page

Table A.9.: Neutron activation analysis of the sample ^{232}Th:CaF$_2$ Melt 1

Peak Nr.	$E_{\gamma M}$ (keV)	Net Peak Area (cts)	Bkgnd (cts)	FWHM (keV)	$CR_{\gamma M}$ (cps)	Error (%)
F11	299.81	29970	5561	1.549	1.498E+000	1.27
F12	311.61	168578	3563	1.541	8.429E+000	0.34
F13	340.19	18657	1564	1.554	9.328E-001	1.24
F14	351.79	321	972	1.324	1.606E-002	30.30
F15	375.15	2538	1010	1.430	1.269E-001	1.96
F16	398.20	5147	861	1.577	2.573E-001	3.73
F17	415.48	6476	829	1.577	3.238E-001	2.45
F18	510.64	801	647	2.875	4.004E-002	16.23
F19	582.98	133	369	1.454	6.636E-003	13.23
F20	609.11	411	482	1.765	2.054E-002	5.56
F21	911.12	127	220	1.138	6.370E-003	41.72
F22	968.67	76	244	1.117	3.817E-003	19.09
F23	1120.33	245	229	1.788	1.225E-002	24.80
F24	1297.09	1103	193	1.985	5.513E-002	7.12
F25	1461.09	1940	123	2.072	9.700E-002	2.19
F26	1765.22	332	50	1.976	1.659E-002	12.83
F27	2205.26	104	24	2.314	5.190E-003	29.44
F28	2616.17	373	6	2.535	1.864E-002	5.08

Table A.9.: Neutron activation analysis of the sample ^{232}Th:CaF$_2$ Melt 1

Sample ^{232}Th:CaF$_2$ Melt 2

Peak Nr.	$E_{\gamma M}$ (keV)	Net Peak Area (cts)	Bkgnd (cts)	FWHM (keV)	$CR_{\gamma M}$ (cps)	Error (%)
F1	4.83	8850	9751	1.301	4.425E-001	1.08
F2	74.52	6938	23224	1.310	3.469E-001	6.92
F3	85.90	9375	23902	1.288	4.687E-001	4.66
M4	93.95	45721	23556	1.466	2.286E+000	0.90
Continued on next page						

Table A.10.: Neutron activation analysis of the sample ^{232}Th:CaF$_2$ Melt 2

Peak Nr.	$E_{\gamma M}$ (keV)	Net Peak Area (cts)	Bkgnd (cts)	FWHM (keV)	$CR_{\gamma M}$ (cps)	Error (%)
m5	97.74	75224	21494	1.472	3.761E+000	0.82
m6	103.18	4334	18147	1.480	2.167E-001	2.58
M7	110.39	29321	16332	1.814	1.466E+000	2.08
m8	114.03	10382	16845	1.819	5.191E-001	2.31
F9	158.96	8761	20531	1.337	4.380E-001	1.35
F10	271.28	1456	5244	1.350	7.281E-002	3.86
F11	299.81	29970	5561	1.549	1.498E+000	1.27
F12	311.61	168578	3563	1.541	8.429E+000	0.34
F13	340.19	18657	1564	1.554	9.328E-001	1.24
F14	351.79	321	972	1.324	1.606E-002	30.30
F15	375.15	2538	1010	1.430	1.269E-001	1.96
F16	398.20	5147	861	1.577	2.573E-001	3.73
F17	415.48	6476	829	1.577	3.238E-001	2.45
F18	510.64	801	647	2.875	4.004E-002	16.23
F19	582.98	133	369	1.454	6.636E-003	13.23
F20	609.11	411	482	1.765	2.054E-002	5.56
F21	911.12	127	220	1.138	6.370E-003	41.72
F22	968.67	76	244	1.117	3.817E-003	19.09
F23	1120.33	245	229	1.788	1.225E-002	24.80
F24	1297.09	1103	193	1.985	5.513E-002	7.12
F25	1461.09	1940	123	2.072	9.700E-002	2.19
F26	1765.22	332	50	1.976	1.659E-002	12.83
F27	2205.26	104	24	2.314	5.190E-003	29.44
F28	2616.17	373	6	2.535	1.864E-002	5.08

Table A.10.: Neutron activation analysis of the sample ^{232}Th:CaF$_2$ Melt 2

Sample ^{232}Th:CaF$_2$ Melt 3

Peak Nr.	$E_{\gamma M}$ (keV)	Net Peak Area (cts)	Bkgnd (cts)	FWHM (keV)	$CR_{\gamma M}$ (cps)	Error (%)
F1	74.54	7297	24122	1.337	3.648E-001	7.13
F2	85.86	9337	26947	1.353	4.669E-001	5.46
M3	93.95	48609	24484	1.502	2.430E+000	0.89
m4	97.74	78688	22396	1.508	3.934E+000	0.80
m5	103.22	4482	18982	1.516	2.241E-001	2.51
m6	110.42	28744	17011	1.527	1.437E+000	0.96
m7	114.00	10230	15469	1.532	5.115E-001	1.42
F8	158.96	8295	18894	1.329	4.148E-001	1.41
F9	248.09	304	5270	1.027	1.521E-002	15.22
F10	271.24	1752	6259	1.427	8.760E-002	12.84
F11	299.84	31076	5502	1.547	1.554E+000	1.27
F12	311.66	174483	3700	1.381	8.724E+000	0.22
F13	340.21	19190	1522	1.557	9.595E-001	1.33
F14	351.66	359	1154	1.547	1.793E-002	7.60
F15	375.13	2776	1135	1.560	1.388E-001	5.23
F16	398.22	5428	1047	1.615	2.714E-001	3.15
F17	415.49	6559	892	1.606	3.280E-001	2.44
F18	488.69	176	503	1.590	8.804E-003	352.56
F19	510.71	699	679	2.292	3.495E-002	3.99
F20	582.77	188	348	1.470	9.402E-003	9.67
F21	609.08	373	456	1.568	1.863E-002	20.68
F22	807.53	119	239	1.460	5.953E-003	46.24
F23	1120.28	264	290	1.976	1.319E-002	7.21
F24	1297.10	1019	166	2.074	5.094E-002	7.60
F25	1461.18	2004	87	2.040	1.002E-001	4.41
F26	1729.97	41	41	1.226	2.052E-003	20.26
						Continued on next page

Table A.11.: Neutron activation analysis of the sample ^{232}Th:CaF$_2$ Melt 3

Peak Nr.	$E_{\gamma M}$ (keV)	Net Peak Area (cts)	Bkgnd (cts)	FWHM (keV)	$CR_{\gamma M}$ (cps)	Error (%)
F27	1765.27	301	39	2.165	1.507E-002	5.72
F28	2205.32	92	20	2.493	4.609E-003	13.75
F29	2616.31	332	9	2.594	1.660E-002	11.60

Table A.11.: Neutron activation analysis of the sample ^{232}Th:CaF$_2$ Melt 3

Sample ^{232}Th:CaF$_2$ 1

Peak Nr.	$E_{\gamma M}$ (keV)	Net Peak Area (cts)	Bkgnd (cts)	FWHM (keV)	$CR_{\gamma M}$ (cps)	Error (%)
F1	74.49	1809	6878	1.220	9.044E-002	14.91
F2	85.88	2400	8254	1.328	1.200E-001	10.13
M3	93.95	11037	7823	1.458	5.519E-001	2.11
m4	97.76	17613	7673	1.464	8.807E-001	1.95
m5	103.18	842	7010	1.472	4.211E-002	7.26
M6	110.37	7011	6491	1.813	3.506E-001	5.83
m7	114.01	2351	7020	1.818	1.175E-001	6.33
F8	158.94	5262	7640	1.473	2.631E-001	5.18
F9	185.37	492	4258	1.471	2.458E-002	34.70
F10	238.34	221	2189	1.163	1.106E-002	44.36
F11	271.22	306	1938	1.247	1.528E-002	10.52
F12	299.86	6838	2389	1.441	3.419E-001	1.16
F13	311.63	39598	1579	1.533	1.980E+000	0.72
F14	340.22	4230	1125	1.568	2.115E-001	3.50
F15	351.73	396	841	1.711	1.982E-002	25.36
F16	375.14	673	904	1.589	3.363E-002	14.25
F17	398.24	1218	703	1.524	6.091E-002	2.91
F18	415.49	1497	756	1.499	7.487E-002	7.27
F19	510.77	618	707	2.606	3.089E-002	18.83
						Continued on next page

Table A.12.: Neutron activation analysis of the sample Th:CaF$_2$ 1

Peak Nr.	$E_{\gamma M}$ (keV)	Net Peak Area (cts)	Bkgnd (cts)	FWHM (keV)	$CR_{\gamma M}$ (cps)	Error (%)
F20	609.08	409	433	1.579	2.044E-002	5.67
F21	910.69	133	373	1.599	6.648E-003	40.11
F22	1120.15	234	213	1.790	1.168E-002	26.57
F23	1297.08	653	203	1.902	3.266E-002	4.06
F24	1461.10	1958	99	2.120	9.790E-002	3.97
F25	1765.13	337	44	2.206	1.685E-002	12.10
F26	2616.23	367	26	2.714	1.837E-002	5.17

Table A.12.: Neutron activation analysis of the sample Th:CaF$_2$ 1

Sample ^{232}Th:CaF$_2$ 2

Peak Nr.	$E_{\gamma M}$ (keV)	Net Peak Area (cts)	Bkgnd (cts)	FWHM (keV)	$CR_{\gamma M}$ (cps)	Error (%)
F1	74.60	3084	11372	1.138	1.542E-001	10.40
F2	85.88	4401	11678	1.329	2.201E-001	7.68
M3	93.95	21429	12484	1.505	1.071E+000	1.40
m4	97.75	34670	11801	1.511	1.734E+000	1.27
m5	103.23	2059	10360	1.519	1.030E-001	3.89
m6	110.42	12637	9451	1.530	6.318E-001	1.51
m7	114.03	4489	8786	1.536	2.245E-001	2.25
F8	158.97	9545	12015	1.344	4.773E-001	1.12
F9	185.39	326	5774	1.000	1.628E-002	47.58
F10	271.27	907	3540	1.504	4.537E-002	17.09
F11	299.84	13375	3382	1.540	6.688E-001	2.01
F12	311.66	75333	2297	1.387	3.767E+000	0.33
F13	340.19	8299	1361	1.533	4.149E-001	2.18
F14	351.79	288	992	1.287	1.442E-002	31.47
F15	375.16	1140	726	1.433	5.702E-002	3.16
Continued on next page						

Table A.13.: Neutron activation analysis of the sample Th:CaF$_2$ 2

Peak Nr.	$E_{\gamma M}$ (keV)	Net Peak Area (cts)	Bkgnd (cts)	FWHM (keV)	$CR_{\gamma M}$ (cps)	Error (%)
F16	398.21	2369	764	1.454	1.184E-001	2.00
F17	415.51	2770	792	1.471	1.385E-001	1.83
F18	488.97	270	663	1.883	1.352E-002	29.18
F19	510.76	778	665	2.448	3.889E-002	16.12
F20	583.10	191	483	1.168	9.555E-003	37.94
F21	609.02	441	484	1.662	2.207E-002	15.91
F22	807.61	173	313	1.707	8.673E-003	10.02
F23	911.17	162	286	1.739	8.078E-003	36.91
F24	1120.32	269	238	1.750	1.345E-002	7.19
F25	1297.09	1194	175	1.972	5.972E-002	2.85
F26	1461.07	1863	129	2.108	9.315E-002	4.22
F27	1765.15	302	43	2.333	1.509E-002	5.66
F28	2616.21	384	6	2.591	1.921E-002	10.15

Table A.13.: Neutron activation analysis of the sample Th:CaF$_2$ 2

Sample ^{232}Th:CaF$_2$ 3

Peak Nr.	$E_{\gamma M}$ (keV)	Net Peak Area (cts)	Bkgnd (cts)	FWHM (keV)	$CR_{\gamma M}$ (cps)	Error (%)
F1	74.52	2536	9092	1.147	1.268E-001	10.42
F2	85.85	3361	11565	1.405	1.681E-001	9.98
M3	93.95	16792	10722	1.452	8.396E-001	1.58
m4	97.75	27517	10315	1.458	1.376E+000	1.45
m5	103.20	1502	9228	1.466	7.508E-002	4.83
M6	110.40	10759	8140	1.800	5.379E-001	3.38
m7	114.06	3911	9735	1.805	1.955E-001	3.72
F8	158.93	7221	10185	1.364	3.611E-001	1.32
F9	185.47	324	3066	1.199	1.620E-002	13.61
						Continued on next page

Table A.14.: Neutron activation analysis of the sample Th:CaF$_2$ 3

Peak Nr.	$E_{\gamma M}$ (keV)	Net Peak Area (cts)	Bkgnd (cts)	FWHM (keV)	$CR_{\gamma M}$ (cps)	Error (%)
F10	238.26	267	2121	1.137	1.335E-002	13.38
F11	271.22	600	2196	1.344	2.998E-002	6.37
F12	299.83	10619	2827	1.506	5.310E-001	3.45
F13	311.61	61685	1761	1.545	3.084E+000	0.60
F14	340.20	6834	1256	1.579	3.417E-001	2.28
F15	351.65	267	723	1.485	1.333E-002	9.12
F16	375.20	949	809	1.516	4.746E-002	3.47
F17	398.24	1872	867	1.459	9.360E-002	2.30
F18	415.48	2346	613	1.556	1.173E-001	5.16
F19	510.74	706	703	2.559	3.532E-002	3.98
F20	582.79	184	377	1.808	9.203E-003	9.69
F21	608.96	380	431	1.529	1.899E-002	6.09
M22	1115.47	71	187	1.691	3.560E-003	19.01
m23	1120.22	282	229	1.693	1.410E-002	6.82
F24	1297.06	833	164	1.849	4.166E-002	3.52
F25	1461.11	1962	111	2.179	9.811E-002	4.81
F26	1765.19	334	45	2.316	1.669E-002	5.36
F27	2205.14	96	32	2.137	4.790E-003	11.48
F28	2616.08	376	16	2.592	1.881E-002	5.06

Table A.14.: Neutron activation analysis of the sample Th:CaF$_2$ 3

Reference Material ThO$_2$ + Vitamine C

Peak Nr.	$E_{\gamma M}$ (keV)	Net Peak Area (cts)	Bkgnd (cts)	FWHM (keV)	$CR_{\gamma M}$ (cps)	Error (%)
F1	9.12	1182212	1557687	1.697	5.911E+001	0.10
M2	71.32	410729	3784956	1.530	2.054E+001	0.74
m3	74.34	1905844	6401052	1.535	9.529E+001	0.48
					Continued on next page	

Table A.15.: Neutron activation analysis of the reference material ThO$_2$ + Vitamine C

A. Appendix

Peak Nr.	$E_{\gamma M}$ (keV)	Net Peak Area (cts)	Bkgnd (cts)	FWHM (keV)	$CR_{\gamma M}$ (cps)	Error (%)
M4	85.72	2434091	5243067	1.672	1.217E+002	0.10
m5	89.75	555269	6435197	1.678	2.776E+001	0.29
m6	93.78	11913951	6304925	1.685	5.957E+002	0.06
m7	97.58	18734568	5221067	1.691	9.367E+002	0.06
m8	103.07	1225926	4567353	1.700	6.130E+001	0.13
m9	110.23	6719013	3946266	1.711	3.360E+002	0.06
m10	113.82	2449769	3829551	1.716	1.225E+002	0.09
F11	142.35	412108	4928582	4.433	2.061E+001	0.71
F12	169.97	143489	3466876	3.110	7.174E+000	1.09
13	184.27	8529	2126307	15.045	4.264E-001	28.16
F14	228.07	6844	972605	1.257	3.422E-001	43.13
F15	247.80	69653	1068366	1.608	3.483E+000	4.63
F16	258.06	33605	1048600	1.538	1.680E+000	1.92
F17	271.08	373005	1138859	1.637	1.865E+001	0.86
M18	279.93	10905	936076	1.417	5.453E-001	5.37
m19	287.82	13802	935300	1.425	6.901E-001	4.38
F20	299.68	7219388	1119707	1.688	3.610E+002	0.09
F21	311.47	40936576	868414	1.702	2.047E+003	0.03
F22	340.06	4491761	176694	1.714	2.246E+002	0.09
F23	364.04	2019	70372	1.710	1.009E-001	8.51
M24	375.00	642667	69078	1.717	3.213E+001	0.29
m25	379.64	3972	65780	1.721	1.986E-001	4.13
m26	386.59	6949	64279	1.727	3.474E-001	2.50
M27	398.07	1279441	61926	1.747	6.397E+001	0.14
m28	405.95	16075	50040	1.753	8.037E-001	1.12
m29	409.84	29701	51752	1.756	1.485E+000	0.71
m30	415.34	1548464	34848	1.760	7.742E+001	0.13
m31	422.29	12278	16751	1.765	6.139E-001	1.06

Table A.15.: Neutron activation analysis of the reference material ThO_2 + Vitamine C

Peak Nr.	$E_{\gamma M}$ (keV)	Net Peak Area (cts)	Bkgnd (cts)	FWHM (keV)	$CR_{\gamma M}$ (cps)	Error (%)
m32	425.91	4607	16419	1.768	2.304E-001	2.19
m33	434.56	1893	16803	1.774	9.465E-002	4.68
m34	438.26	3162	15711	1.777	1.581E-001	2.99
M35	486.58	4721	10147	1.750	2.360E-001	6.81
m36	492.27	538	11354	1.754	2.688E-002	12.63
m37	496.19	838	10677	1.757	4.190E-002	9.45
M38	509.89	1796	7777	2.306	8.979E-002	16.83
m39	513.22	1376	9071	2.309	6.878E-002	15.19
M40	530.41	154	4266	1.498	7.676E-003	29.63
m41	536.89	1582	5312	1.503	7.909E-002	3.67
F42	582.77	2021	4891	1.791	1.011E-001	10.84
F43	599.49	1436	4312	1.998	7.180E-002	15.38
F44	611.36	14901	4377	1.904	7.450E-001	2.38
F45	623.11	39952	3234	1.936	1.998E+000	1.12
F46	639.87	1479	1849	1.807	7.396E-002	9.68
F47	651.67	9090	1666	2.003	4.545E-001	2.58
F48	667.29	405	937	1.562	2.025E-002	7.38
M49	680.26	397	869	1.917	1.986E-002	12.70
m50	686.60	1263	1218	1.920	6.315E-002	9.87
F51	698.08	341	901	1.469	1.703E-002	28.59
M52	709.64	2585	1035	2.022	1.293E-001	4.32
m53	715.15	696	1040	2.025	3.479E-002	5.77
m54	723.77	1007	989	2.030	5.035E-002	6.13
m55	726.95	3249	905	2.032	1.625E-001	3.99
F56	738.26	258	595	2.047	1.292E-002	8.52
M57	751.22	317	640	2.137	1.585E-002	11.39
m58	756.12	1395	738	2.139	6.973E-002	7.78
m59	765.40	619	713	2.145	3.095E-002	8.70
Continued on next page						

Table A.15.: Neutron activation analysis of the reference material ThO_2 + Vita-mine C

Peak Nr.	$E_{\gamma M}$ (keV)	Net Peak Area (cts)	Bkgnd (cts)	FWHM (keV)	$CR_{\gamma M}$ (cps)	Error (%)
m60	772.27	406	734	2.148	2.031E-002	9.78
F61	815.32	1674	644	1.933	8.368E-002	7.59
F62	867.31	335	459	2.135	1.676E-002	6.52
M63	910.75	921	431	2.010	4.604E-002	3.37
m64	919.15	169	487	2.014	8.433E-003	10.55
m65	924.93	441	478	2.017	2.206E-002	5.31
M66	964.27	177	328	1.807	8.836E-003	19.08
m67	968.65	593	485	1.809	2.966E-002	13.91
F68	1120.26	273	335	1.814	1.363E-002	7.50
F69	1461.01	2028	221	2.227	1.014E-001	5.05
F70	1596.52	3881	172	2.339	1.941E-001	3.40
F71	1765.16	306	76	2.429	1.530E-002	17.53
F72	2522.92	108	24	2.036	5.397E-003	28.57
F73	2616.11	803	27	2.643	4.016E-002	7.33

Table A.15.: Neutron activation analysis of the reference material ThO_2 + Vitamine C

A.4. Transmittance Measurements

E_p (J)	ΔE_p (J)	E_{pc} (J)	ΔE_{pc} (J)
$1.249 \cdot 10^{-5}$	$1.137 \cdot 10^{-6}$	$9.346 \cdot 10^{-6}$	$8.054 \cdot 10^{-7}$
$2.838 \cdot 10^{-5}$	$1.712 \cdot 10^{-6}$	$1.537 \cdot 10^{-5}$	$9.668 \cdot 10^{-7}$
$4.039 \cdot 10^{-5}$	$1.409 \cdot 10^{-6}$	$1.892 \cdot 10^{-5}$	$8.983 \cdot 10^{-7}$
$4.156 \cdot 10^{-5}$	$3.230 \cdot 10^{-6}$	$2.017 \cdot 10^{-5}$	$1.053 \cdot 10^{-6}$
$4.616 \cdot 10^{-5}$	$1.414 \cdot 10^{-6}$	$2.113 \cdot 10^{-5}$	$9.277 \cdot 10^{-7}$
$6.146 \cdot 10^{-5}$	$5.497 \cdot 10^{-6}$	$3.220 \cdot 10^{-5}$	$1.699 \cdot 10^{-6}$
$7.822 \cdot 10^{-5}$	$6.644 \cdot 10^{-6}$	$3.596 \cdot 10^{-5}$	$2.857 \cdot 10^{-6}$
$9.078 \cdot 10^{-5}$	$6.748 \cdot 10^{-6}$	$4.746 \cdot 10^{-5}$	$2.018 \cdot 10^{-6}$
$1.240 \cdot 10^{-4}$	$4.244 \cdot 10^{-6}$	$5.609 \cdot 10^{-5}$	$2.133 \cdot 10^{-6}$
$2.039 \cdot 10^{-4}$	$8.346 \cdot 10^{-6}$	$8.471 \cdot 10^{-5}$	$4.417 \cdot 10^{-6}$

Table A.16.: Energy per pulse CaF$_2$ - sample "Small Chip"

E_p (J)	ΔE_p (J)	E_{pc} (J)	ΔE_{pc} (J)
$2{,}779 \cdot 10^{-5}$	$1{,}946 \cdot 10^{-6}$	$9{,}815 \cdot 10^{-6}$	$7{,}740 \cdot 10^{-7}$
$3{,}761 \cdot 10^{-5}$	$1{,}309 \cdot 10^{-6}$	$1{,}002 \cdot 10^{-5}$	$7{,}809 \cdot 10^{-7}$
$4{,}156 \cdot 10^{-5}$	$3{,}230 \cdot 10^{-6}$	$1{,}223 \cdot 10^{-5}$	$4{,}726 \cdot 10^{-7}$
$1{,}187 \cdot 10^{-4}$	$4{,}458 \cdot 10^{-6}$	$1{,}273 \cdot 10^{-5}$	$6{,}474 \cdot 10^{-7}$
$1{,}240 \cdot 10^{-4}$	$4{,}244 \cdot 10^{-6}$	$1{,}049 \cdot 10^{-5}$	$7{,}931 \cdot 10^{-7}$
$2{,}034 \cdot 10^{-4}$	$8{,}229 \cdot 10^{-6}$	$1{,}404 \cdot 10^{-5}$	$9{,}730 \cdot 10^{-7}$

Table A.17.: Energy per pulse - CaF$_2$ sample "Big Chip"

E_p (J)	ΔE_p (J)	E_{pc} (J)	ΔE_{pc} (J)
$1{,}249 \cdot 10^{-5}$	$1{,}137 \cdot 10^{-6}$	$1{,}118 \cdot 10^{-5}$	$9{,}136 \cdot 10^{-7}$
$2{,}7289 \cdot 10^{-5}$	$1{,}688 \cdot 10^{-6}$	$2{,}231 \cdot 10^{-5}$	$1{,}470 \cdot 10^{-6}$
$3{,}937 \cdot 10^{-5}$	$3{,}077 \cdot 10^{-6}$	$3{,}422 \cdot 10^{-5}$	$2{,}413 \cdot 10^{-6}$
$4{,}039 \cdot 10^{-5}$	$1{,}409 \cdot 10^{-6}$	$3{,}382 \cdot 10^{-5}$	$1{,}150 \cdot 10^{-6}$
$4{,}963 \cdot 10^{-5}$	$7{,}406 \cdot 10^{-6}$	$4{,}793 \cdot 10^{-5}$	$1{,}007 \cdot 10^{-5}$
$5{,}595 \cdot 10^{-5}$	$5{,}531 \cdot 10^{-6}$	$2{,}872 \cdot 10^{-5}$	$1{,}515 \cdot 10^{-6}$
$7{,}822 \cdot 10^{-5}$	$6{,}644 \cdot 10^{-6}$	$6{,}079 \cdot 10^{-5}$	$4{,}111 \cdot 10^{-6}$
$8{,}961 \cdot 10^{-5}$	$4{,}012 \cdot 10^{-6}$	$5{,}541 \cdot 10^{-5}$	$2{,}826 \cdot 10^{-6}$
$1{,}059 \cdot 10^{-4}$	$8{,}844 \cdot 10^{-6}$	$8{,}113 \cdot 10^{-5}$	$6{,}552 \cdot 10^{-6}$
$1{,}240 \cdot 10^{-4}$	$4{,}244 \cdot 10^{-6}$	$7{,}439 \cdot 10^{-5}$	$5{,}090 \cdot 10^{-6}$
$1{,}631 \cdot 10^{-4}$	$7{,}781 \cdot 10^{-6}$	$1{,}251 \cdot 10^{-4}$	$5{,}593 \cdot 10^{-6}$
$1{,}882 \cdot 10^{-4}$	$3{,}517 \cdot 10^{-6}$	$1{,}440 \cdot 10^{-4}$	$3{,}623 \cdot 10^{-6}$
$1{,}952 \cdot 10^{-4}$	$7{,}621 \cdot 10^{-6}$	$1{,}635 \cdot 10^{-4}$	$5{,}375 \cdot 10^{-6}$

Table A.18.: Energy per pulse - sample ^{232}Th:CaF$_2$

E_p (J)	ΔE_p (J)	E_{pc} (J)	ΔE_{pc} (J)
$1{,}514 \cdot 10^{-5}$	$9{,}117 \cdot 10^{-7}$	$1{,}355 \cdot 10^{-5}$	$9{,}079 \cdot 10^{-7}$
$2{,}345 \cdot 10^{-5}$	$1{,}105 \cdot 10^{-6}$	$1{,}773 \cdot 10^{-5}$	$9{,}575 \cdot 10^{-7}$
$3{,}884 \cdot 10^{-5}$	$1{,}760 \cdot 10^{-6}$	$3{,}274 \cdot 10^{-5}$	$1{,}553 \cdot 10^{-6}$
$3{,}960 \cdot 10^{-5}$	$3{,}456 \cdot 10^{-6}$	$3{,}682 \cdot 10^{-5}$	$3{,}602 \cdot 10^{-6}$
$5{,}366 \cdot 10^{-5}$	$1{,}427 \cdot 10^{-6}$	$4{,}317 \cdot 10^{-5}$	$1{,}429 \cdot 10^{-6}$
$8{,}110 \cdot 10^{-5}$	$4{,}780 \cdot 10^{-6}$	$7{,}149 \cdot 10^{-5}$	$4{,}514 \cdot 10^{-6}$
$1{,}089 \cdot 10^{-4}$	$5{,}206 \cdot 10^{-6}$	$9{,}016 \cdot 10^{-5}$	$4{,}162 \cdot 10^{-6}$
$1{,}334 \cdot 10^{-4}$	$4{,}229 \cdot 10^{-6}$	$1{,}171 \cdot 10^{-4}$	$3{,}391 \cdot 10^{-6}$
$1{,}887 \cdot 10^{-4}$	$5{,}835 \cdot 10^{-6}$	$1{,}588 \cdot 10^{-4}$	$5{,}333 \cdot 10^{-6}$

Table A.19.: Energy per pulse - CaF$_2$ sample "Hellma disc"

E_p (J)	ΔE_p (J)	E_{pc} (J)	ΔE_{pc} (J)
$1{,}211 \cdot 10^{-5}$	$8{,}681 \cdot 10^{-7}$	$1{,}086 \cdot 10^{-5}$	$7{,}886 \cdot 10^{-7}$
$2{,}877 \cdot 10^{-5}$	$1{,}074 \cdot 10^{-6}$	$2{,}032 \cdot 10^{-5}$	$9{,}309 \cdot 10^{-7}$
$5{,}632 \cdot 10^{-5}$	$1{,}811 \cdot 10^{-6}$	$4{,}071 \cdot 10^{-5}$	$1{,}153 \cdot 10^{-6}$
$7{,}889 \cdot 10^{-5}$	$1{,}881 \cdot 10^{-6}$	$5{,}791 \cdot 10^{-5}$	$1{,}433 \cdot 10^{-6}$
$1{,}197 \cdot 10^{-4}$	$3{,}707 \cdot 10^{-6}$	$7{,}289 \cdot 10^{-5}$	$1{,}874 \cdot 10^{-6}$
$1{,}563 \cdot 10^{-4}$	$6{,}464 \cdot 10^{-6}$	$8{,}250 \cdot 10^{-5}$	$2{,}361 \cdot 10^{-6}$
$1{,}928 \cdot 10^{-4}$	$3{,}719 \cdot 10^{-6}$	$1{,}300 \cdot 10^{-4}$	$2{,}709 \cdot 10^{-6}$

Table A.20.: Energy per pulse - sample YLF

E_p (J)	ΔE_p (J)	E_{pc} (J)	ΔE_{pc} (J)
$9{,}913 \cdot 10^{-6}$	$8{,}502 \cdot 10^{-7}$	$9{,}415 \cdot 10^{-6}$	$8{,}240 \cdot 10^{-7}$
$1{,}592 \cdot 10^{-5}$	$3{,}226 \cdot 10^{-6}$	$1{,}300 \cdot 10^{-5}$	$2{,}304 \cdot 10^{-6}$
$4{,}337 \cdot 10^{-5}$	$6{,}949 \cdot 10^{-6}$	$3{,}359 \cdot 10^{-5}$	$4{,}428 \cdot 10^{-6}$
$4{,}872 \cdot 10^{-5}$	$3{,}011 \cdot 10^{-6}$	$3{,}737 \cdot 10^{-5}$	$2{,}539 \cdot 10^{-6}$
$8{,}331 \cdot 10^{-5}$	$2{,}830 \cdot 10^{-6}$	$6{,}130 \cdot 10^{-5}$	$2{,}209 \cdot 10^{-6}$
$1{,}294 \cdot 10^{-4}$	$5{,}681 \cdot 10^{-6}$	$9{,}718 \cdot 10^{-5}$	$3{,}424 \cdot 10^{-6}$
$1{,}649 \cdot 10^{-4}$	$4{,}593 \cdot 10^{-6}$	$1{,}011 \cdot 10^{-4}$	$2{,}148 \cdot 10^{-6}$

Table A.21.: Energy per pulse - sample LiF

E_p (J)	ΔE_p (J)	E_{pc} (J)	ΔE_{pc} (J)
$1{,}023 \cdot 10^{-5}$	$8{,}858 \cdot 10^{-7}$	$8{,}247 \cdot 10^{-6}$	$8{,}042 \cdot 10^{-7}$
$2{,}425 \cdot 10^{-5}$	$3{,}618 \cdot 10^{-6}$	$9{,}457 \cdot 10^{-6}$	$9{,}888 \cdot 10^{-7}$
$4{,}809 \cdot 10^{-5}$	$5{,}168 \cdot 10^{-6}$	$2{,}098 \cdot 10^{-5}$	$1{,}677 \cdot 10^{-6}$
$6{,}004 \cdot 10^{-5}$	$2{,}459 \cdot 10^{-6}$	$2{,}031 \cdot 10^{-5}$	$1{,}005 \cdot 10^{-6}$
$8{,}603 \cdot 10^{-5}$	$2{,}290 \cdot 10^{-6}$	$2{,}868 \cdot 10^{-5}$	$1{,}027 \cdot 10^{-6}$
$1{,}341 \cdot 10^{-4}$	$4{,}938 \cdot 10^{-6}$	$4{,}301 \cdot 10^{-5}$	$1{,}737 \cdot 10^{-6}$
$1{,}836 \cdot 10^{-4}$	$6{,}093 \cdot 10^{-6}$	$4{,}310 \cdot 10^{-5}$	$1{,}470 \cdot 10^{-6}$

Table A.22.: Energy per pulse - sample Nd doped LiLuF$_4$

E_p (J)	ΔE_p (J)	E_{pc} (J)	ΔE_{pc} (J)
$1{,}023 \cdot 10^{-5}$	$8{,}858 \cdot 10^{-7}$	$8{,}830 \cdot 10^{-6}$	$8{,}177 \cdot 10^{-7}$
$2{,}425 \cdot 10^{-5}$	$3{,}618 \cdot 10^{-6}$	$1{,}856 \cdot 10^{-5}$	$2{,}625 \cdot 10^{-6}$
$4{,}809 \cdot 10^{-5}$	$5{,}168 \cdot 10^{-6}$	$4{,}110 \cdot 10^{-5}$	$2{,}850 \cdot 10^{-6}$
$6{,}004 \cdot 10^{-5}$	$2{,}459 \cdot 10^{-6}$	$4{,}479 \cdot 10^{-5}$	$1{,}812 \cdot 10^{-6}$
$8{,}603 \cdot 10^{-5}$	$2{,}290 \cdot 10^{-6}$	$6{,}825 \cdot 10^{-5}$	$1{,}810 \cdot 10^{-6}$
$1{,}341 \cdot 10^{-4}$	$4{,}938 \cdot 10^{-6}$	$9{,}214 \cdot 10^{-5}$	$4{,}088 \cdot 10^{-6}$
$1{,}836 \cdot 10^{-4}$	$6{,}093 \cdot 10^{-6}$	$1{,}092 \cdot 10^{-4}$	$3{,}847 \cdot 10^{-6}$

Table A.23.: Energy per pulse - sample $LiCaAlF_6$

List of Figures

List of Tables

Bibliography

[1]   S.L. Baldochi I.M. Ranieri G.E. Brito A.F.H. Librantz L. Gomes. "Luminescence study of the $4f^25d$ configuration of Nd^{3+} in $LiYF_4$, $LiLuF_4$ and BaY_2F_8 crystals". In: *Journal of Luminescence* 121 (2006), p. 11.

[2]   Luiz Vicente Gomes Tarelho Izilda Marcia Ranieri Andre Felipe Henriques Librantz Laercio Gomes. "Investigation of energy shift of $4f^3$ and $4f^25d$ levels in Nd-doped YLF and LLF crystals". In: *Exacta* 4 (2006), p. 5.

[3]   Avantes. URL: http://www.avantes.com.

[4]   B. R. Beck et al. "Energy Splitting of the Ground-State Doublet in the Nucleus ^{229}Th". In: *Phys. Rev. Lett.* 98 (14 2007), p. 142501. DOI: 10.1103/PhysRevLett.98.142501. URL: http://link.aps.org/doi/10.1103/PhysRevLett.98.142501.

[5]   National Nuclear Data Center. Brookhaven National Laboratory. URL: http://www.nndc.bnl.gov.

[6]   K. Mann Ch. Görling U. Leinhos. "Self-trapped exciton luminescence and repetition rate dependence of two-photon absorption in CaF_2 at 193 nm". In: *Optics Communications* 216 (2003), pp. 369–378.

[7]   K. Mann Ch. Görling U. Leinhos. "Surface and bulk absorption in CaF_2 at 193 and 157 nm". In: *Optics Communications* 249 (2005).

[8]   P. Dessovic private communication.

[9]   Loren Paul Cramer. "Defect in calcium fluoride generated by 157 nm laser and low-energy electrons". In: *Dissertation Washington State University* (2004).

[10] Prof. Dr. Wolfgang Demtröder. *Experimentalphysik 2*. Ed. by Leipzig LE-TeX Jelonek Schmidt & Völker GbR. Springer-Verlag, 2004.

[11]   Prof. Dr. Wolfgang Demtröder. *Experimentalphysik 3*. Ed. by Leipzig LE-TeX Jelonek Schmidt & Völker GbR. Springer-Verlag, 2005.

[12]   Gam Laser Inc. VUV 157nm Fluorine Lasers. URL: `http://www.gamlaser.com/Brochures/F2.pdf`.

[13]   R. I. Eglitis* H. Shi and G. Borstel. "First-principles calculations of the CaF_2 bulk and surface electronic structure". In: (2005).

[14]   R.I. Eglitis H. Shi and G. Borstel. "Ab initio calculations of the CaF2 electronic structure and F centers". In: *Phys. Rev. B* 72 (2005).

[15]   M. N. Kabler and R. T. Williams. "Vacancy-interstitial pair production via electron-hole recombination in halide crystals". In: *Phys. Rev. B18* (1978).

[16]   Mayeen Uddin Khandaker. "High purity germanium detector in gamma-ray spectrometry". In: *International Journal of Fundamental Physical Sciences* (2011), p. 5.

[17]   W. J. Manthey. "Crystal Field and Site Symmetry of Trivalent Cerium Ions in CaF_2: the C_{4v} and C_{3v} Centers with Interstitial-Fluoride Charge Compensator". In: *Physical Review B* 8 (1973), p. 13.

[18]   ElBaradei M.M. and Burkart W. *Handbook of Radioactivity Analysis*. Ed. by L'annunziata M.F. Academic Press, Great Britain, 2003.

[19]   Vaidya Nathan and A. H. Guenther. "Review of multiphoton absorption in crystalline solids". In: *J. Opt. Soc. Am. B* 2 (1984).

[20]   Thomas E Parker. "Long-term comparison of caesium fountain primary frequency standards". In: *Metrologia* 47 (2010), p. 10.

[21]   Asylum Research. URL: `http://www.asylumresearch.com/Products/MFP-3D-BIO/MFP-3D-BIO.shtml`.

[22]   Vincet P. Sokira Revecca S. Retherford Robert Sabia. "Effect of surface quality on transmission performance for (111) CaF_2". In: *Applied Surface Science* 183 (2001), pp. 264–269.

[23]   Pyroelectric Energy Sensor. URL: `www.optoscience.com/maker/ophir/pdf/catalog2010.pdf.`.

Bibliography

[24] K.S. Song and R.T. Williams. "Self-Trapped Excitons: Second Edition". In: (1996).

[25] K. Tanimura. "Lattice relaxation of highly excited self-trapped excitons in CaF_2". In: . *Phys. Rev. B* 40 (1989).

[26] V. Nagirnyi V. Denks T. Savikhina. "Dependence of luminescence processes and transmission in vacuum-ultraviolet region on surface condition in CaF_2 single crystals". In: *Applied Surface Science* 158 (2000).

[27] Matthieu Verstraete and Xavier Gonze. "First-principles calculation of the electronic, dielectric, and dynamical properties of CaF_2". In: *Phys. Rev. B* (2003), p. 7.

Acknowledgements